NASA CONTRACTOR REPORT 177443

GPS VERTICAL AXIS PERFORMANCE ENHANCEMENT

HELICOPTER PRECISION APPROACH

ROBERT P. DENARO AND JACQUES BESER

CONTRACT NAS2-11791

NASA

NASA CONTRACTOR REPORT 177443

GPS VERTICAL AXIS PERFORMANCE ENHANCEMENT

HELICOPTER PRECISION APPROACH

ROBERT P. DENARO AND JACQUES BESER

Prepared for
Ames Research Center
Under Contract NAS2-11791

National Aeronautics and
Space Administration

Ames Research Center
Moffett Field, California 94035

TABLE OF CONTENTS

TABLE OF CONTENTS

LIST OF FIGURES

LIST OF FIGURES

LIST OF TABLES

GLOSSARY OF ACRONYMS USED IN FIGURES

1. X , Y, and Z correspond to Local Tangent Plane (LTP) East, North, and Up unless otherwise noted.

2. ECEF = Earth-Centered, Earth-Fixed

3. NAV x(+) refers to the navigation (coordinate) state immediately following Kalman filter update.

4. PV = Position/Velocity State vector

5. PVAC = Position/Velocity/Constant Acceleration state vector

6. PVAT = Position/Velocity/Turn Rate Dynamics state vector

7. ALT = Altimeter-aided filter

8. C = Conventional GPS Solution

9. D = Differential GPS Solution

10. Statistics below plots are, from left to right, mean, standard deviation, and root-mean-square (RMS)

11. The "ephemeris date" refers to the almanac used to propagate the satellite motion and the basis for the time scale.

I. INTRODUCTION

1.1 BACKGROUND

The Navstar Global Positioning System (GPS) is a highly accurate radionavigation system being developed for military and civil use by the Department of Defense (DoD). Due to the proposed global availability of this extremely accurate positioning system, GPS promises to be a major national resource for civil aviation and other navigation users. Of particular interest to NASA is a derivative of GPS, called differential GPS, which has direct applicability to many high-priority rotorcraft operations. Differential GPS affords increased levels of precision which will be essential for such rotorcraft applications as non-precision approach, off-shore oil operations, search and rescue, and oil pipeline servicing.

Preliminary studies have been conducted by NASA to investigate differential GPS concept mechanizations and cost, and to theoretically predict navigation performance and the impact of degradation of the GPS C/A-code for national security reasons. The results of these studies show that GPS performance, even in the differential mode, may be inadequate (compared to FAA landing and approach navigation accuracy requirements) to support precision approach [1]. This is particularly true of the vertical axis accuracy of differential GPS, which must meet the most demanding specification.

However, several attractive alternatives exist for improving GPS vertical axis performance, such as receiver "tuning" to the landing environment, optional selection of tracked satellites, and receiver aiding with other sensors. The objective of this effort was to investigate such techniques using available NASA simulation facilities, and recommend a composite system which meets approach and landing navigation accuracy requirements. In addition, flight tests were conducted with post-test differential GPS processing to establish a performance baseline for future flight tests of these advanced concepts. Results of this preliminary flight test are presented in this report as well.

1.2 DIFFERENTIAL GPS CONCEPT

The Navstar GPS is a satellite-based radionavigation system that will provide extremely accurate position, velocity, and time on a worldwide, continuous basis. User receivers make ranging and Doppler measurements from digitally encoded L-band signals transmitted from a constellation of 18 to 21 satellites. Four signals are required from four of the possible six to eight satellites in view to solve for three coordinates of position, velocity, and an unknown user clock bias (hence the term, pseudorange).

User receivers employ delay lock loops and phase lock loops for tracking the signals and extracting the coded information to complete the triangulation-type navigation computations. In addition to residual phase and frequency errors from these tracking loops, other sources of ranging errors include mismodeled signal propagation delays, ephemeris errors, multipath errors, and intentional signal degradation imposed by the DoD for national security reasons. However, since the satellites are at half-synchronous altitude, the major contributor to user navigation error is non-orthogonal ranging signals which causes geometric dilution of precision (GDOP).

The sequential nature of pseudorange measurements in the receiver lends very well to recursive Kalman filtering, which is the usual technique for computing the navigation solution. A low-cost C/A-code tracking set will typically employ an 8-state linearized (indirect) Kalman filter. To maximize efficiency and satisfy real-time constraints, the filter can be implemented using the upper triangular diagonal factorization of the state covariance matrix, using the modified Cholesky algorithm. In addition, the filter will need an adaptive fading memory feature to control possible filter divergence by increasing diagonal elements of the state covariance matrix whenever smoothed pseudorange measurement residuals are large. Aiding sensors can be useful to GPS for improving tracking bandwidths (and hence receiver noise ranging errors) and for improving the geometry of the ranging solutions. Kalman filter state vectors will typically be modified to estimate relevant sensor states.

Differential GPS is a concept that eliminates some of the common, bias errors experienced by conventional GPS. Differential GPS derives its potential from the fact that the measurement errors are highly correlated between different users (as well as being highly correlated in time, or autocorrelation). By employing a second GPS receiver with comparison to truth, slowly varying, correlated errors can be isolated and eliminated. In addition, depending on the relative rates, intentional degradation of the C/A-signal may be eliminated by differential GPS as well [2]. A popular implementation is illustrated in Figure 1-1.

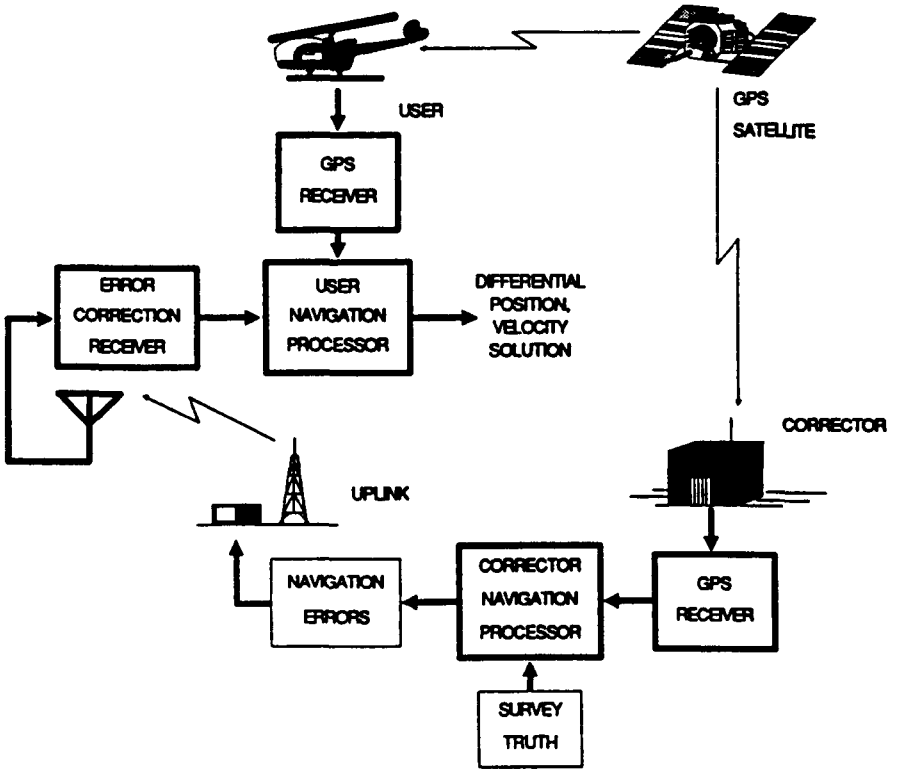

Figure 1-1. Differential GPS Concept

1.3 ROTORCRAFT APPROACH AND LANDING

The attractive application of GPS to the rotorcraft community is for remote, low visibility meteorological conditions where other reliable and precise forms of navigation are unavailable. Specific examples include Alaskan inter-city navigation; off-shore oil rig navigation, approach, and landing; and mountainous operations where precise beacons are unavailable. Also, special operations such as search and rescue, police work, and fire fighting can benefit from enhanced navigation precision.

For landing operations in these locations and applications, even more precise positioning data is required. Such precision may be available by employing differential GPS. Thus, a differential GPS user may be totally independent of visibility conditions, which for many of the locations postulated constitutes a large percentage of the operations.

Rotorcraft approach profiles vary, but are generally flown at six to ten degree glideslopes. Low visibility approaches usually include long straight-in finals, but finals as short as one mile or less are feasible. Speeds vary by equipment flown, from as fast as small fixed-wing aircraft to much slower speeds. The controllability of speed as well as flight path is a factor that may have potential in relaxing landing navigation standards, currently established for fixed and rotor wing aircraft in general.

However, for the present, FAA Navigation System Accuracy Standards are as shown in Table 1-1. As stated, the elevation accuracy requirement is more demanding than the lateral error. Even at Category I decision heights, the vertical axis requirement presents a formidable challenge to differential GPS. At these accuracy levels, every known error source in differential GPS must be exploited in full to have any hope of reducing cumulative error budgets below required levels. Furthermore, because GPS solutions often lack a satellite directly at zenith, the vertical axis suffers the greatest accumulation of multiple sources of errors.

Table 1-1. Approach and Landing Navigation Accuracy Requirements

Phase	Sub-Phase		Altitude (Flight Level)	Traffic Density	Route Width (NM)	Accuracy 2 drms (meters)		System Use Accuracy 2 drms (meters)
Approach and Landing	Non-Precision		250 to 3000 ft. above Surface	Normal				
	Precision	Cat I	100 to 3000 ft. above Surface	Normal		± 3.1 Meters**	± 3 Meters***	
						at 100 ft. above Surface		
		Cat II	50 to 3000 ft. above Surface	Normal		± 4.6 Meters	± 1.4 Meters	
						at 50 ft. above Surface		
		Cat III	8 to 3000 ft. above Surface	Normal		± 4.1 Meters	± 0.4 Meters	
						8 ft. above Surface		

** This column is lateral position 2 sigma accuracy in meters for Precision Approach and Landing

*** This column is vertical position 2 sigma accuracy in meters for Precision Approach and Landing

II. PROBLEM DEFINITION AND SCOPE

2.1 OBJECTIVES

The objectives of this effort were to improve the vertical axis performance of GPS to potentially support precision helicopter landing approach operations.

Analysis of differential GPS performance have shown that while the system may provide adequate (with respect to current FAA standards) accuracy in the lateral axis to support precision approach, further improvements are necessary in the vertical axis. Fortunately, investigation of GPS error sources indicates that several receiver and navigation filter design changes are possible which may improve vertical axis accuracy for this particular application. Such error models and filter components are inherent in the NASA DIFFGPS simulation, thus providing a readily available facility for verifying this hypothesis. The purpose of this effort is to determine improvements that can be realized in rotorcraft landing approach differential GPS vertical axis performance using the DIFFGPS simulation. Specific areas of investigation included receiver measurement processing improvements, state modeling improvements, adaptive covariance modeling, mission-tailored satellite selection, and integration of external aiding sensors.

2.2 SYSTEM SIMULATION FACILITY

The major GPS evaluation tool used for this study was DIFFGPS. DIFFGPS is an analytical simulation of the Navstar GPS and its environment. In addition to conventional GPS, the simulation models the differential implementation of GPS, where a second, static receiver at a surveyed location is used to compute measurement corrections and augment the dynamic user's solution via telemetry data link. Figure 2-1 illustrates the DIFFGPS program.

DIFFGPS was designed as a Monte Carlo simulation to provide realism of the environment and its non-linear features, and to provide direct relevance to field test programs [3]. Satellite motion is modeled by classic Keplerian equations. Constellation alternatives are selectable for up to 24 satellites. User motion in the User Route Planning Program is produced by the operator establishing a "route plan" by specifying either latitude/longitude/altitude or range/bearing/altitude from an initial location. The simulation generates accelerating turns, climbs, dives and linear speed changes, automatically checking for adequate acceleration distances in the route plan.

Particular emphasis was placed on the development of the error models, since they explicitly determine navigation performance. Care was taken to assure that empirically-backed error levels were incorporated. Dynamics of the errors due to user-satellite and user-corrector geometry were faithfully reproduced to support representative differential GPS performance conclusions. This caused consideration and modeling of somewhat undefined relationships, such as spatial and temporal variations of ionospheric and tropospheric delays. Magnitudes of the errors may be adjusted so that the relative comparison of different filters should produce very robust conclusions based on the error model fidelity used. This last feature, reliability of the comparative performance of the filters, was the major design methodology driver in developing the various error models.

GPS navigation algorithm analysis is the primary emphasis of the simulation. To enable an efficient and fair comparison of implementation techniques under the Monte Carlo driver environment, the simulation can run three corrector and six user navigation algorithms simultaneously during any run, although only one corrector is permitted to provide the differential reference solution for a particular run. Therefore, five user receiver navigation algorithms can process identical motion, satellite geometry, and error model inputs during a simulation run. Due to the modular nature of the simulation, it is possible to substitute different sets of variations of filters into the six user and three corrector slots prior to the run. Of course, it is equally easy to substitute in variations of error models or even satellite/user motion models if the need arises. Interface specifications are well defined for such flexibility.

The post-run analysis module provides the analyst extensive observation of relative motion, error model outputs, and Kalman filter operation. This is accomplished by providing menu-selectable plots, with selectable data periods and scales, for all parameters of interest. The operator can essentially retrieve all significant input, intermediate, and output variables from a large data file produced during the run. A high-performance plotting package and high-resolution graphics provide the display medium, including multiple plots per page and multiple curves per plot for comparative analysis.

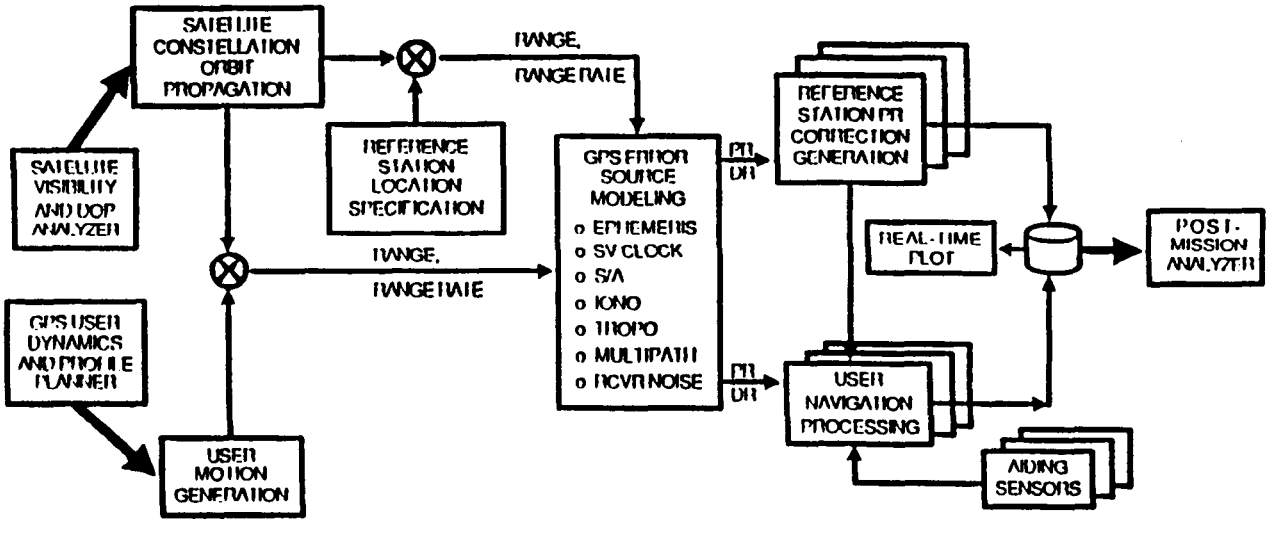

Figure 2-1. DIFFGPS Monte Carlo Simulation

III. RECEIVER NAVIGATION FILTER ENHANCEMENT

This section describes enhancements to the receiver measurement processing and Kalman filter development. The measurement processing change involves continuous deltaranging and is discussed in Section 3.1.

The two significant improvements to the earlier modeled Z-Set type filter were acceleration state modeling and improvements to adaptive covariance modeling. Such models improve the fidelity of the plant model to the known dynamics of the vehicle, yet allow graceful boost of process noise when the model is inadequate. It is generally true that when the plant model is more precise, the process noise modeling must be responsive to preserve optimal filter operations in all conditions, particularly in those conditions for which the modeling was not designed and may be in error. Acceleration state modeling improvements are discussed in Section 3.2 and Adaptive Covariance modeling is discussed in Section 3.3.

3.1 MEASUREMENT PROCESSING IMPROVEMENTS

Since the baseline GPS receiver technology for this effort was the Magnavox Z-Set, an analysis was made of the receiver measurement process to determine possible improvements.

The major area for improvement and a technique that is being implemented in modern receivers is continuously integrated Doppler (carrier processing). In the Z-Set, the effective Doppler integration interval is only 1/4 of the pseudorange measurement interval. This was necessary because of the delta-pseudorange technique of deriving integrated Doppler. That is, during the 1/4 interval Doppler integration process, the code loop is disabled so that the end-of-deltarange-interval pseudorange measurement is precise to relative Doppler accuracies, but this technique causes the deltarange to be non-contiguous in time. Therefore, use of deltarange for velocity determination requires extrapolation which will be in error under accelerating conditions. In particular, the "smoothing" advantage of continuous, precise deltarange measurments is lost to a great extent in this method.

In current, multi-channel GPS receivers with sufficient tracking loop processing power, measurement processing can achieve full-interval deltarange averaging or nearly so. This deltarange is a very precise (fraction of a carrier wavelength, 19 cm, typically 1-2 cm) measure of change in pseudorange and therefore, has a tremendous effect on smoothing the less accurate (3-6 m, 1 σ typically) pseudorange measurements if applied correctly. Although periodic loss of carrier lock would force "reinitialization" of this smoothing process, the process quickly converges, so if positive coherent tracking indication is present, the advantage of having contiguous deltaranging is still apparent.

To account for this tracking implementation improvement in DIFFGPS, the receiver tracking model was modified to emulate full-interval deltarange tracking. Figure 3-1 compares the performance of an 8-state (position-velocity) filter tracking aircraft motion during a constant acceleration turn followed by a constant linear acceleration.

The full internal deltaranging had a dramatic effect on performance. In fact, the effects of the acceleration are virtually undetectable. This is due to the fact that the process noise is (and is modeled as) nearly zero, since the deltarange is a very accurate measurement of the true change in velocity over the interval, not unlike the use of delta velocity inputs from an INS. The error excursions of 20-40 meters in the Z-set modeled case are typical of the case of partial interval doppler measurement.

Full Interval Deltaranging

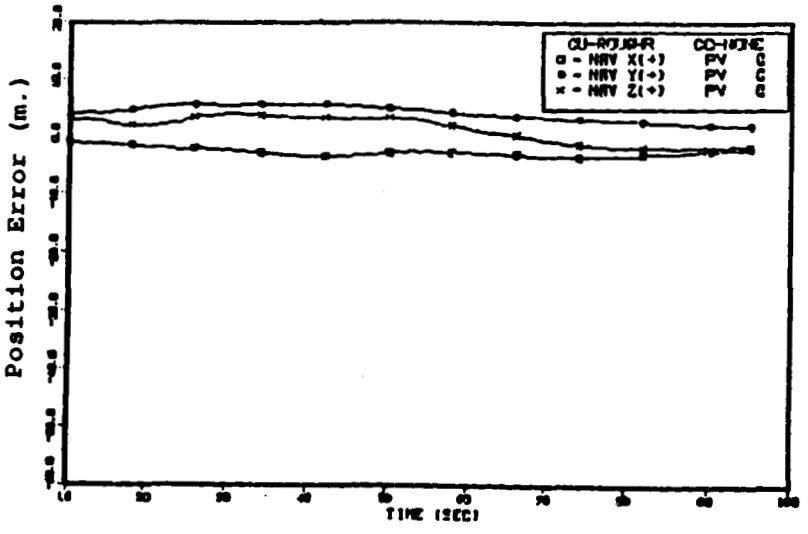

Statistics:		$\bar{x}$	σ
	x	-2.74	.69
	y	4.09	1.25
	z	1.30	2.19

Quarter Interval Deltaranging

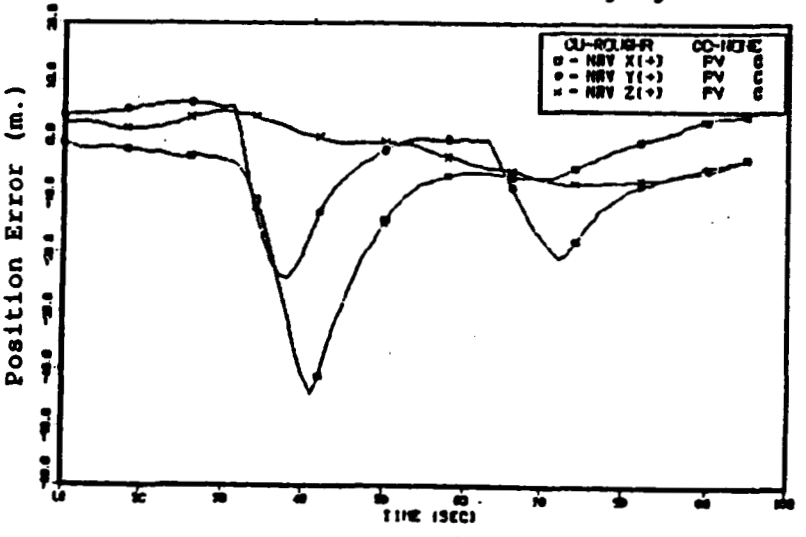

Statistics:		$\bar{x}$	σ
	x	-7.80	11.04
	y	-4.90	6.68
	z	-1.75	4.18

Figure 3-1. Comparison of Performance for 1/4-Interval and Full-Interval Deltarange Integration

For acronym definition refer to glossary on page vi.

3.2 ACCELERATION STATE MODELING

In general, the inclusion of acceleration states in the Kalman Filter, allowing for the estimation of the vehicle acceleration should provide for a better dynamic tracking of the vehicle motion. However, since the only direct observations in the measurement vector are range and range rate, any acceleration is observable only as the derivative of the rate and therefore, lags the velocity estimate. For this reason, acceleration state modeling will work well only when the vehicle acceleration is reasonably constant, allowing the filter to build up that state and stay there. Conversely, changes in accelerations will be a transient to this process and will cause the filter to lag in its response unless adequate process noise is introduced to deweight the process (constant acceleration) modeling.

Of course, it is important to remember that the state modeling is related to the measurement and computation intervals. For example, if the measurement and computation intervals are 1 second, then it is important to closely model the dynamics over that 1 second interval rather than be concerned with longer term effects. The significance of this is that, as tracking intervals get shorter for the same vehicle dynamics, the structure and perhaps even order of the state modeling becomes less important.

The models considered in this study were the baseline position-velocity state vector (with the contiguous deltaranging discussed in Section 3.1), constant acceleration state modeling, and a concept called constant turn-rate dynamics. Comparisons for a constant contripetal acceleration, level turn were performed using the DIFFGPS Simulation and are shown in this section with the various modeling discussions. The most attractive models were later tested with the other design improvements in the landing simulation which is reported in Section VI.

3.2.1 No Acceleration Modeling: PV Filter

This model, which emulates the baseline Z-Set Kalman filter (except for the addition of contiguous delta-ranging) investigated in an earlier study [3], uses an eight-state filter containing the three position states and three velocity states, the user clock bias, and the user clock drift rate, as follows:

$$
\begin{aligned}
\dot{x} &= v_x \\
\dot{y} &= v_y \\
\dot{z} &= v_z \\
\dot{v}_x &= w_{v_x} \\
\dot{v}_y &= w_{v_y} \\
\dot{v}_z &= w_{v_z} \\
\dot{b} &= f + w_b \\
\dot{f} &= -f/\tau + w_f
\end{aligned}
\qquad (1)
$$

where the w terms are white process noise with normal distribution, zero mean and power spectral density N, i.e., $w_{v_x} \sim N(0, N_{v_x})$. This formulation models, or at least accounts for, acceleration related effects in the process noise matrix, Q. The impact of this is to boost Q, and hence, the covariance, P, more than would be done for the acceleration state case which would incorporate only jerk-related effects in the Q-matrix. With larger Q then, the position-velocity (PV) filter will deweight the state modeling (state extrapolation) and weight higher the measurements, resulting in greater response to measurement errors and noise.

3.2.2 Constant Acceleration: PVAC Filter

In this model, a constant acceleration is assumed in each of three axes. The filter consists of 11 states, including the three positions, three velocities, three accelerations, the clock bias and drift rate.

The principle behind this model is that, as long as actual accelerations are constant, the acceleration state estimates will attain constant values. Constant acceleration is, in fact, a good assumption for most flight situations since power changes normally result in reasonably constant linear accelerations while coordinated turns, in zero wind conditions, result in constant centripetal acceleration. Of course, the ECEF components of total acceleration are not constant as defined in the model, which is a disadvantage of this technique if modeled in the ECEF frame.

The acceleration is modeled as a random walk, i.e., a white noise forcing function is used as process noise.

The equations are:

$$
\begin{aligned}
\dot{x} &= v_x \\
\dot{y} &= v_y \\
\dot{z} &= v_z \\
\dot{v}_x &= a_x \\
\dot{v}_y &= a_y \\
\dot{v}_z &= a_z \\
\dot{a}_y &= w_{a_x} \\
\dot{a}_y &= w_{a_y} \\
\dot{a}_z &= w_{a_z} \\
\dot{b} &= f + w_b \\
\dot{f} &= -f/\tau + w_f
\end{aligned}
\qquad (2)
$$

3.2.3 Turn Rate Dynamics: PVAT Filter

In this model, a constant turn rate is assumed, i.e.,

$$\dot{\underline{a}}(t) = -\omega^2 \underline{v}(t) + \underline{w}(t) \tag{3}$$

where $\underline{\omega}$ is the turn-rate, or

$$\underline{\omega} = \frac{\underline{v}(t) \times \underline{a}(t)}{\underline{v}(t)^2} \tag{4}$$

Note that $\underline{\omega}$ is not a constant, but rather a variable non-linear function of time.

Clearly, the use of this model will add a certain amount of computational burden and the discussion below trades off this burden against the improved accuracy over simpler models.

This model takes advantage of the assumption of coordinated turns where the acceleration vector is perpendicular to the instantaneous velocity vector. The model identifies such a situation and adjusts the acceleration state accordingly.

3.2.4 Discrete Formulation

The continuous formulation provided in the previous sections can be summarized as:

$$\dot{X} = FX + W \tag{5}$$

The equivalent discrete formulation is obtained by

$$X(k+1) = \phi(k)X(k) + W(k) \tag{6}$$

with

$$\phi(k) = L^{-1}(sI - F)^{-1} \tag{7}$$

where L^{-1} is the Inverse Laplace transform and

$$W(k) = \int_{t_k}^{t_k+1} \phi(t_{k+1}, \tau)\, W(\tau)\, d\tau \tag{8}$$

These calculations were performed for the three models described previously and are included in Appendix A, along with the discrete noise covariance matrix,

$$Q(k) = \int_{t_k}^{t_k+1} \phi(t_{k+1}, \tau)\, N(\tau)\, \phi^T(t_{k+1}, \tau)\, d\tau \tag{9}$$

Note that all matrices are constant, except for the turning dynamics model, where they are functions of time (through the turning rate ω).

3.2.5 Simulations

Simulations were performed using the DIFFGPS program to assess performance for the various models during both conventional and differential GPS operation and for several levels of dynamics.

Although the object of the study is vertical accuracy enhancement, the performance of the various filters was initially assessed using a level Constant Acceleration Turn type pattern. It was felt that accelerations were experienced in all axes, so that improvements laterally would imply similar improvements in the vertical axis. Performance in the vertical axis is described in later sections where an actual descending glidepath profile is simulated. The path is plotted in Figure 3-2.

The Constant Acceleration Turn profile selected for the simulations consisted of:

a. a straight, level, constant velocity segment at 1000 ft altitude, 100 knots, and -80 degrees bearing (duration: 29 seconds);

b. a level turn, constant velocity segment at 1000 ft altitude, 100 knots to a bearing of +10 degrees (duration: 11 seconds);

c. a straight, level, constant velocity segment at 1000 ft altitude, 100 knots, and +10 degrees bearing (duration: 22 seconds);

d. a straight, level, accelerating segment at 1000 ft altitude, +10 degrees bearing, and final velocity of 155 knots (duration: 9 seconds);

e. a straight, level, constant velocity segment at 1000 ft altitude, 155 knots, and +10 degrees bearing (duration: 23 seconds).

3.2.5.1 PV Filter

The PV filter performance is presented in Figures 3-3 and 3-4 for this type of process noise matrices.

The baseline Z-Set model used a diagonal process noise matrix, ignoring cross terms. While this formulation is technically incorrect, it will not necessarily result in poorer performance due to the reduced order state vector, non-linearities, and measurement characteristics. In particular, Eller [4] pointed out in his study that the high precision of the deltarange measurements compared with pseudorange measurements (factor of 100 or 200-to-1) encourages decoupling of the position states form velocity (and acceleration, if modeled) states in the process noise matrix.

In Figure 3-3, a diagonal process noise matrix is used, while in Figure 3-4, the full process noise matrix is used.

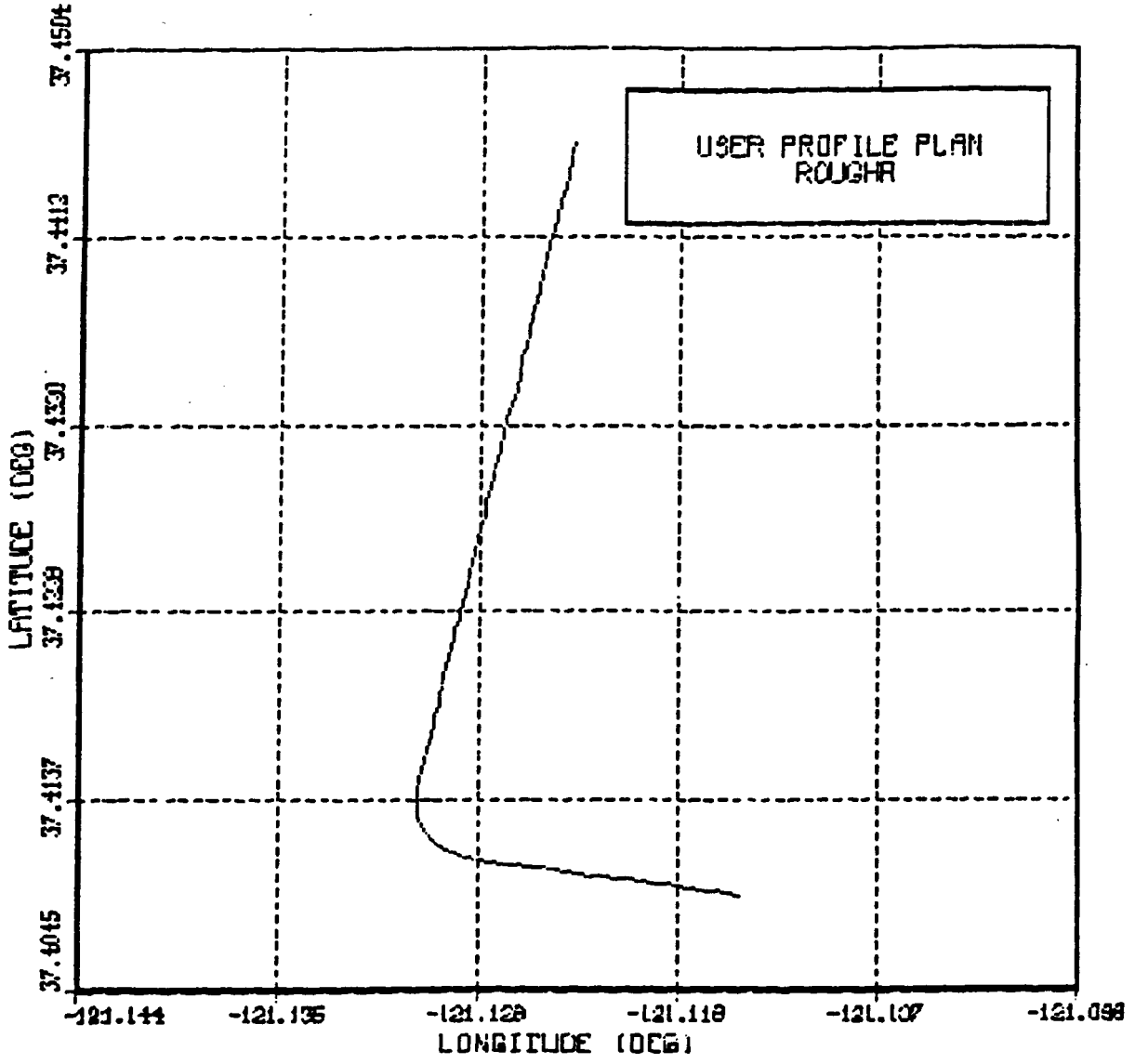

Figure 3-2. Constant Acceleration Turn Flight Profile

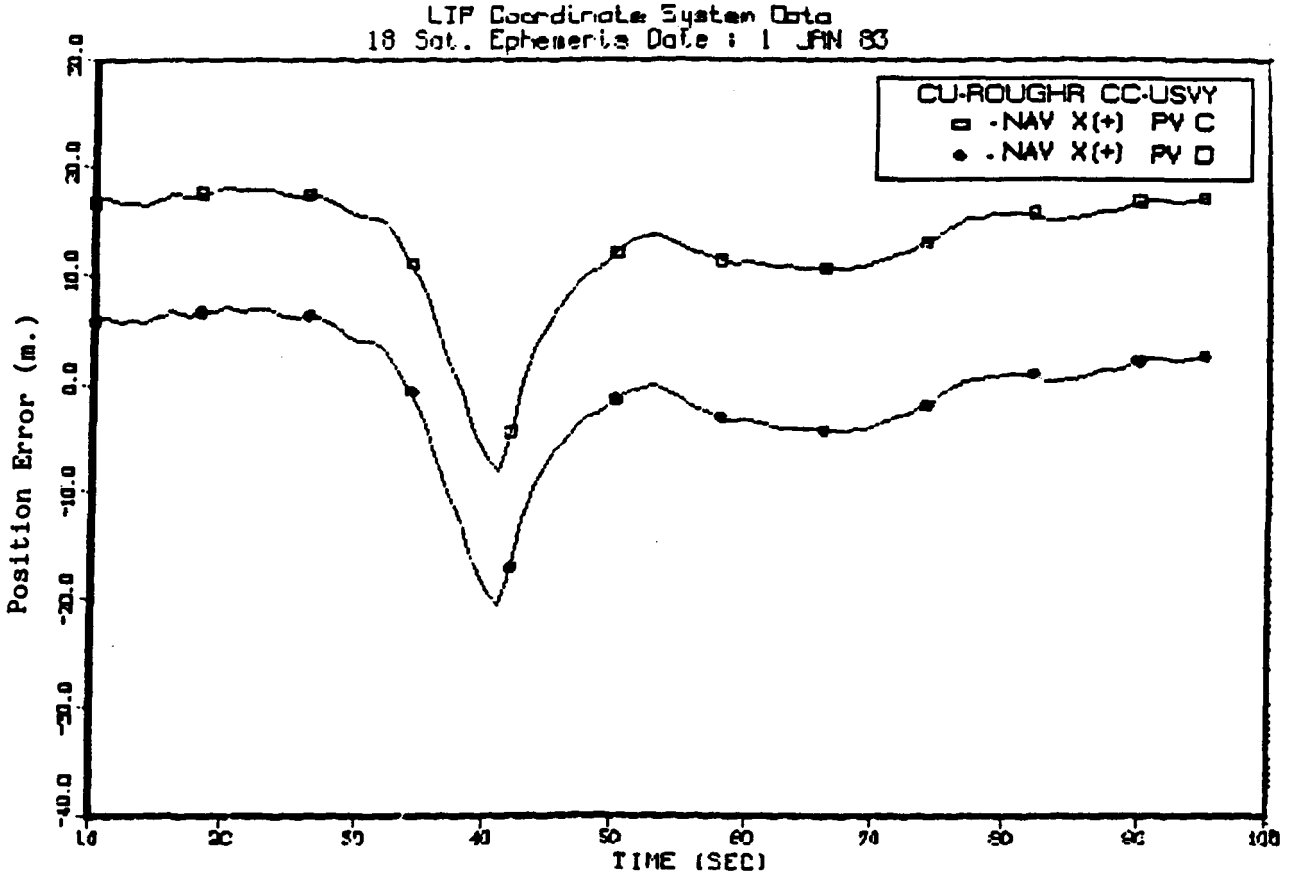

For acronym definition refer to glossary on page vi.

Figure 3-3a. PV Filter Performance, X-Axis Diagonal Q-Matrix

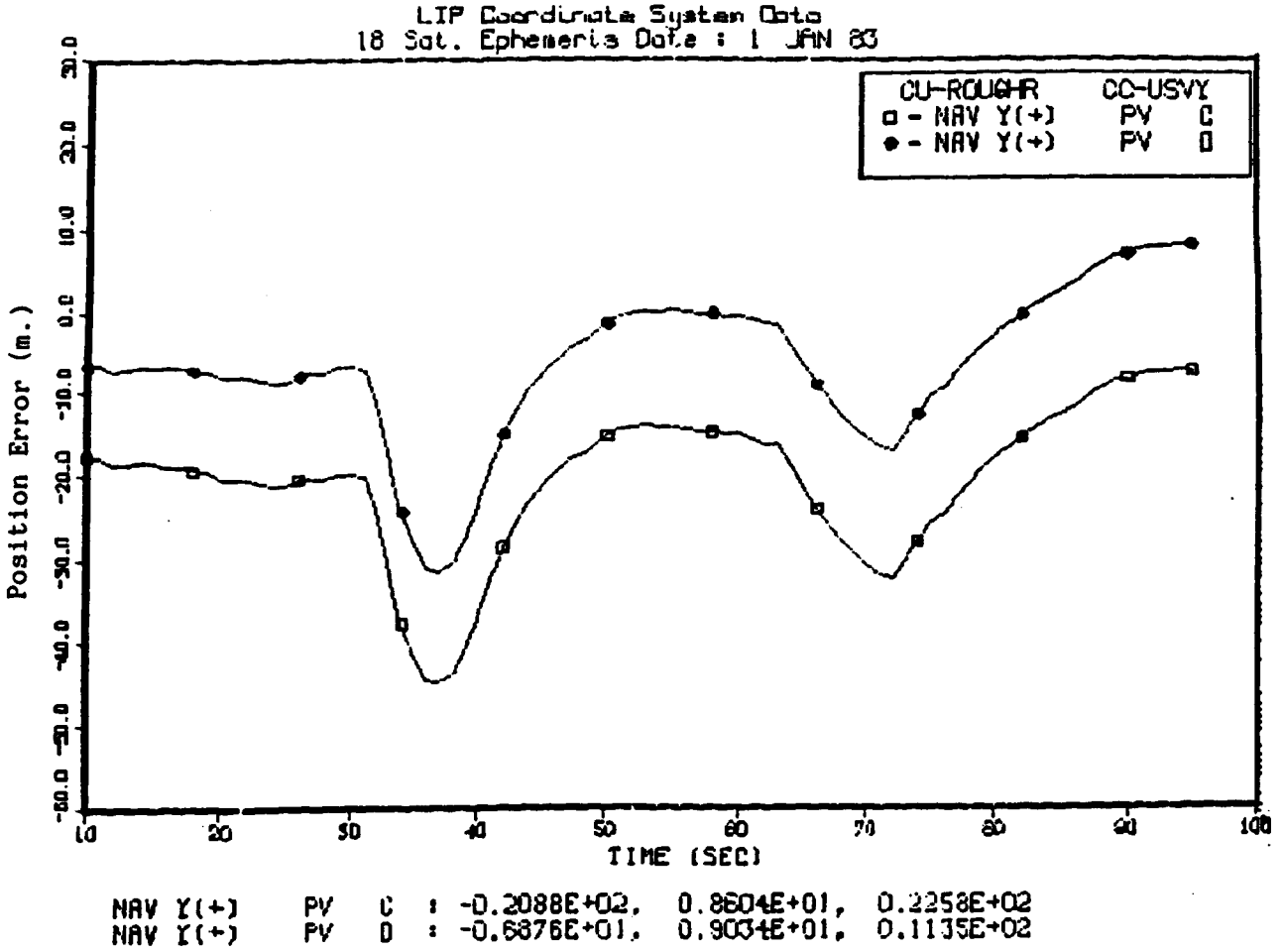

For acronym definition refer to glossary on page vi.

Figure 3-3b. PV Filter Performance, Y-Axis Diagonal Q-Matrix

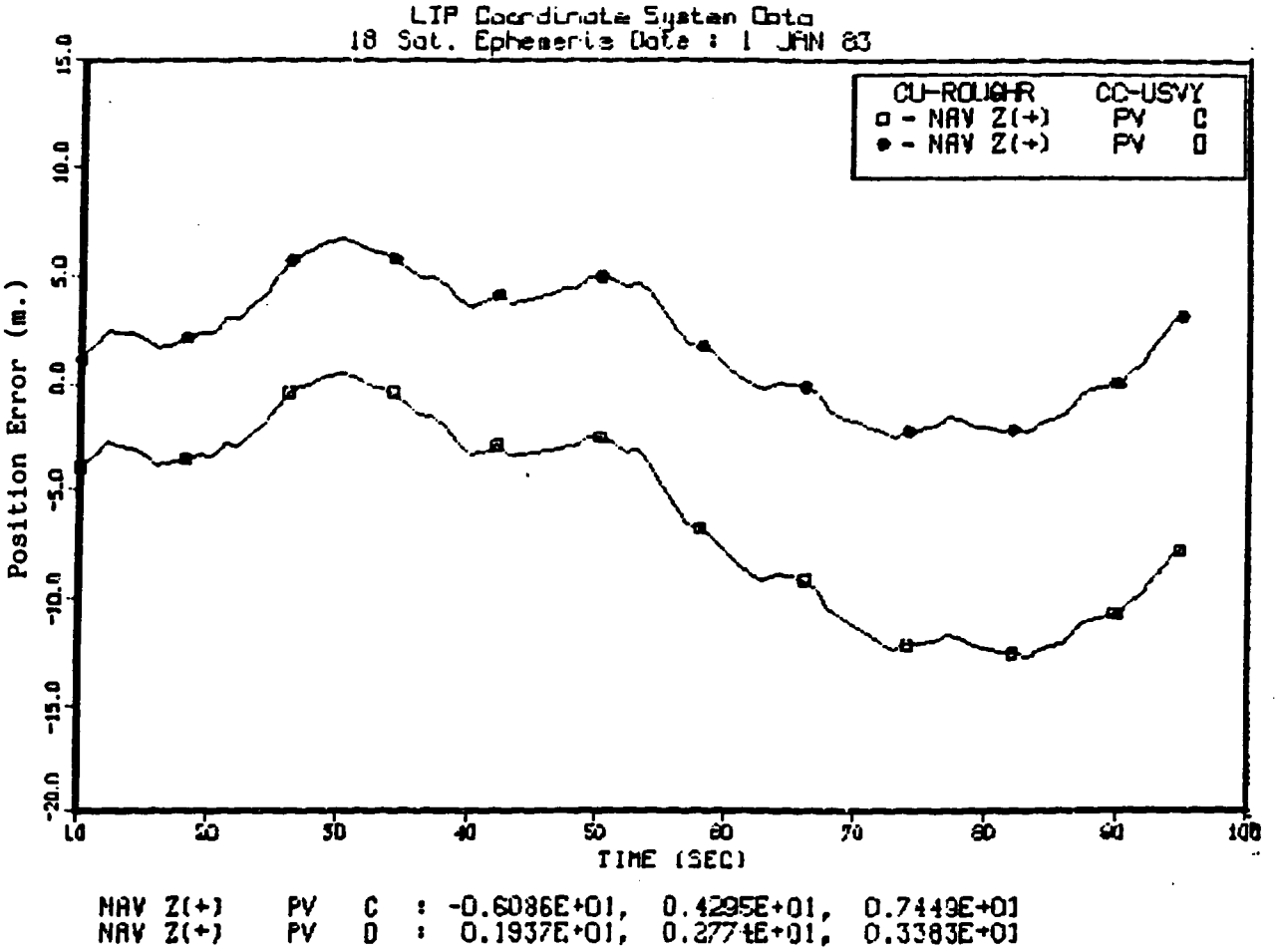

NAV Z(+) PV C : -0.6086E+01, 0.4295E+01, 0.7449E+01
NAV Z(+) PV D : 0.1937E+01, 0.2774E+01, 0.3383E+01

For acronym definition refer to glossary on page vi.

Figure 3-3c. PV Filter Performance, Z-Axis Diagonal Q-Matrix

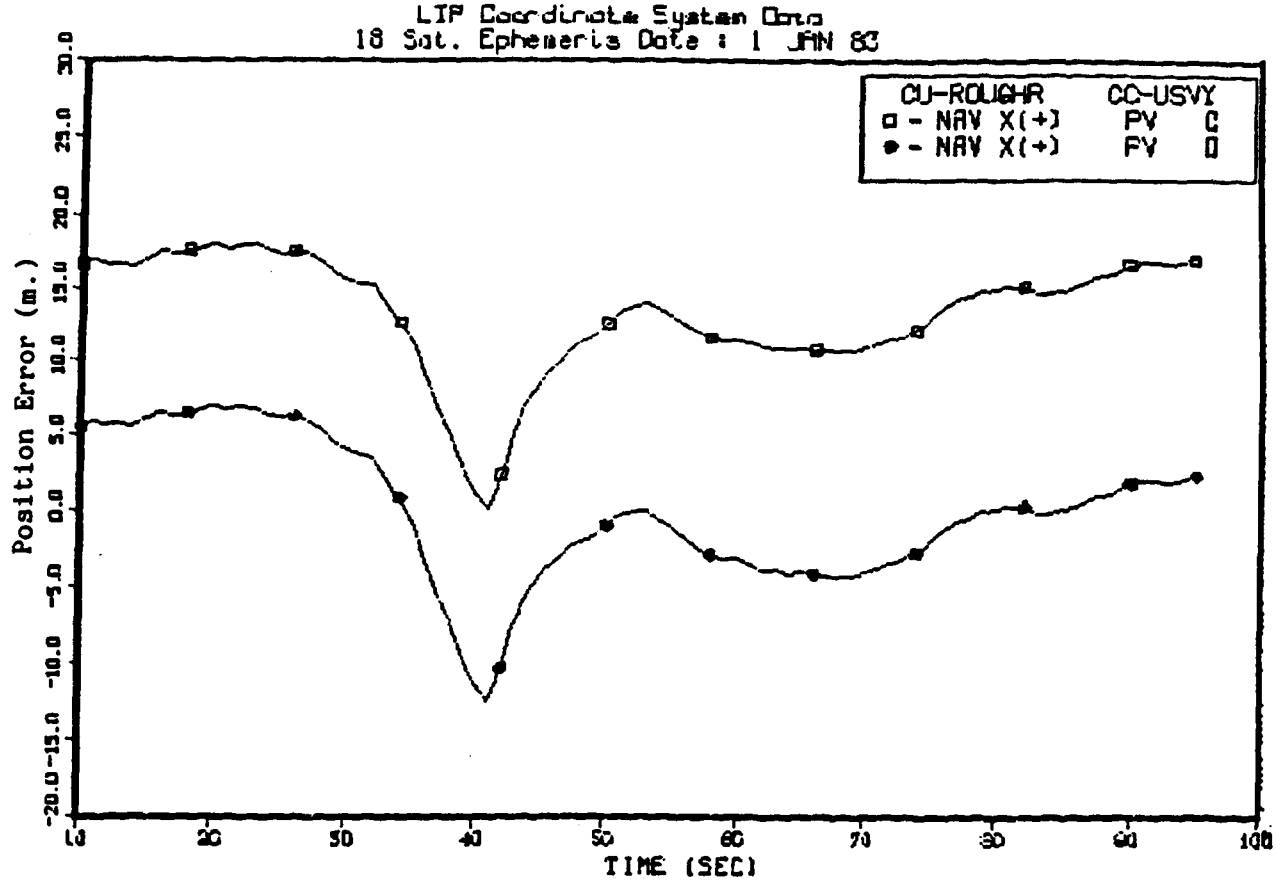

For acronym definition refer to glossary on page vi.

Figure 3-4a. PV Filter Performance, X-Axis Full Q-Matrix

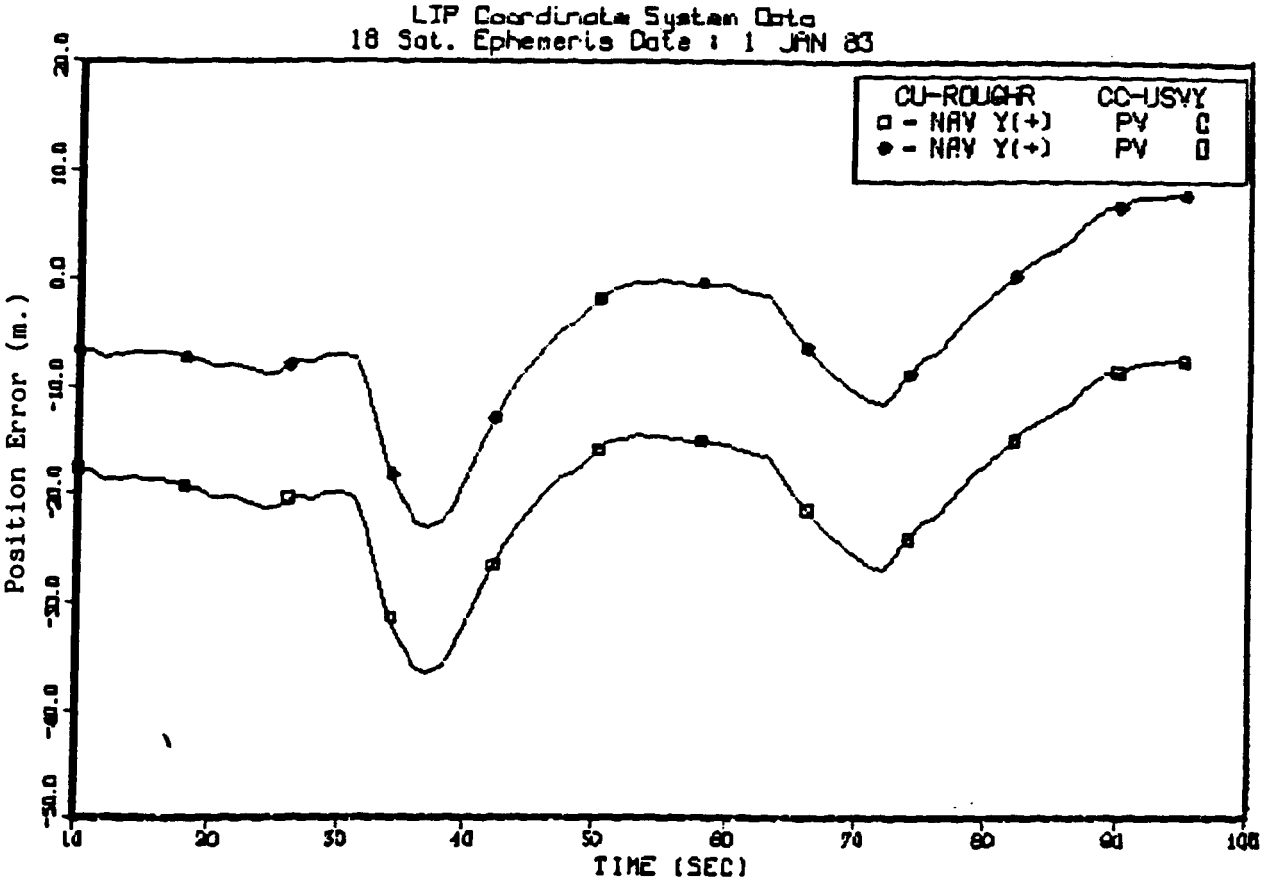

For acronym definition refer to glossary on page vi.

Figure 3-4b. PV Filter Performance, Y-Axis Full Q-Matrix

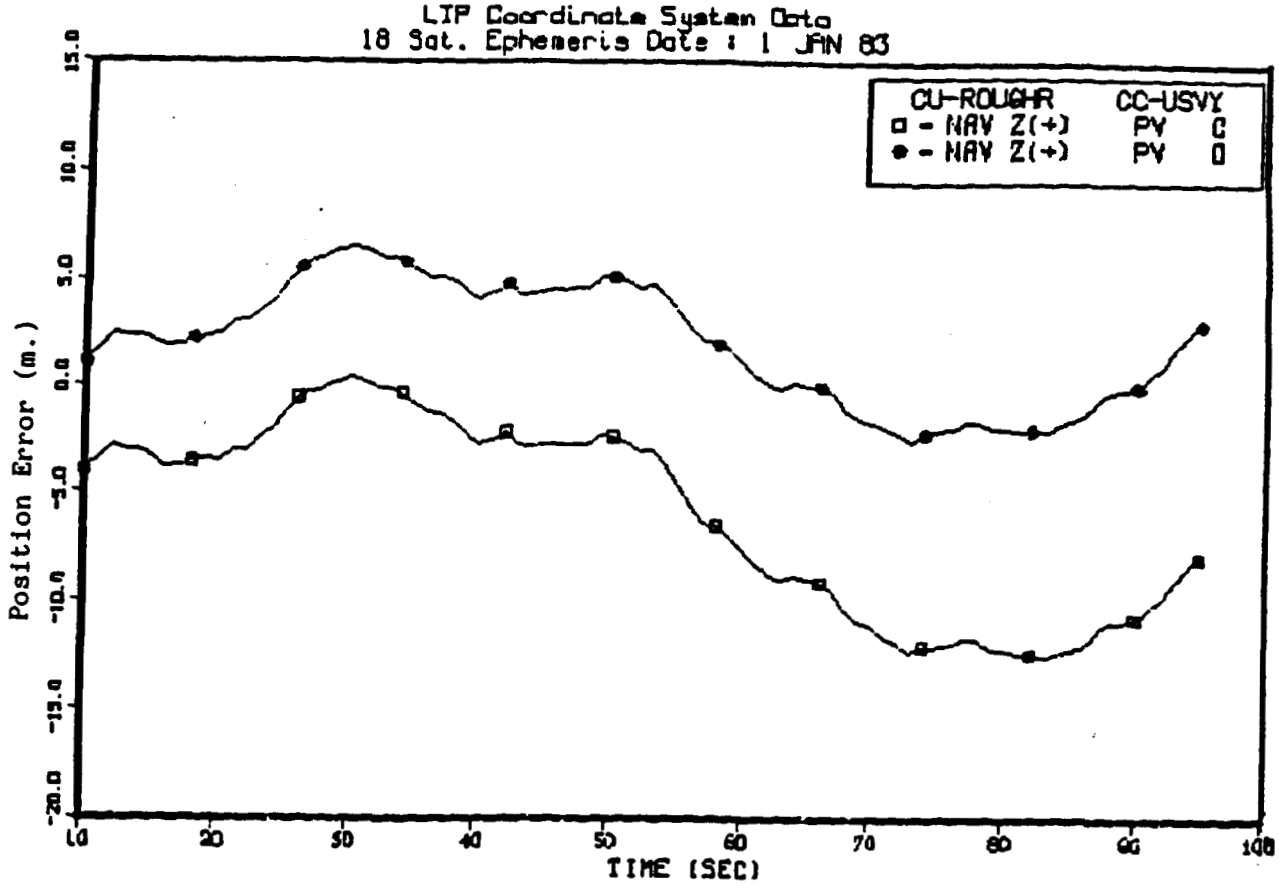

NAV Z(+) PV C : -0.5991E+01, 0.4289E+01, 0.7368E+01
NAV Z(+) PV D : 0.2011E+01, 0.2792E+01, 0.3442E+01

For acronym definition refer to glossary on page vi.

Figure 3-4c. PV Filter Performance, Z-Axis Full Q-Matrix

A comparison between the two cases indicates little difference over the entire path in both the conventional and differential modes. RMS and Standard deviations are listed in Table 3-2 for all three axes.

Table 3-1. PV Filter Performance (Meters), Constant Acceleration Turn Pattern

		FULL Q MATRIX		DIAGONAL Q MATRIX	
VALUES IN METERS		RMS	STANDARD DEVIATION	RMS	STANDARD DEVIATION
CONVENTIONAL GPS	x	13.8	4.0	13.8	5.7
	y	30.6	8.5	22.5	8.8
	z	7.3	4.3	7.4	4.3
DIFFERENTIAL GPS	x	4.5	4.5	6.0	5.3
	y	9.0	7.1	11.3	2.0
	z	3.4	2.8	3.3	2.8

The table shows that the differences between the two filters are not large and that they are not favoring one over the other. This is true for both the conventional and differential modes. During the filter tuning, it became clear, however, that one had to be very careful in the case of the full Q matrix since the presence of the off-diagonal terms could lead to an ill-defined Q matrix (i.e., non-positive definite). The data presented in Table 3-1 is for the full Constant Acceleration Turn pattern. Table 3-2 presents the data if only the turn segment is considered and, therefore, shows better how each filter tracks during the higher dynamics. Here, too, differences are not clearly in favor of one model or the other, although the standard deviations are generally smaller for the full Q matrix filter. Overall, though, conclusions are difficult to draw with the PV filter as to the advisability to use a full or diagonal Q matrix.

Table 3-2. PV Filter Performance, Turning Segment of Constant Acceleration Turn Pattern

VALUES IN METERS		FULL Q MATRIX RMS	FULL Q MATRIX STANDARD DEVIATION	DIAGONAL Q MATRIX RMS	DIAGONAL Q MATRIX STANDARD DEVIATION
CONVENTIONAL GPS	x	10.1	4.6	9.3	7.2
	y	26.8	6.8	30.6	10.1
	z	2.1	1.1	2.4	1.3
DIFFERENTIAL GPS	x	5.9	4.8	9.6	7.3
	y	14.3	6.9	18.5	10.2
	z	5.1	0.7	4.2	2.5

3.2.5.2 PVAC Filter

Figure 3-5 presents the PVAC filter performance for the Constant Acceleration Turn pattern and using a full process noise matrix. In Figure 3-6, the performance is presented for the diagonal process noise matrix where the position states are decoupled from the velocity and acceleration states, leaving cross terms between velocity and acceleration only. Table 3-3 shows the RMS and standard deviations for all axes and for both the conventional and differential modes. As for the PV filter, the performance for both filters are not significantly different. Table 3-4 shows the performance during the turning segment only, and, here too, the differences are minor and do not advantage one implementation over the other.

Table 3-3. PVAC Filter Performance (Meters), Constant Acceleration Turn Pattern

		FULL Q MATRIX RMS	FULL Q MATRIX STANDARD DEVIATION	DIAGONAL Q MATRIX RMS	DIAGONAL Q MATRIX STANDARD DEVIATION
CONVENTIONAL GPS	x	14.3	2.8	14.6	2.5
	y	17.8	4.8	17.6	5.2
	z	7.2	4.4	7.5	4.5
DIFFERENTIAL GPS	x	3.8	3.7	3.8	3.7
	y	6.3	5.3	6.6	6.1
	z	3.5	2.9	3.7	3.0

Table 3-4. PVAC Filter Performance (Meters), Turning Segment of Constant Acceleration Turn Pattern

		FULL Q MATRIX		DIAGONAL Q MATRIX	
		RMS	STANDARD DEVIATION	RMS	STANDARD DEVIATION
CONVENTIONAL GPS	x	15.2	2.3	9.2	4.6
	y	22.7	2.7	26.4	2.8
	z	1.7	1.4	3.0	0.15
DIFFERENTIAL GPS	x	4.3	2.8	6.1	4.8
	y	9.8	2.7	14.1	2.8
	z	5.5	1.3	4.9	0.16

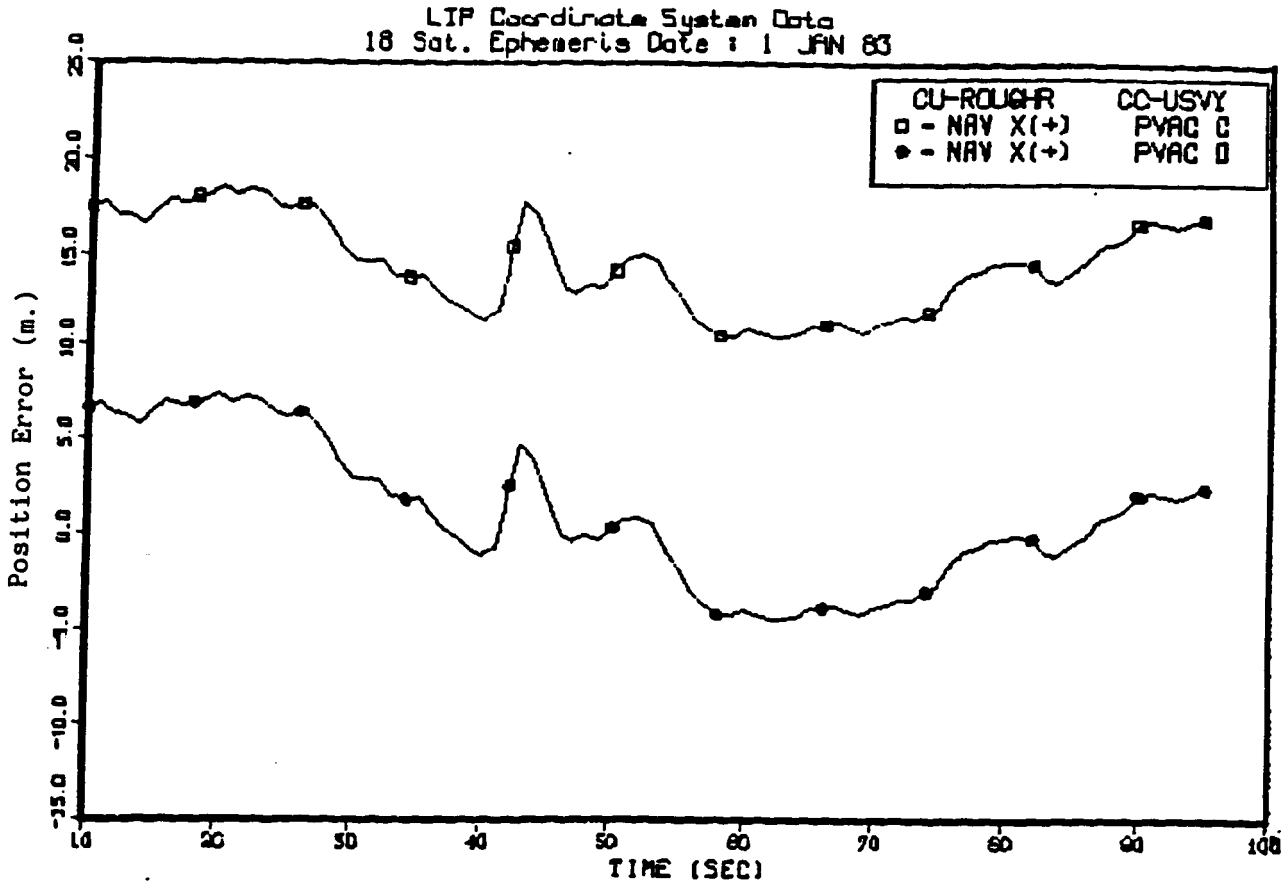

NAV X(+) PVAC C : 0.1438E+02, 0.2460E+01, 0.1459E+02
NAV X(+) PVAC D : 0.9649E+00, 0.3696E+01, 0.3820E+01

For acronym definition refer to glossary on page vi.

Figure 3-5a. PVAC Filter Performance, X-Axis Full Q-Matrix

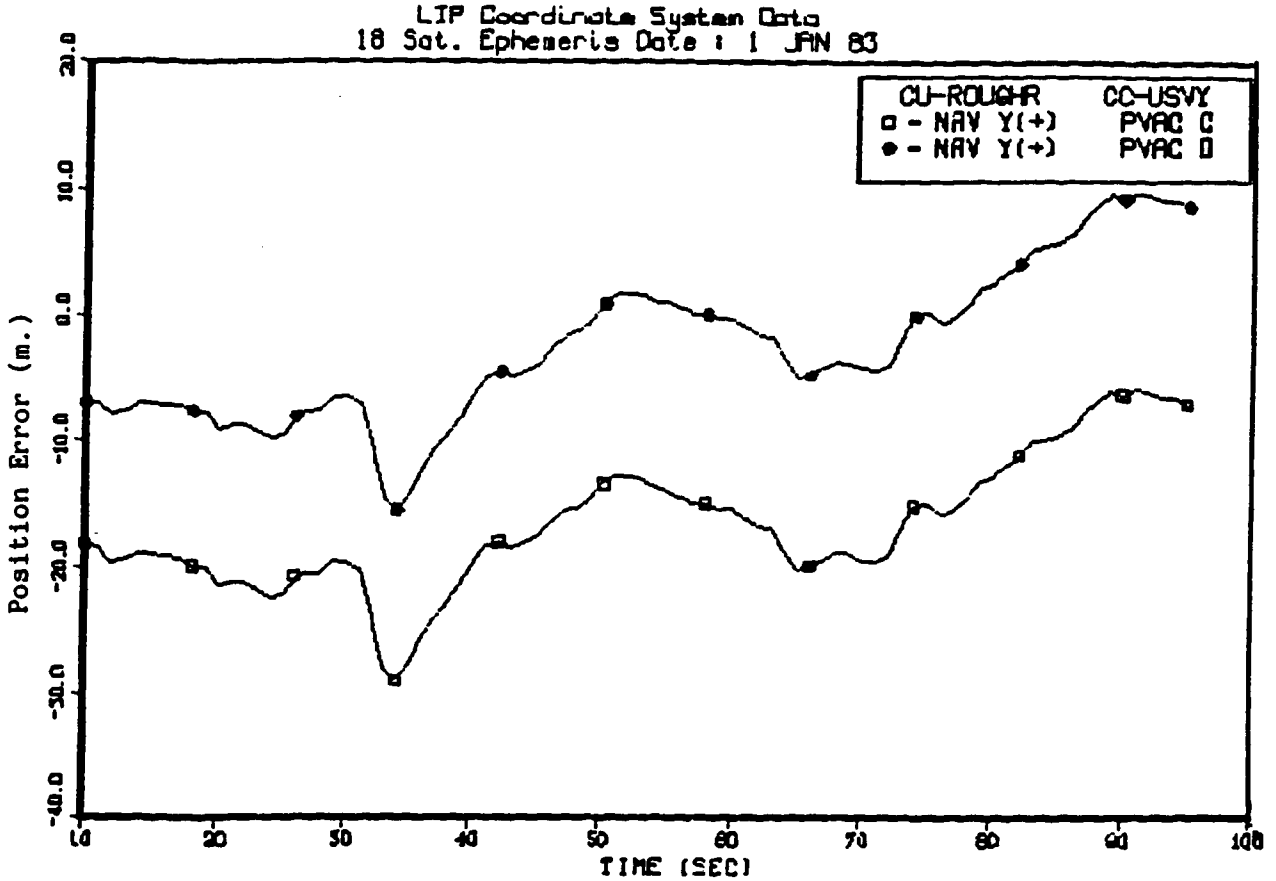

For acronym definition refer to glossary on page vi.

Figure 3-5b. PVAC Filter Performance, Y-Axis Full Q-Matrix

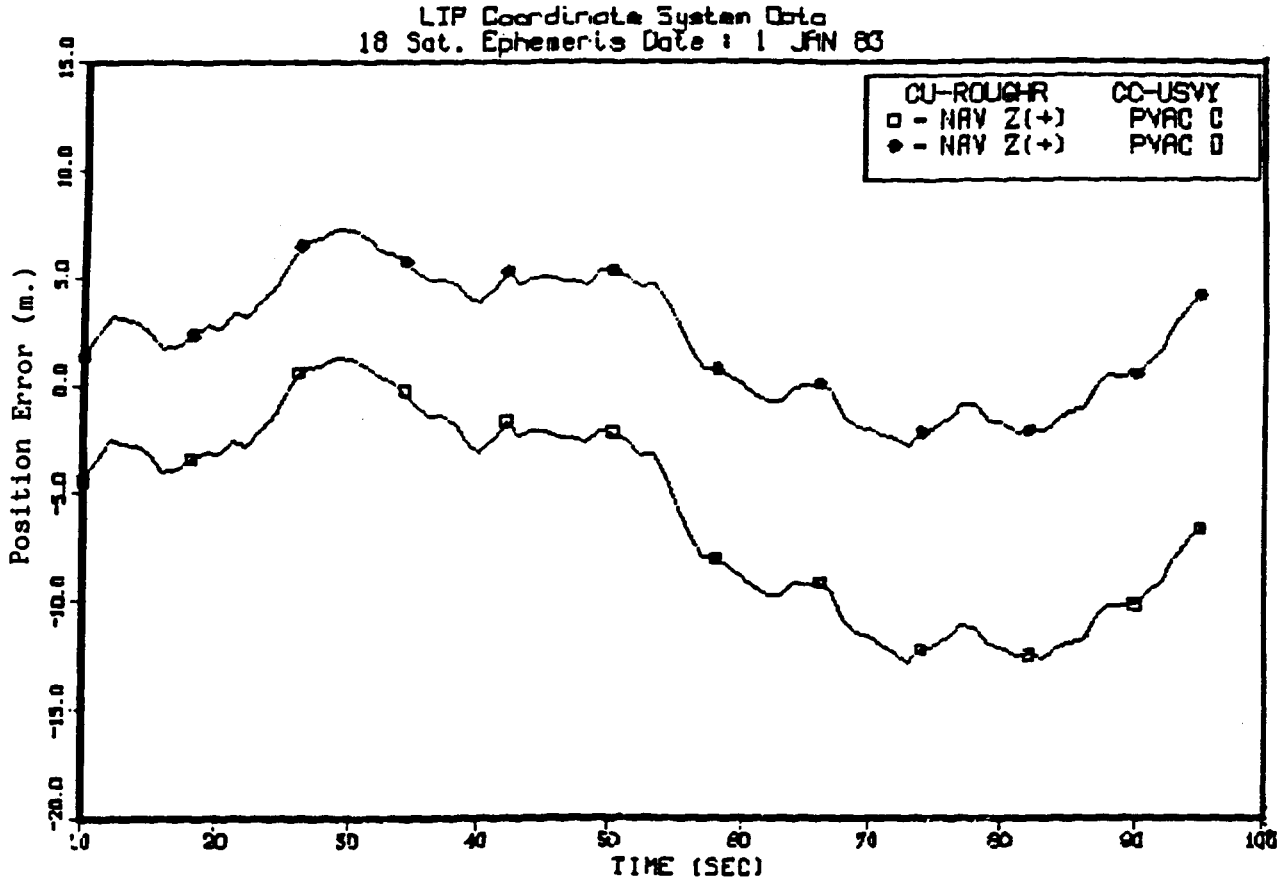

NAV Z(+) PVAC C : -0.5963E+01, 0.4499E+01, 0.7469E+01
NAV Z(+) PVAC D : 0.2140E+01, 0.2972E+01, 0.3662E+01

For acronym definition refer to glossary on page vi.

Figure 3-5c. PVAC Filter Performance, Z-Axis Full Q-Matrix

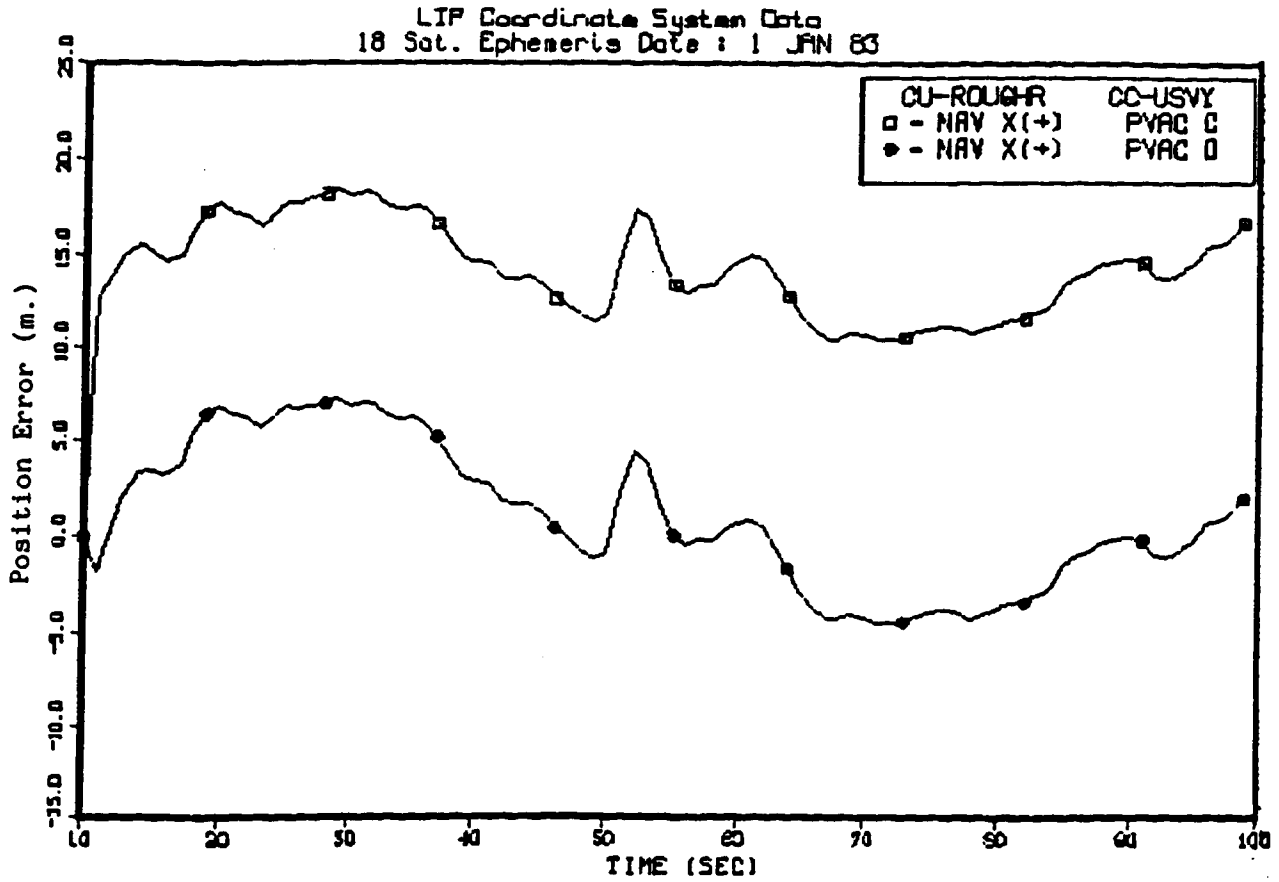

NAV X(+) PVAC C : 0.1411E+02, 0.2778E+01, 0.1438E+02
NAV X(+) PVAC D : 0.1042E+01, 0.3672E+01, 0.3817E+01

For acronym definition refer to glossary on page vi.

Figure 3-6a. PVAC Filter Performance, X-Axis Diagonal Q-Matrix

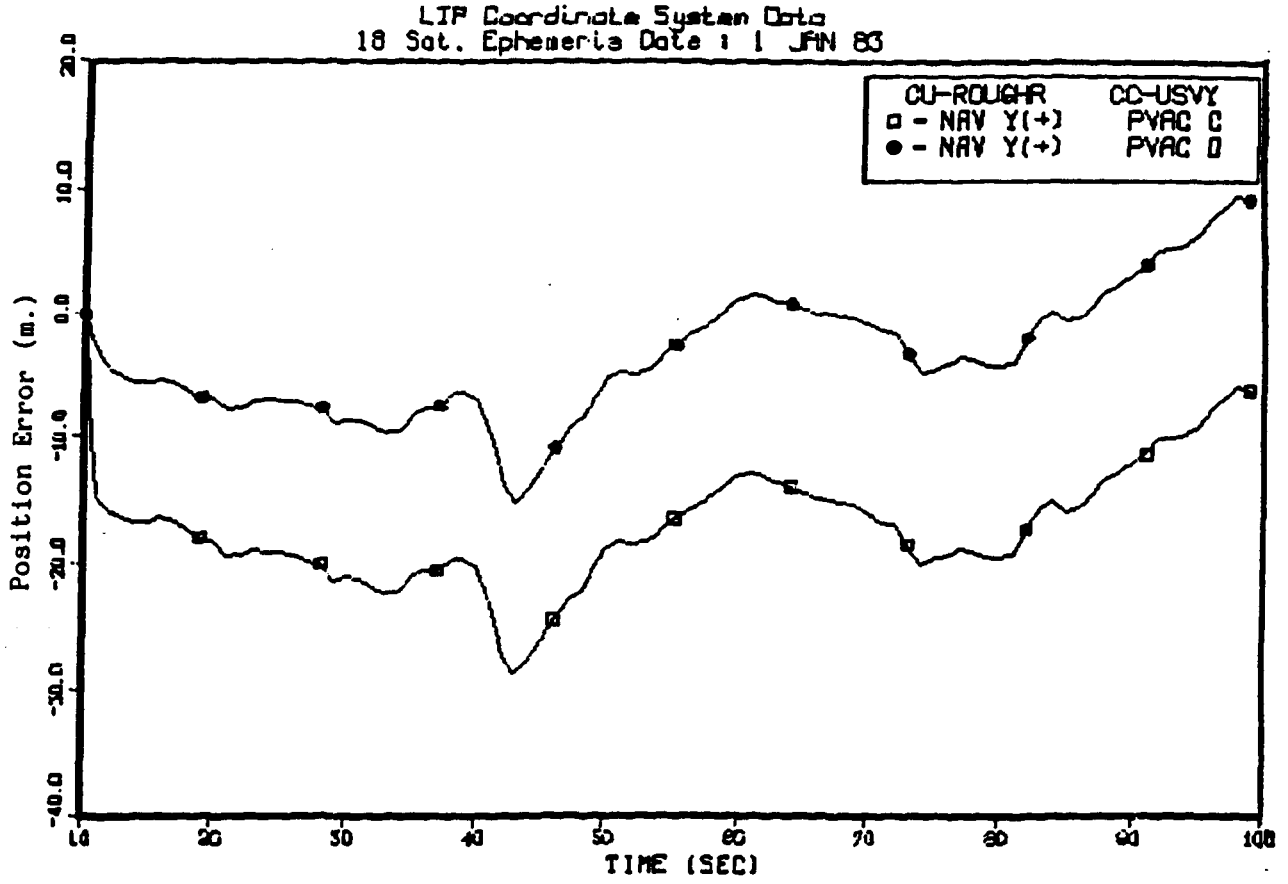

NAV Y(+)	PVAC C	:	-0.1716E+02,	0.4768E+01, 0.1781E+02
NAV Y(+)	PVAC D	:	-0.3489E+01,	0.5252E+01, 0.6305E+01

For acronym definition refer to glossary on page vi.

Figure 3-6b. PVAC Filter Performance, Y-Axis Diagonal Q-Matrix

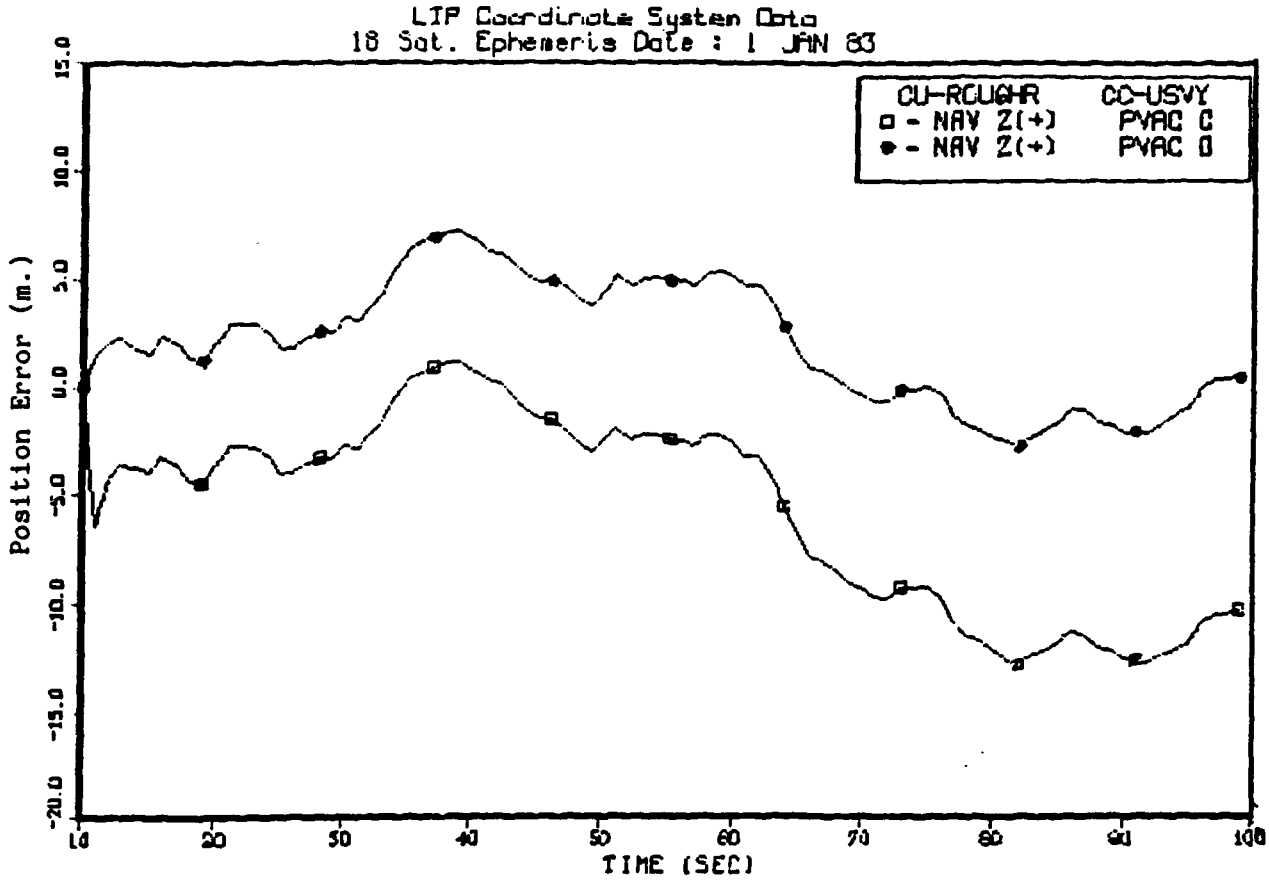

NAV Z(+) PVAC C : -0.5650E+01, 0.4396E+01, 0.7159E+01
NAV Z(+) PVAC D : 0.2067E+01, 0.2868E+01, 0.3535E+01

For acronym definition refer to glossary on page vi.

Figure 3-6c. PVAC Filter Performance, Z-Axis Diagonal Q-Matrix

Comparing the PVAC filter performance with the PV filter performance, based on the full Constant Acceleration Turn pattern, performance is usually slightly better for the PVAC filter, although the impact of any major improvement achieved during the turning segment would be somewhat reduced due to the averaging with the straight segments. Comparisons of the turning segments alone (Tables 3-2 and 3-4) show a clear advantage (factor two or three) in favor of the PVAC filter for the standard deviation. This is not as clear for the RMS values, however. This can be explained by realizing that during periods of poor tracking by the filter, the errors can actually grow in a way to reduce the absolute value of the mean over the path and therefore reduce the RMS, providing therefore a false indication of improved performance. The standard deviation, however, indicates the fluctuations in the error and is a better indication of the filter performance.

3.2.5.3 PVAT Filter

As was mentioned in Section 3.2.3, the turn rate is a function of time. Since the process noise matrix is a function of the turn rate, it, too, is therefore a function of time. Performance was evaluated using both a time variable and a constant process noise matrix. The diagonal noise matrix was used, i.e., the position states are decoupled from both the velocity and acceleration states, learning cross terms between velocity and acceleration only. Figure 3-7 shows the performance for the Constant Acceleration Turn pattern with the variable process noise matrix. Performance with the constant process noise matrix is presented in Figure 3-8.

In Table 3-5, the RMS and standard deviation of the errors are provided for all axes and for both the conventional and differential modes. clearly, the effects of the variable Q matrix are insignificant in the filter performance. Table 3-6 shows the performance with both the constant and variable Q matrices during the turning segments of the Constant Acceleration Turn pattern. Here, too, the effects are very small. Time variable process noise matrices are therefore not necessary and certainly not worth the additional processing load.

Table 3-5. PVAT Filter Performance (Meters), Constant Acceleration Turn Pattern

Diagonal Q Matrix

		VARIABLE Q MATRIX		CONSTANT Q MATRIX	
		RMS	STANDARD DEVIATION	RMS	STANDARD DEVIATION
CONVENTIONAL GPS	x	14.5	2.4	14.5	2.5
	y	17.5	5.0	17.4	5.2
	z	7.5	4.5	7.5	4.5
DIFFERENTIAL GPS	x	3.8	3.7	3.8	3.7
	y	6.6	6.1	6.5	6.0
	z	3.7	2.4	3.6	2.3

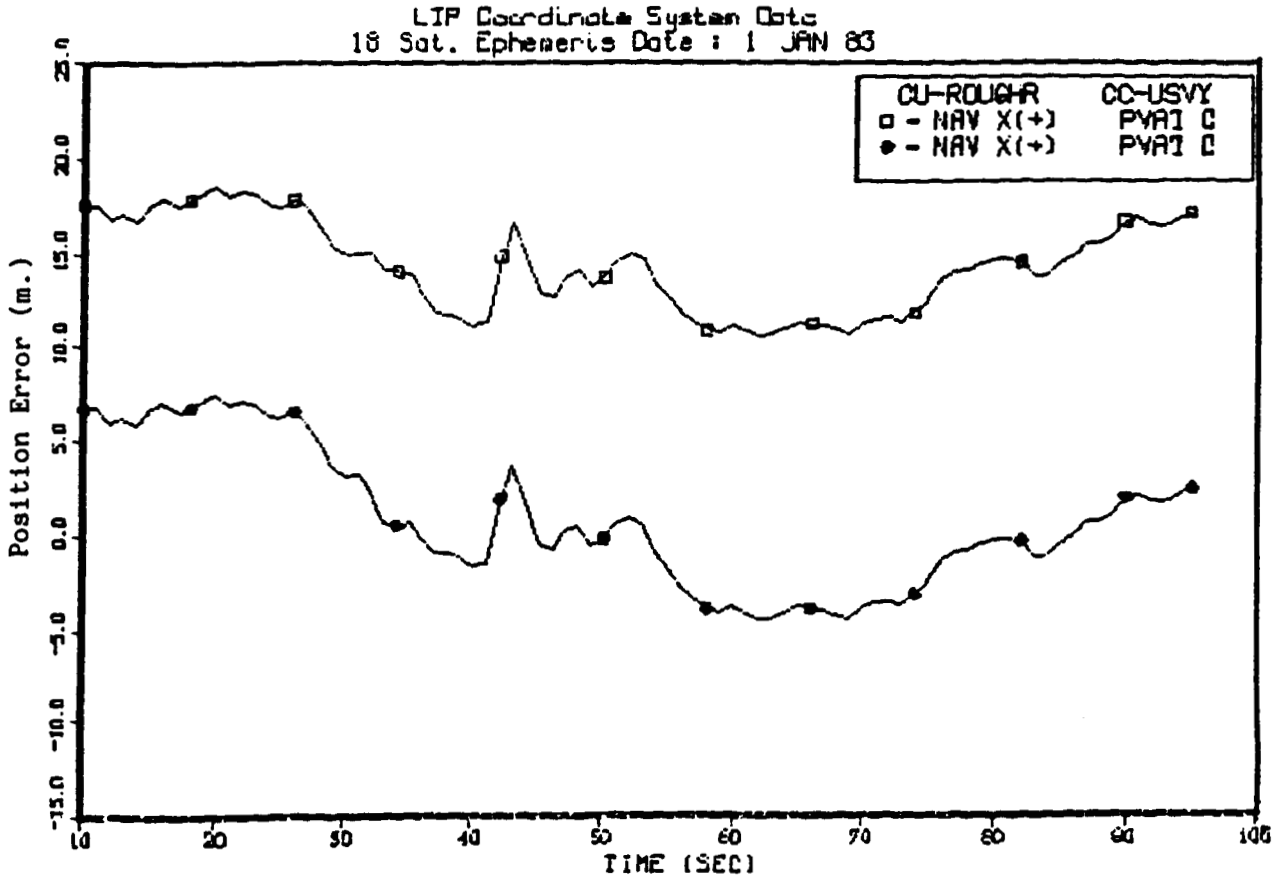

NAV X(+) PVAT C : 0.1428E+02, 0.2441E+01, 0.1449E+02
NAV X(+) PVAT D : 0.7962E+00, 0.3664E+01, 0.3750E+01

For acronym definition refer to glossary on page vi.

Figure 3-7a. PVAT Filter Performance, X-Axis Diagonal Q-Matrix

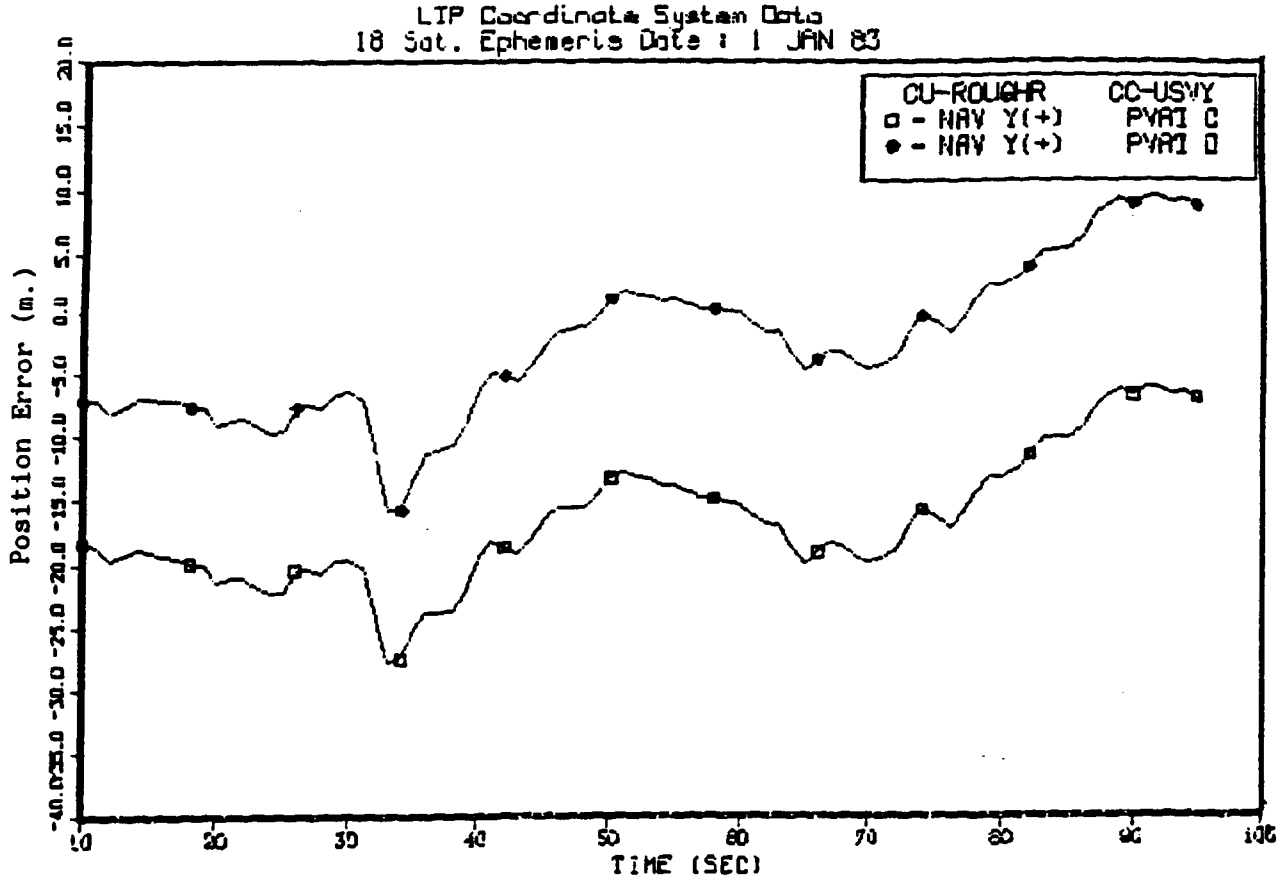

NAV Y(+) PVAT C : -0.1675E+02, 0.5017E+01, 0.1748E+02
NAV Y(+) PVAT D : -0.2676E+01, 0.6079E+01, 0.6642E+01

For acronym definition refer to glossary on page vi.

Figure 3-7b. PVAT Filter Performance, Y-Axis Diagonal Q-Matrix

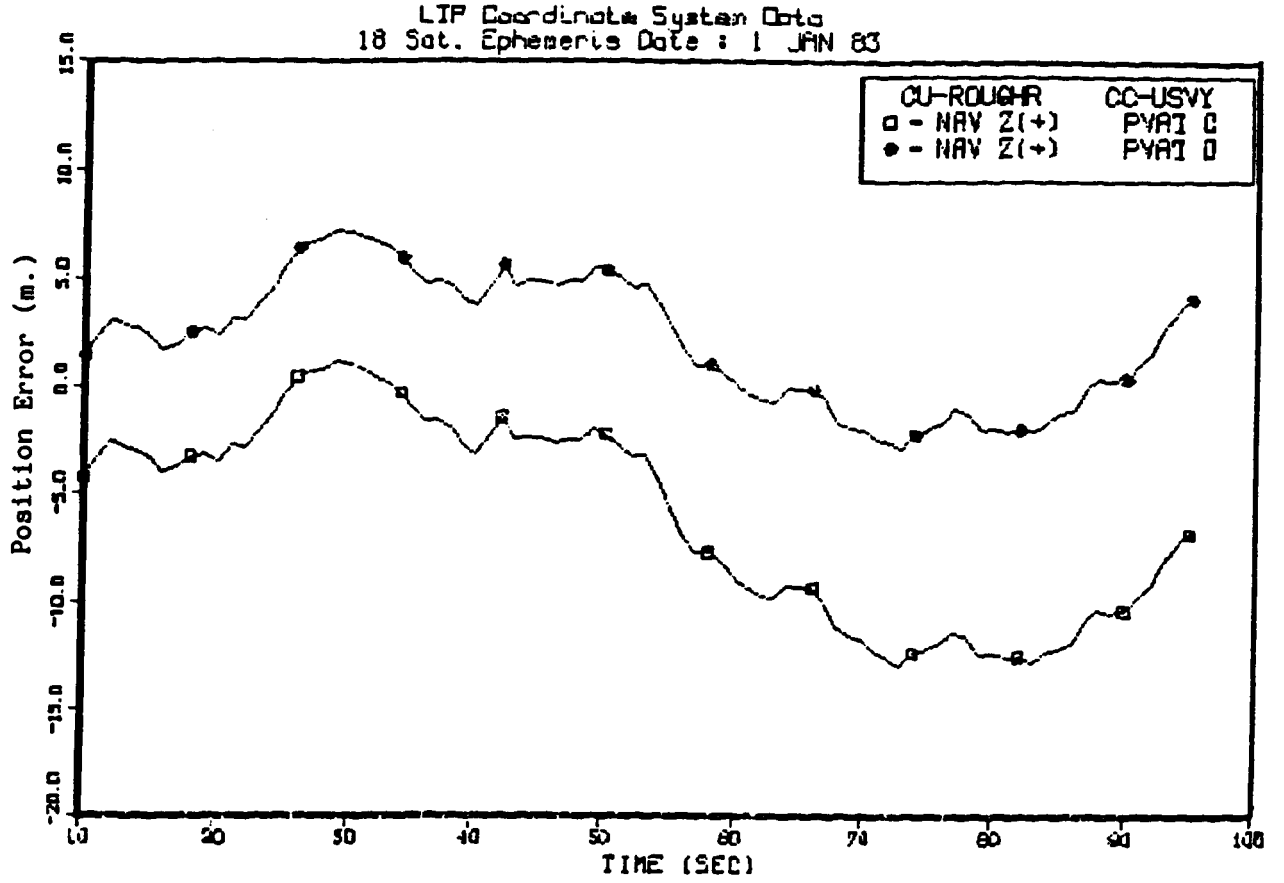

NAV Z(+) PVAT C : -0.5996E+01, 0.1483E+01, 0.7487E+01
NAV Z(+) PVAT D : 0.2144E+01, 0.2991E+01, 0.3680E+01

For acronym definition refer to glossary on page vi.

Figure 3-7c. PVAT Filter Performance, Z-Axis Diagonal Q-Matrix

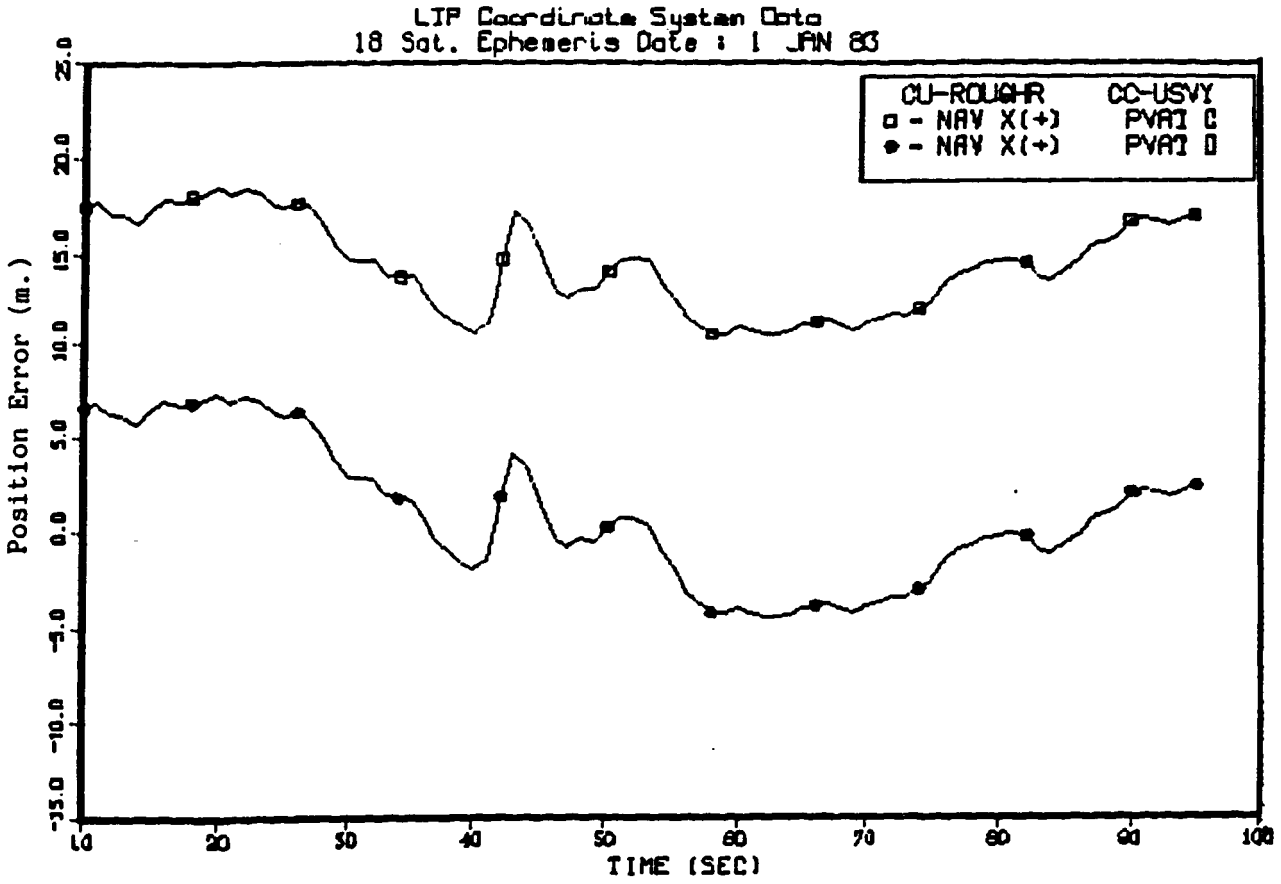

NAV X(+) PVAT C : 0.1429E+02, 0.2501E+01, 0.1451E+02
NAV X(+) PVAT D : 0.8710E+00, 0.3711E+01, 0.3812E+01

For acronym definition refer to glossary on page vi.

Figure 3-8a. PVAT Filter Performance, X-Axis Constant Diagonal Q-Matrix

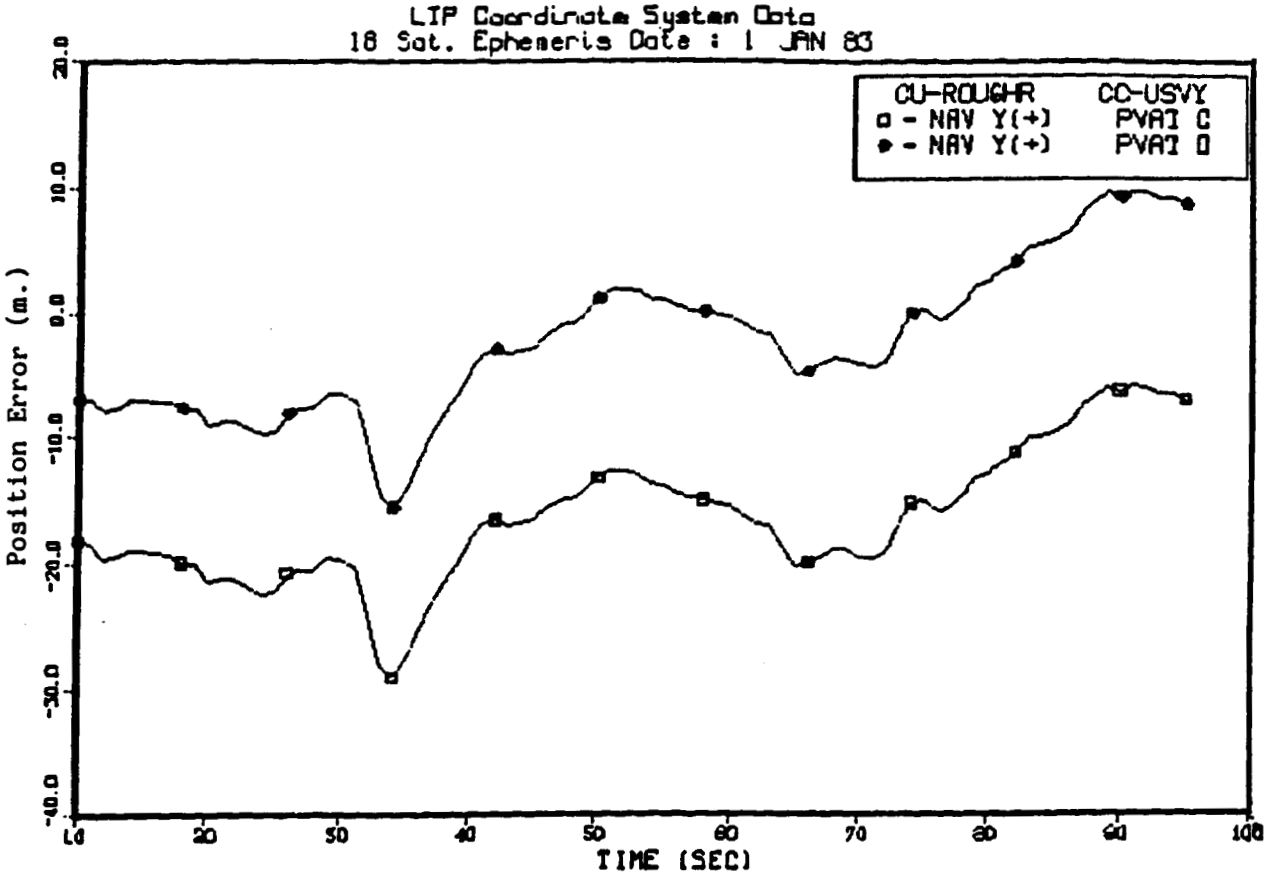

NAV Y(+) PVAT C : -0.1657E+02, 0.5156E+01, 0.1735E+02
NAV Y(+) PVAT D : -0.2369E+01, 0.6045E+01, 0.6493E+01

For acronym definition refer to glossary on page vi.

Figure 3-8b. PVAT Filter Performance, Y-Axis Constant Diagonal Q-Matrix

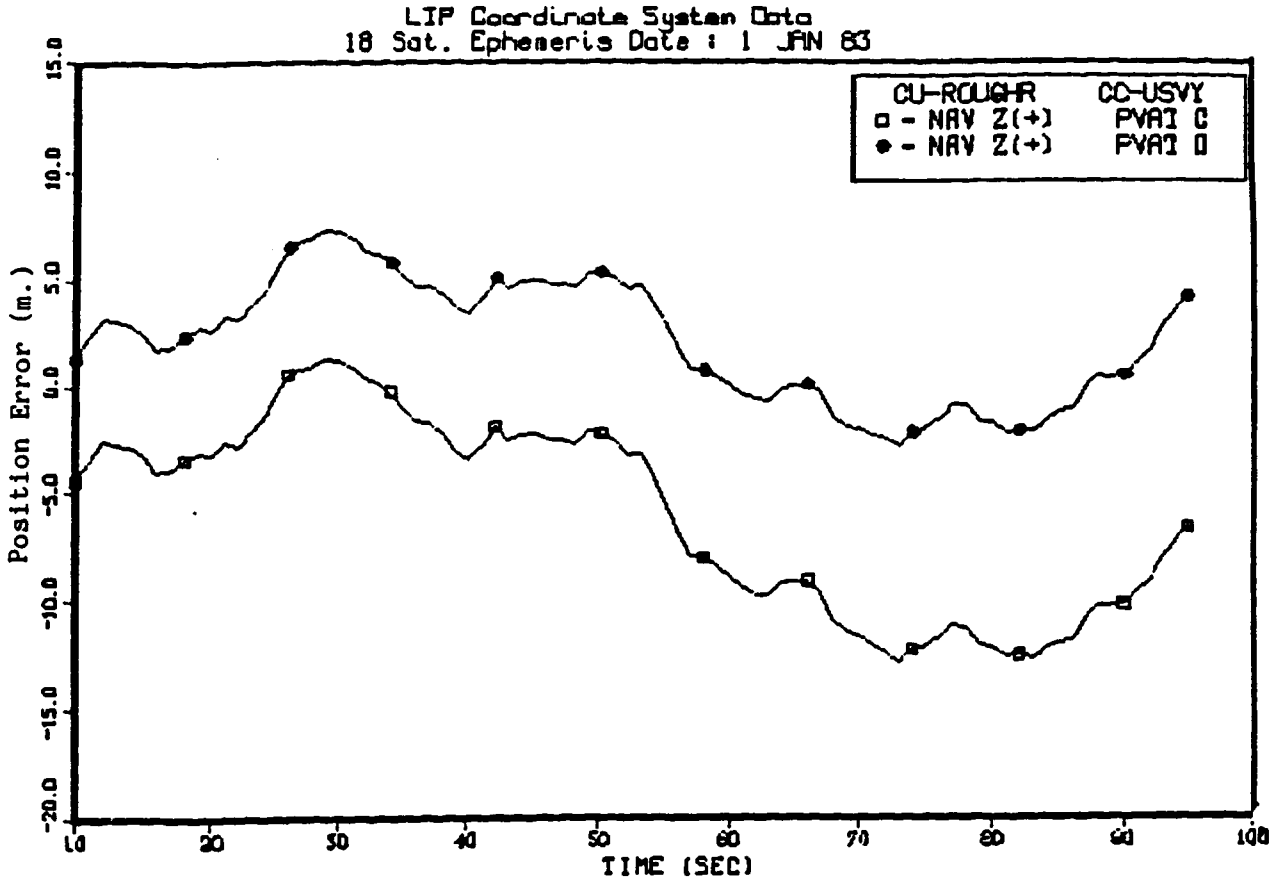

NAV Z(+) PVAT C : -0.5992E+01, 0.4471E+01, 0.7476E+01
NAV Z(+) PVAT D : 0.2111E+01, 0.2943E+01, 0.3622E+01

For acronym definition refer to glossary on page vi.

Figure 3-8c. PVAT Filter Performance, Z-Axis Constant Diagonal Q-Matrix

Table 3-6. PVAT Filter Performance (Meters), Turning Segment of Constant Acceleration Turn Pattern

		Diagonal Q Matrix			
		VARIABLE Q MATRIX		CONSTANT Q MATRIX	
		RMS	STANDARD DEVIATION	RMS	STANDARD DEVIATION
CONVENTIONAL GPS	x	13.5	1.4	13.6	1.7
	y	20.6	4.1	20.2	4.7
	z	2.0	1.2	2.1	1.3
DIFFERENTIAL GPS	x	1.6	1.5	1.9	1.8
	y	6.4	4.8	7.8	4.7
	z	5.4	0.7	5.2	0.9

Comparing the PVAT filter performance with the PV and PVAC filters, very little difference can be noted for the full Constant Acceleration Turn pattern. For the Turning segment only, PVAT filter standard deviation is much smaller (by a factor of 2 or 3) than that obtained with the PV filter. Comparison with the PVAC filter does not show, however, a clear cut advantage for either the PVAT or PVAC filter. At the RMS level, however, the PVAT filter seems to perform better although this could be incidental to this particular run only.

3.2.5.4 Conclusions for Constant Acceleration Turn Pattern

Comparison of the PV, PVAC, and PVAT showed a clear improvement obtained by modeling the acceleration. The performance of the PVAC filter, which models the acceleration on a constant use, however, not significantly different than that of the PVAT filter which models the acceleration as centripetal. The performance obtained by using the full theoretical process noise matrix was not significantly different than that obtained using an diagonal Q matrix, in which position states are decoupled from both velocity and acceleration states.

The PVAT filter performance using a time varying process noise matrix did not improve much over that obtained with a constant process noise matrix. It appears, therefore, that the PVAC filter seems best suited overall for a Constant Acceleration Turn type pattern, considering both performance and complexity factors.

The PV, PVAC, and PVAT filters were further tested using a landing type pattern. Results are discussed in Section 6.

3.3 ADAPTIVE COVARIANCE FEATURES

In the PVAT filter, continuous centripetal acceleration is modeled. However, since dynamics is rarely a continuous centripetal acceleration, this modeling could, in some cases, be worse than for a simpler filter, assuming either constant (PVAT) or just noisy (PV) acceleration. In that case, an increase in the process noise would be required to offset the modeling errors. High dynamics transitions (i.e., large changes in turning

rate, ω) should be accompanied by increased in the process noise, Q. This was simulated here in the following way:

At $t = 0$, $Q = Q_o$

At $t = t + 1$,

If $[(\Delta\omega)^2$ greater than $10^{-2}]$

then $t = 0$

$Q = Q_o\ [1 + a(\Delta\omega)^2\ (1 - t/5)]$.

If [t.greater than. 5]

then $Q = Q_o$

Basically, if $(\Delta\omega)^2$ exceeds a threshold, the process noise is multiplied by $[1 + \alpha(\Delta\omega)^2]$ and then allowed to reduce back to Q_o in five seconds, unless a new larger $\Delta\omega$ occurs first, in which case, the clock gets reset to zero, Q gets reset to a higher value and reduces back to Q_o in five seconds. The term α is a multiplicative factor that can be set by the simulation operator.

The Constant Acceleration Turn pattern, used in the previous tests, is used here. The PVAT filter was run with a constant process noise (diagonal) matrix and then with an adaptive process noise (diagonal) matrix. The multiplicative factor "a" was set to 50,000.

In Section 3.2.5.3, the performance of the PVAT filter was studied and plots were provided. Little difference was noted when the adaptive scheme was tried using the same process noise matrix, even with very large multiplicative factors. This would tend to indicate that the filter does not rely much on the model so that increased process noise is of little or no effect.

To determine if adaptive schemes could provide improved performance, the PVAT filter was run with a reduced process noise matrix. The performance is presented in Figure 3-9. Clearly, the filter experiences difficulty during the turn segment. Figure 3-10 presents the performance of the PVAT filter using the adaptive process noise matrix with the same initial value as that used for the constant case, indicating a 50% reduction in the error due to the turn.

Table 3-7 shows the RMS and standard deviations for all axes and for both the conventional and differential modes for each of the PVAT filters discussed above. A slight improvement is noted in one direction while some degradation is observed in the vertical direction when using the adaptive scheme. The figure shows, however, that the adaptive filter tracks better in the turn, even if the RMS error turns out to be larger (due to biases).

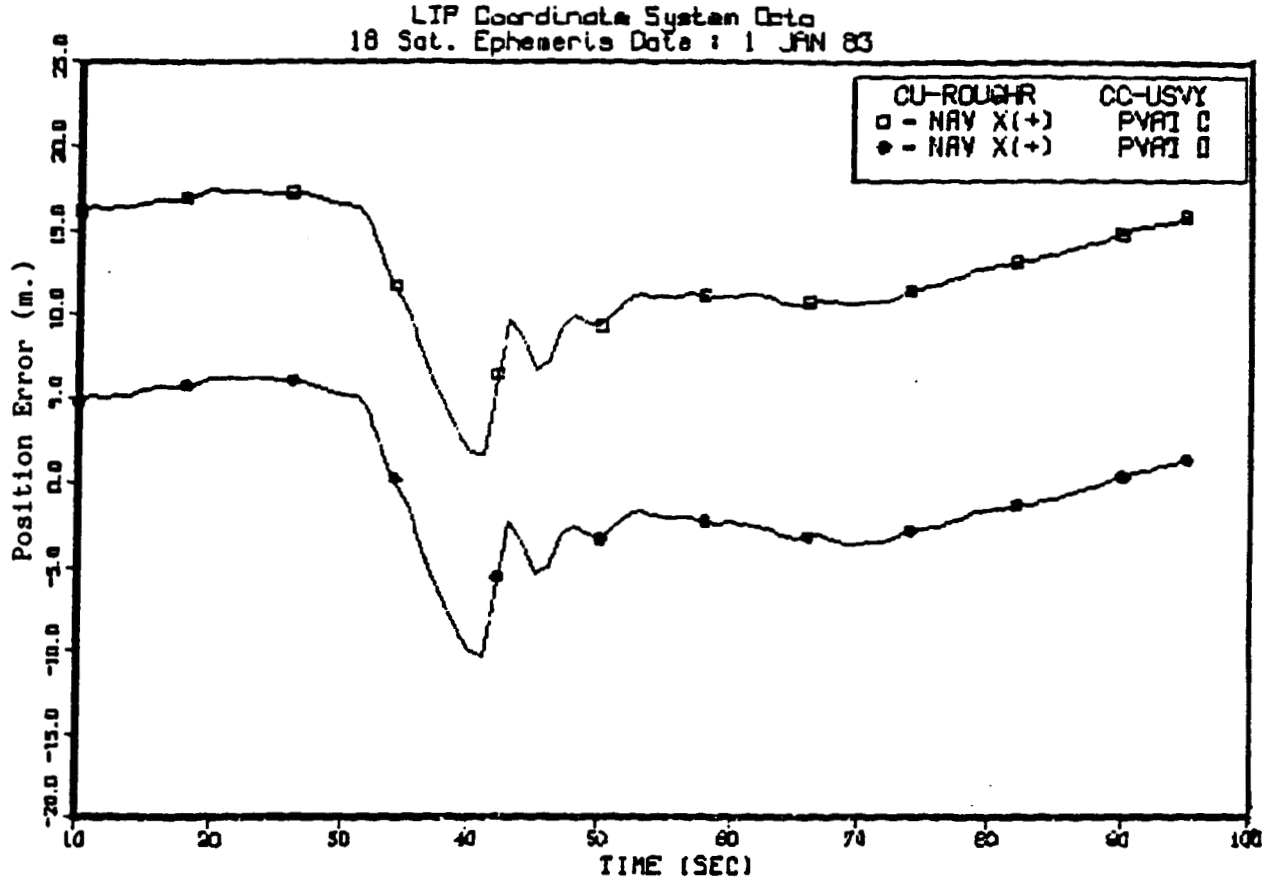

For acronym definition refer to glossary on page vi.

Figure 3-9a. PVAT Filter Performance, X-Axis Reduced, Constant, Diagonal Q-Matrix

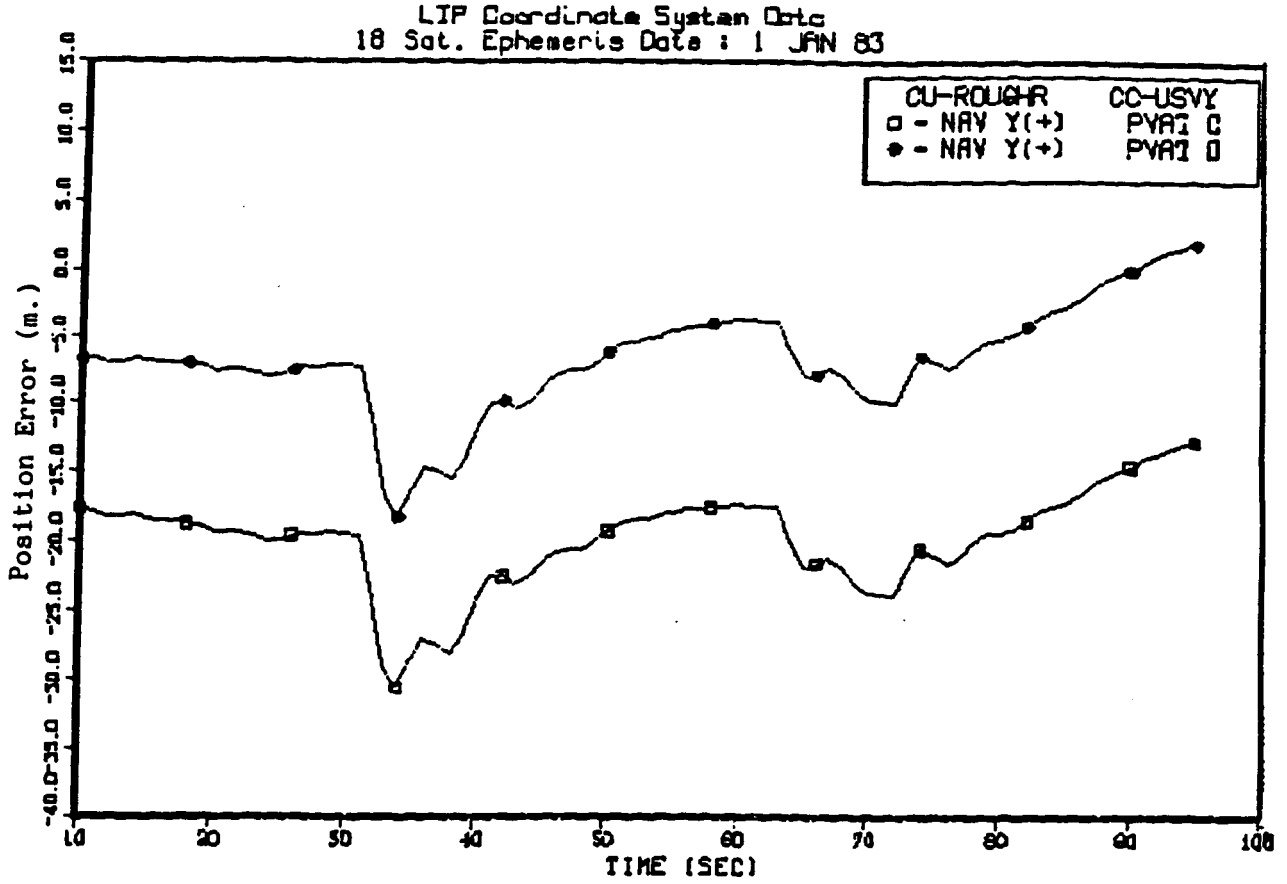

NAV Y(+) PVAT C : -0.1990E+02, 0.3539E+01, 0.2021E+02
NAV Y(+) PVAT D : -0.6752E+01, 0.3984E+01, 0.7840E+01

For acronym definition refer to glossary on page vi.

Figure 3-9b. PVAT Filter Performance, Y-Axis Reduced, Constant, Diagonal Q-Matrix

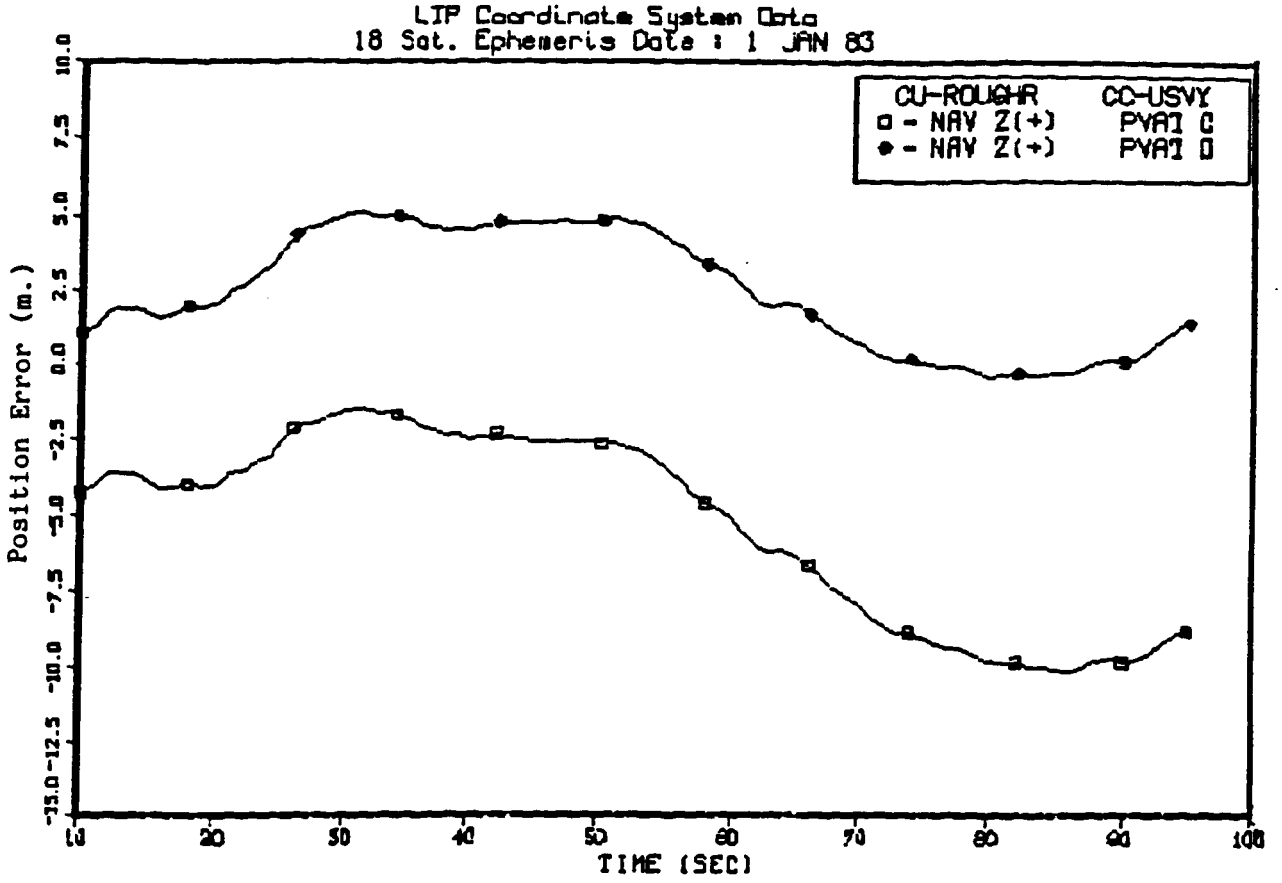

NAV Z(+) PVAT C : -0.5274E+01, 0.3022E+01, 0.6079E+01
NAV Z(+) PVAT D : 0.2468E+01, 0.1933E+01, 0.3135E+01

For acronym definition refer to glossary on page vi.

Figure 3-9c. PVAT Filter Performance, Z-Axis Reduced, Constant, Diagonal Q-Matrix

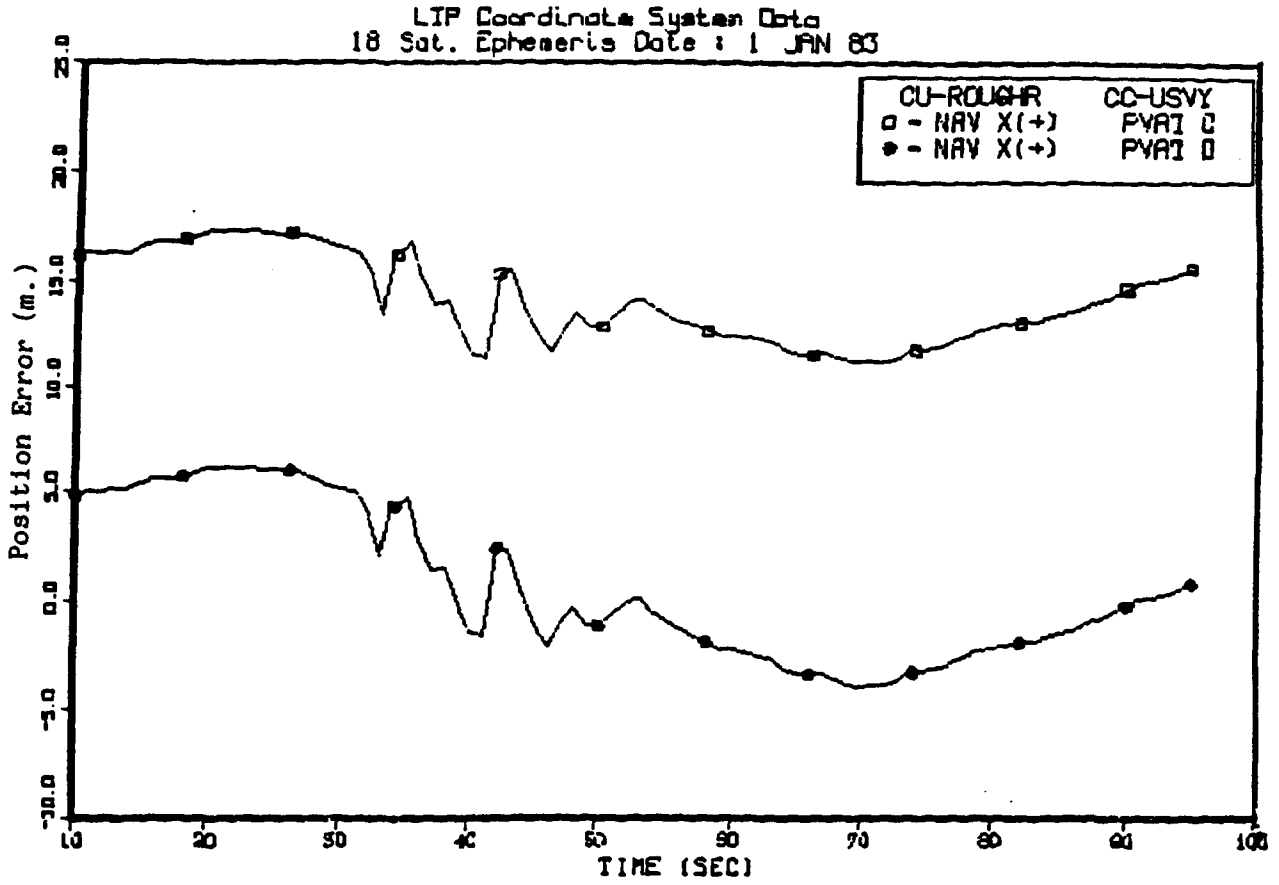

NAV X(+)	PVAT C	:	0.1409E+02,	0.2045E+01,	0.1424E+02
NAV X(+)	PVAT D	:	0.6671E+00,	0.3383E+01,	0.3449E+01

For acronym definition refer to glossary on page vi.

Figure 3-10a. PVAT Filter Performance, X-Axis Adaptive Process Noise Q-Matrix

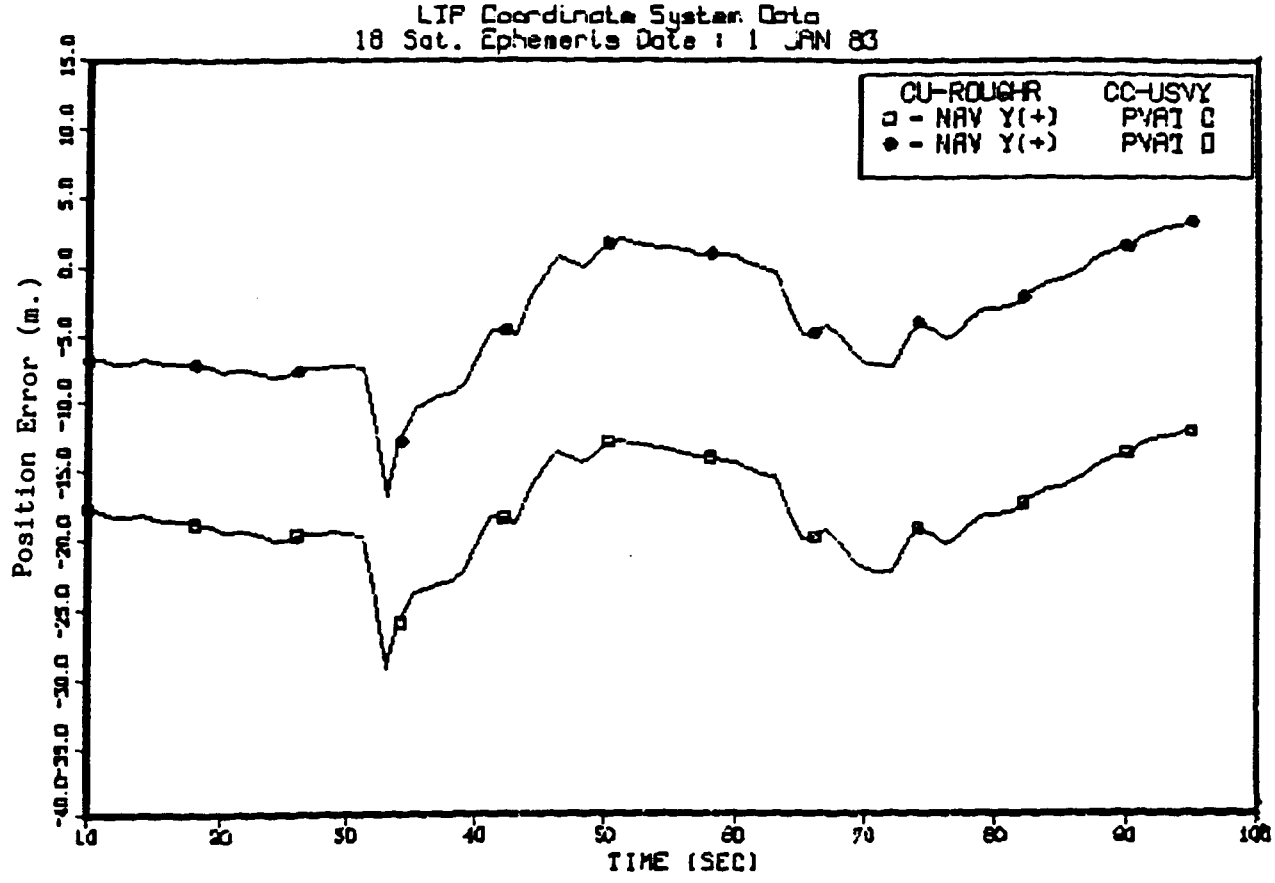

For acronym definition refer to glossary on page vi.

Figure 3-10b. PVAT Filter Performance, Y-Axis Adaptive Process Noise Q-Matrix

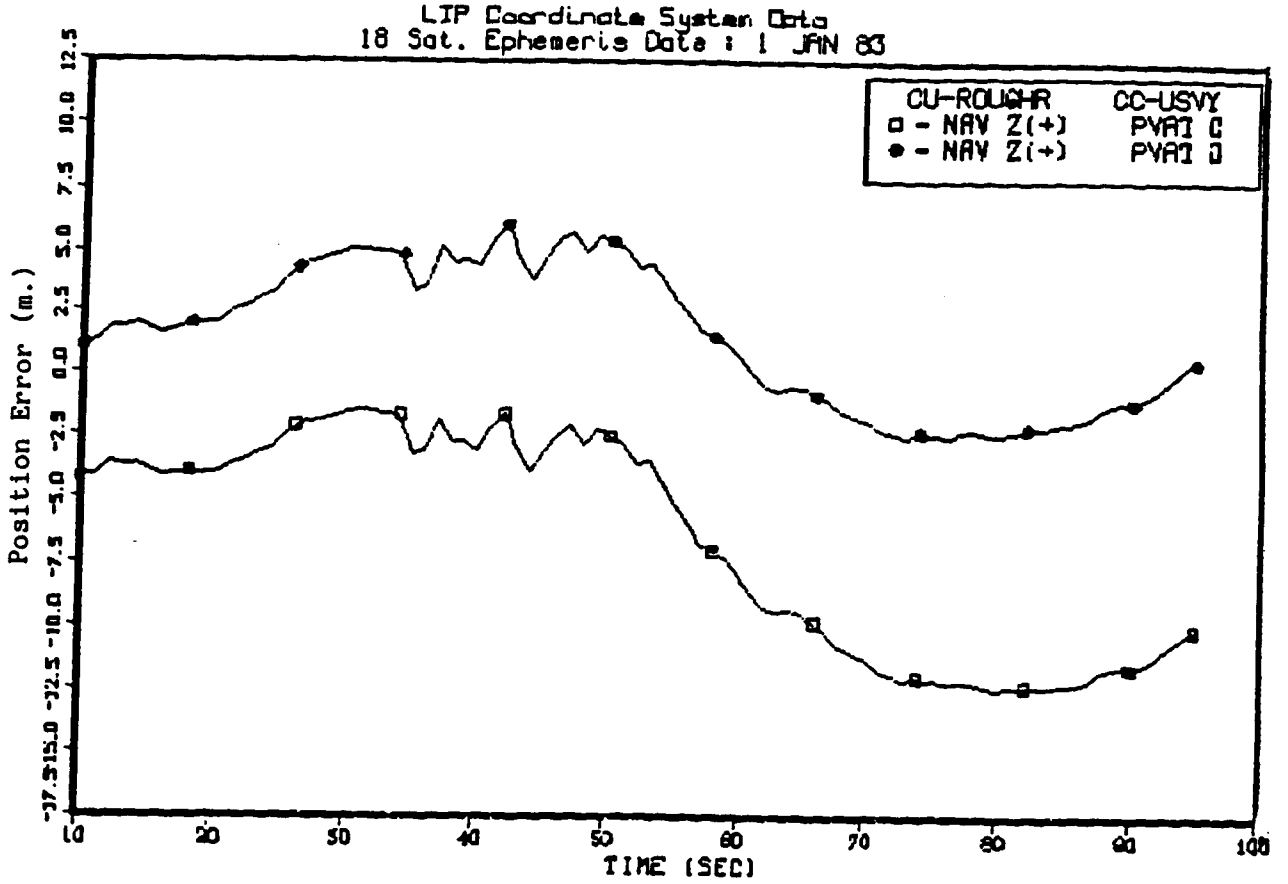

For acronym definition refer to glossary on page vi.

Figure 3-10c. PVAT Filter Performance, Z-Axis Adaptive Process Noise Q-Matrix

Table 3-7. PVAT Filter Performance (Meters), Adaptive Mode

Diagonal Q Matrix

VALUES IN METERS		CONSTANT Q MATRIX RMS	CONSTANT Q MATRIX STANDARD DEVIATION	ADAPTIVE Q MATRIX RMS	ADAPTIVE Q MATRIX STANDARD DEVIATION
CONVENTIONAL GPS	x	13.0	3.9	14.2	2.0
	y	20.2	3.5	18.1	3.5
	z	6.1	3.0	7.8	4.1
DIFFERENTIAL GPS	x	4.1	4.1	3.4	3.4
	y	7.8	3.3	5.7	4.3
	z	3.1	1.3	3.2	2.8

Figures 3-11 and 3-12 show the performances for the constant case and for the adaptive case, respectively, during the turning segment only. Table 3-8 compares the RMS and standard deviations for both cases. Figure 3-13 shows the process noise history during the turn.

Table 3-8. PVAT Filter Performance (Meters), Adaptive Mode
Turning Segment Only

Diagonal Q Matrix

VALUES IN METERS		CONSTANT Q MATRIX RMS	CONSTANT Q MATRIX STANDARD DEVIATION	ADAPTIVE Q MATRIX RMS	ADAPTIVE Q MATRIX STANDARD DEVIATION
CONVENTIONAL GPS	x	9.8	4.2	14.1	1.7
	y	24.0	3.5	19.9	4.5
	z	2.2	0.4	2.5	0.7
DIFFERENTIAL GPS	x	5.3	4.3	2.7	2.4
	y	11.7	3.7	7.7	5.0
	z	4.8	0.16	4.3	0.65

In this case, the filter seems to track better in the adaptive mode in the x direction (smaller standard deviation) but the performance is slightly degraded in the other directions. In the differential mode, the RMS accuracies are improved in all axes.

Overall, though, the improvement of the adaptive scheme is not dramatic and is characteristic of the other schemes tried on the GPS program for various receivers. One such method is described in the next section. Later in this study, we report on results during landing approach type patterns where increased dynamics takes place.

3.3.2 Residuals Tests

This method was implemented by Magnavox in their Z-set. It consisted of calculating four filtered pseudorange and four filtered deltarange residuals

and multiplying the diagonal elements in the Cholesky covariance matrix by their simple average. Although this method was not repeated, it is similar to the one used here in that it increased the covariance (and therefore increases the gains) when the residuals get large (indicating poor filter tracking). Since the Z-set method is a simpler version with weaker assumptions about how the various axes can be combined, the Z-set method will be less responsive than the method applied here.

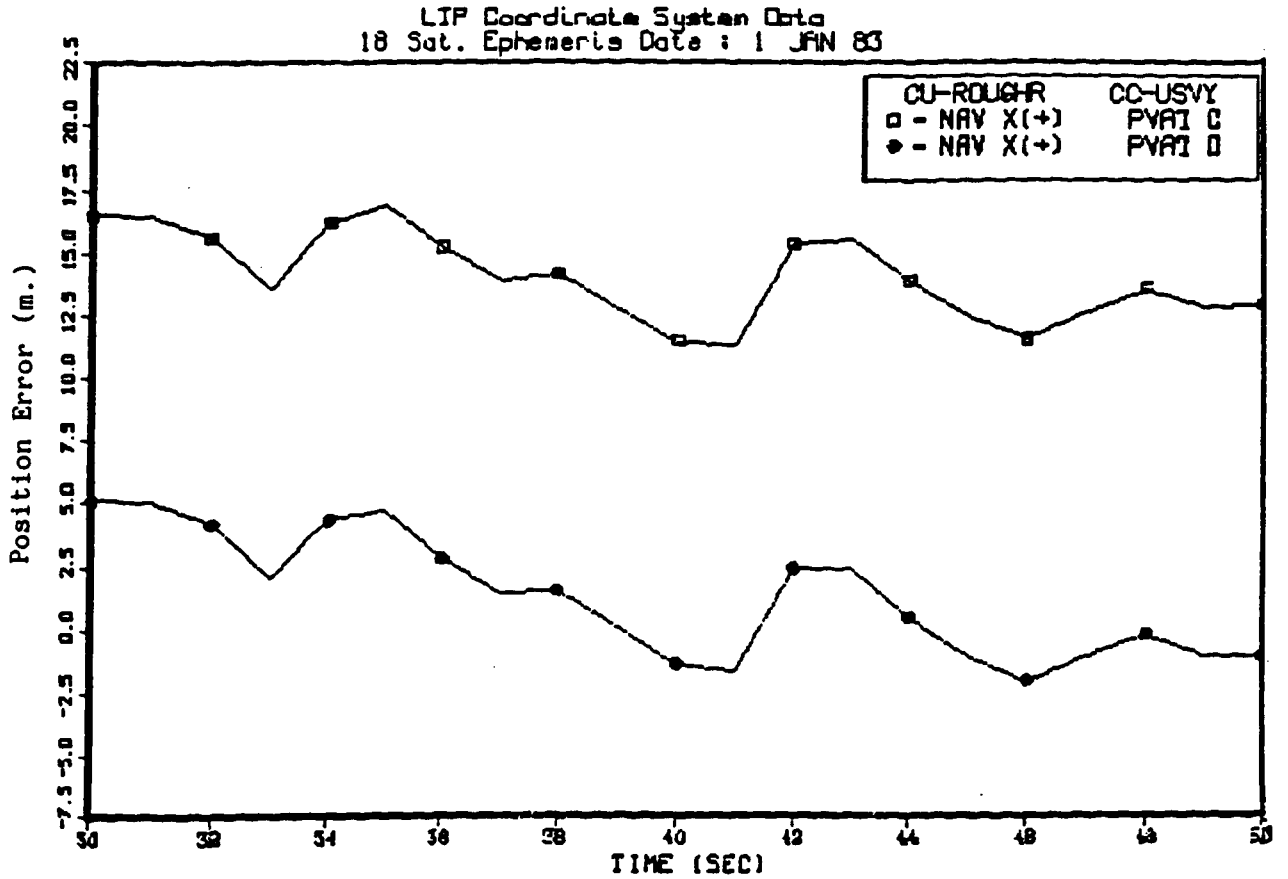

NAV X(+) PVAT C : 0.1400E+02, 0.1728E+01, 0.1411E+02
NAV X(+) PVAT D : 0.1283E+01, 0.2351E+01, 0.2678E+01

For acronym definition refer to glossary on page vi.

Figure 3-11a. PVAT Filter Performance During Turn, X-Axis Constant Q-Matrix

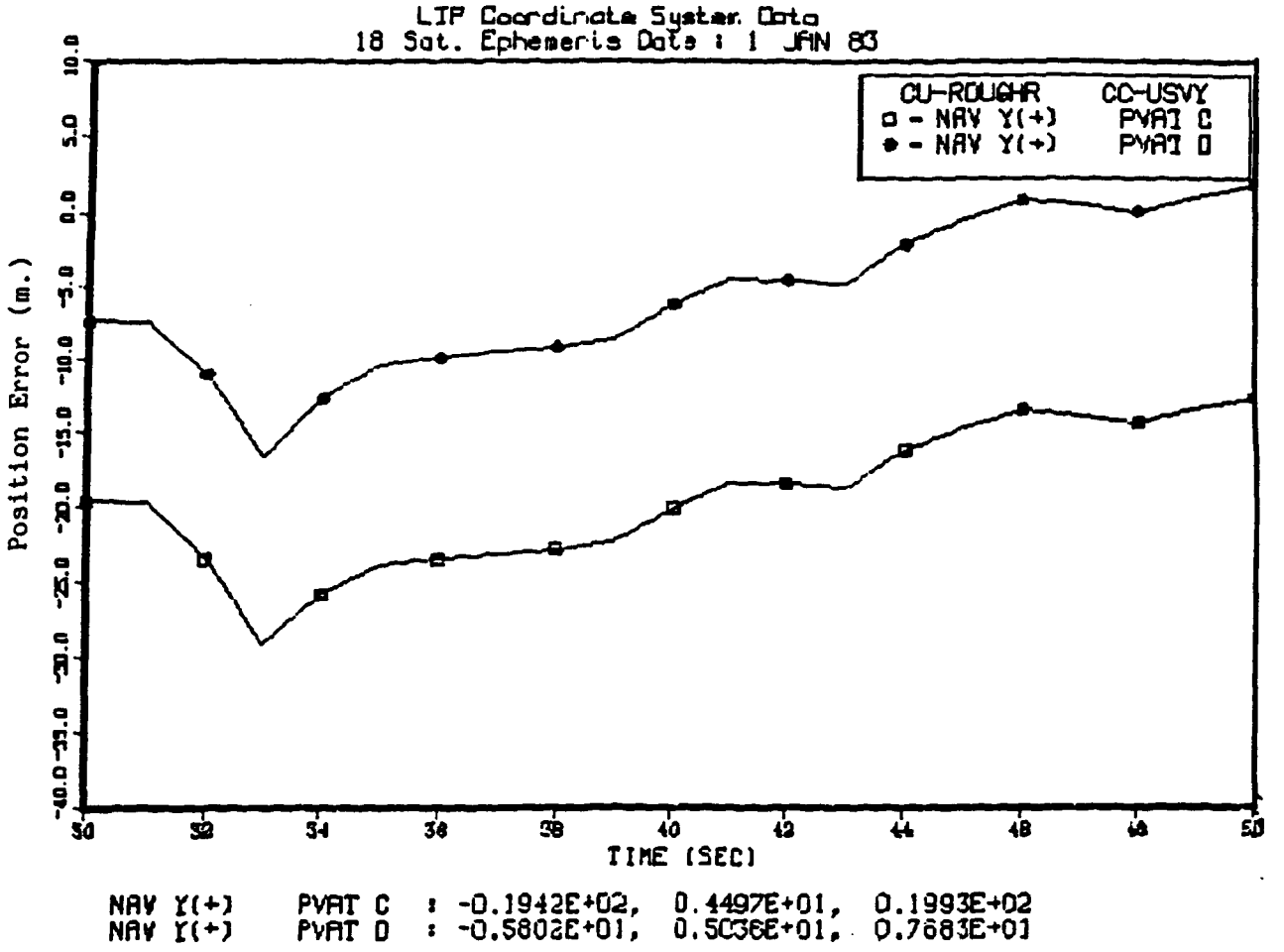

NAV Y(+) PVAT C : -0.1942E+02, 0.4497E+01, 0.1993E+02
NAV Y(+) PVAT D : -0.5802E+01, 0.5036E+01, 0.7683E+01

For acronym definition refer to glossary on page vi.

Figure 3-11b. PVAT Filter Performance During Turn, Y-Axis Constant Q-Matrix

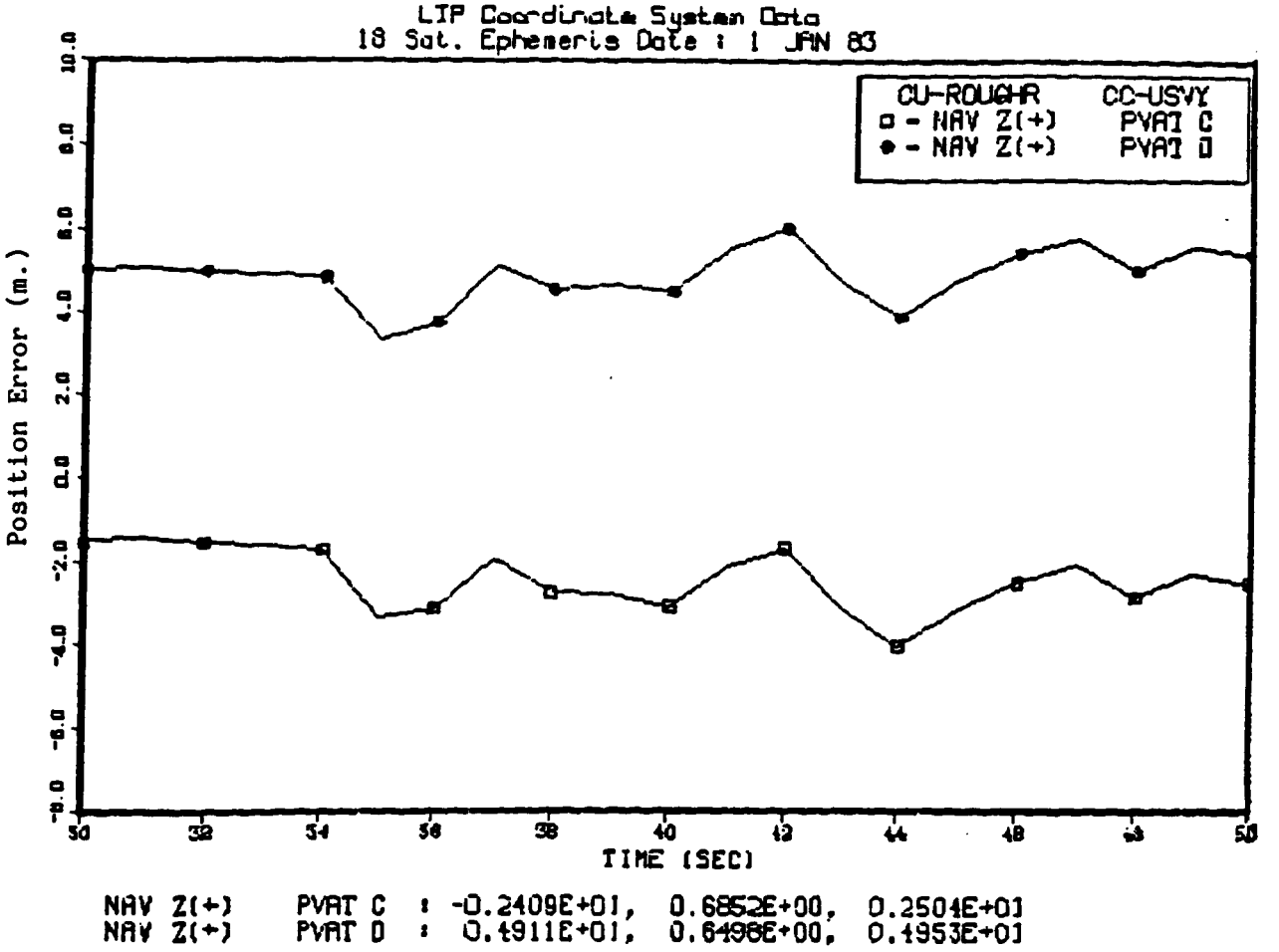

For acronym definition refer to glossary on page vi.

Figure 3-11c. PVAT Filter Performance During Turn, Z-Axis Constant Q-Matrix

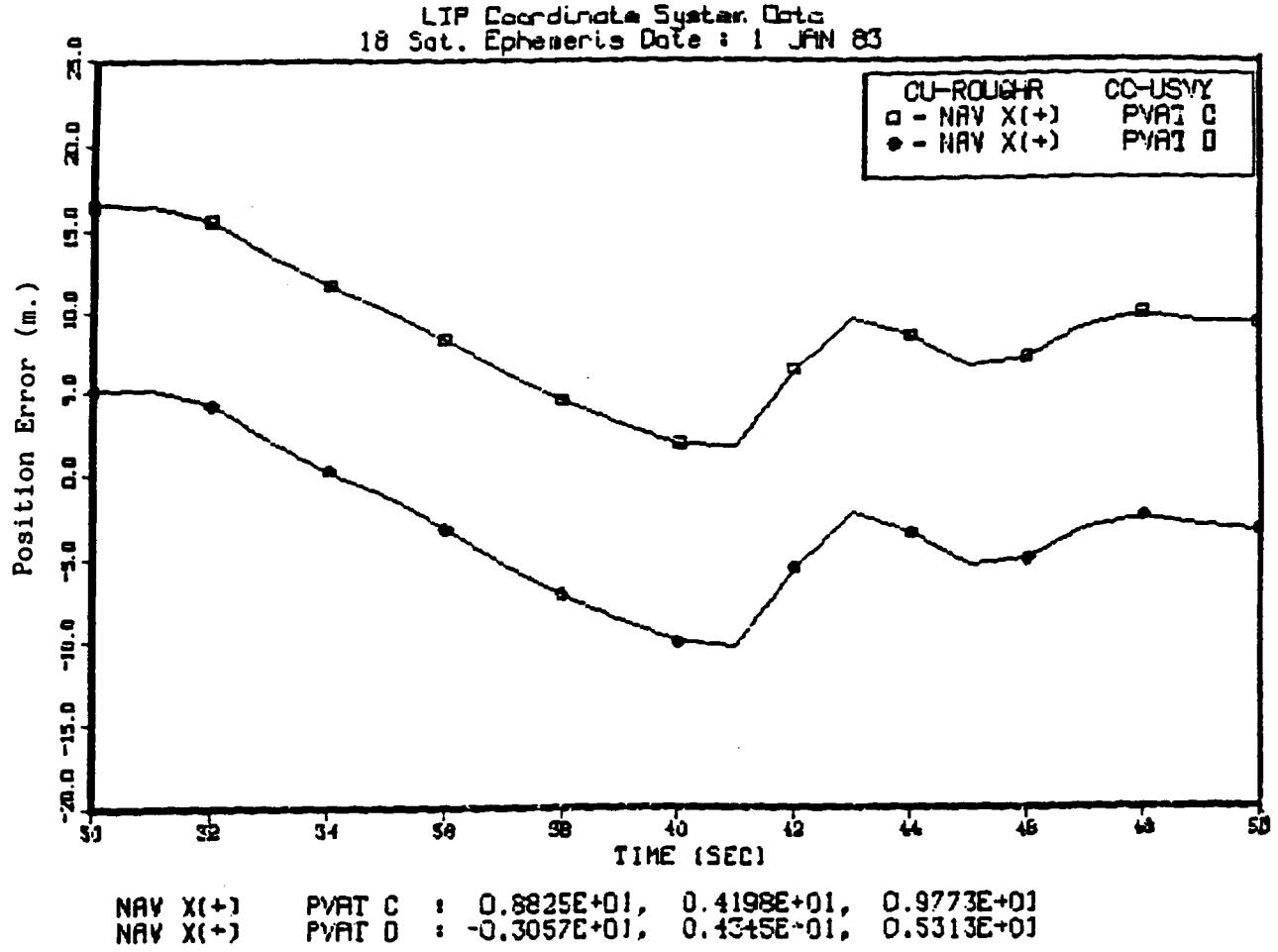

For acronym definition refer to glossary on page vi.

Figure 3-12a. PVAT Filter Performance During Turn, X-Axis Adaptive Q-Matrix

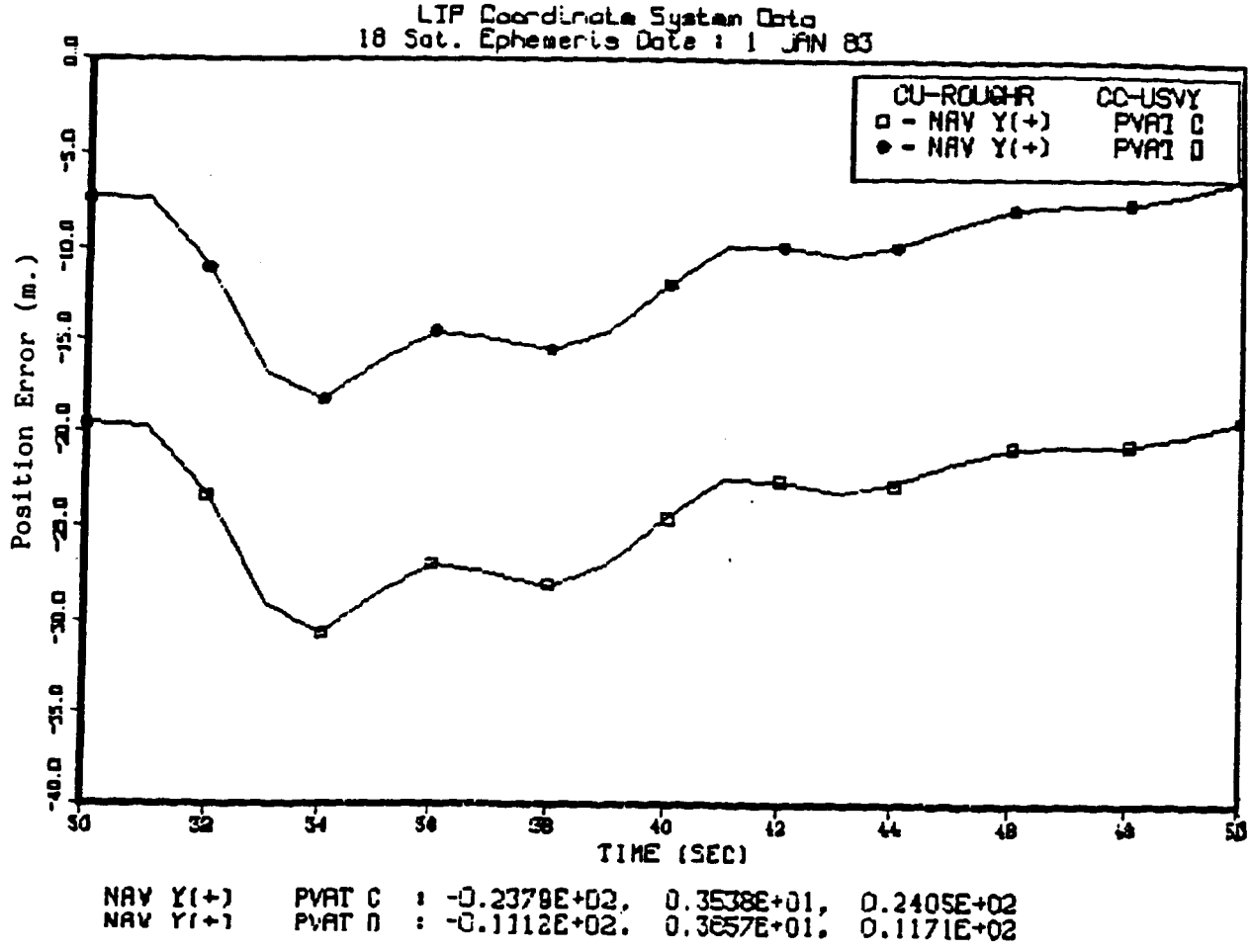

For acronym definition refer to glossary on page vi.

Figure 3-12b. PVAT Filter Performance During Turn, Y-Axis Adaptive Q-Matrix

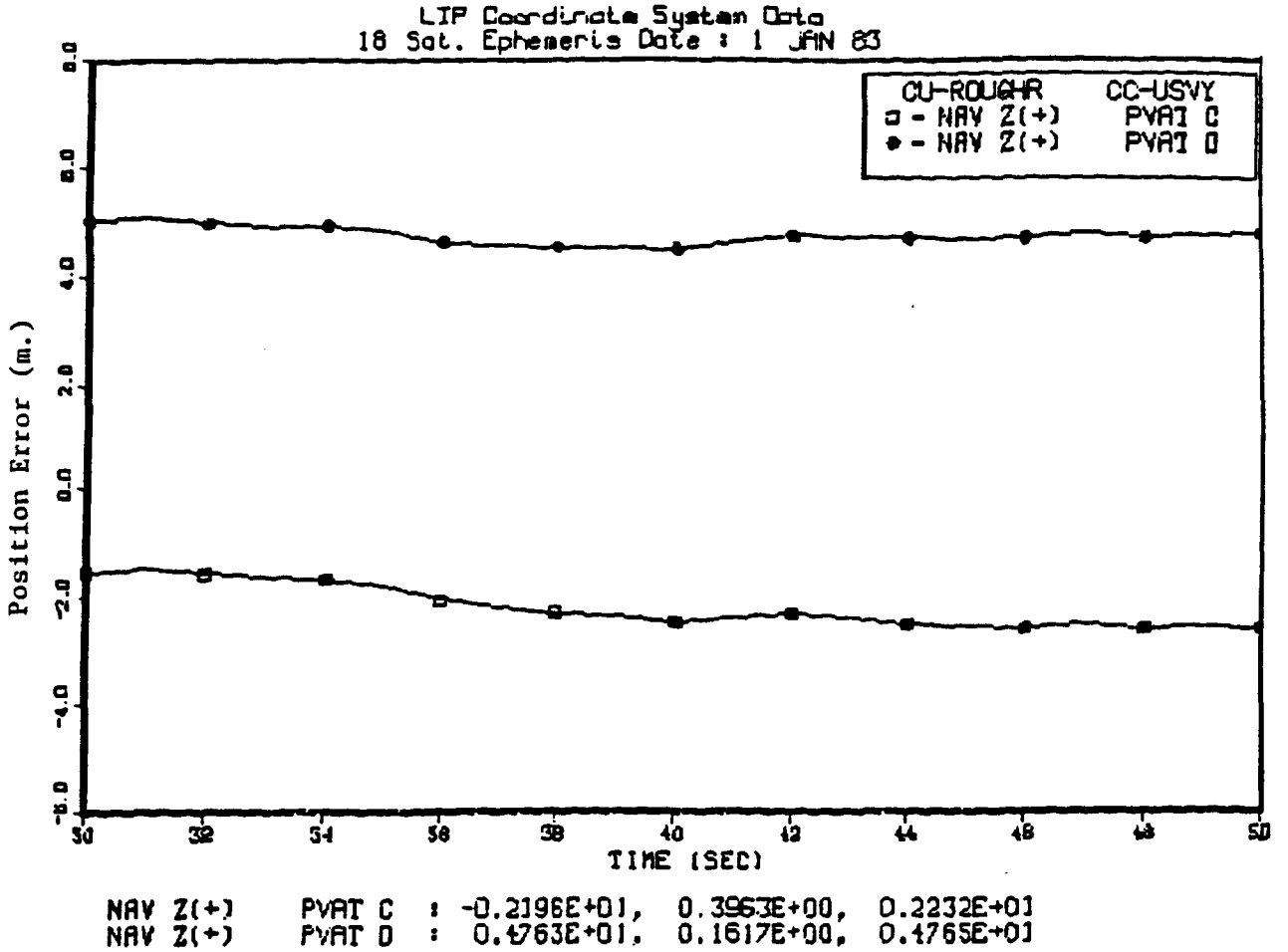

NAV Z(+) PVAT C : -0.2196E+01, 0.3963E+00, 0.2232E+01
NAV Z(+) PVAT D : 0.4763E+01, 0.1617E+00, 0.4765E+01

Figure 3-12c. PVAT Filter Performance During Turn, Z-Axis Adaptive Q-Matrix

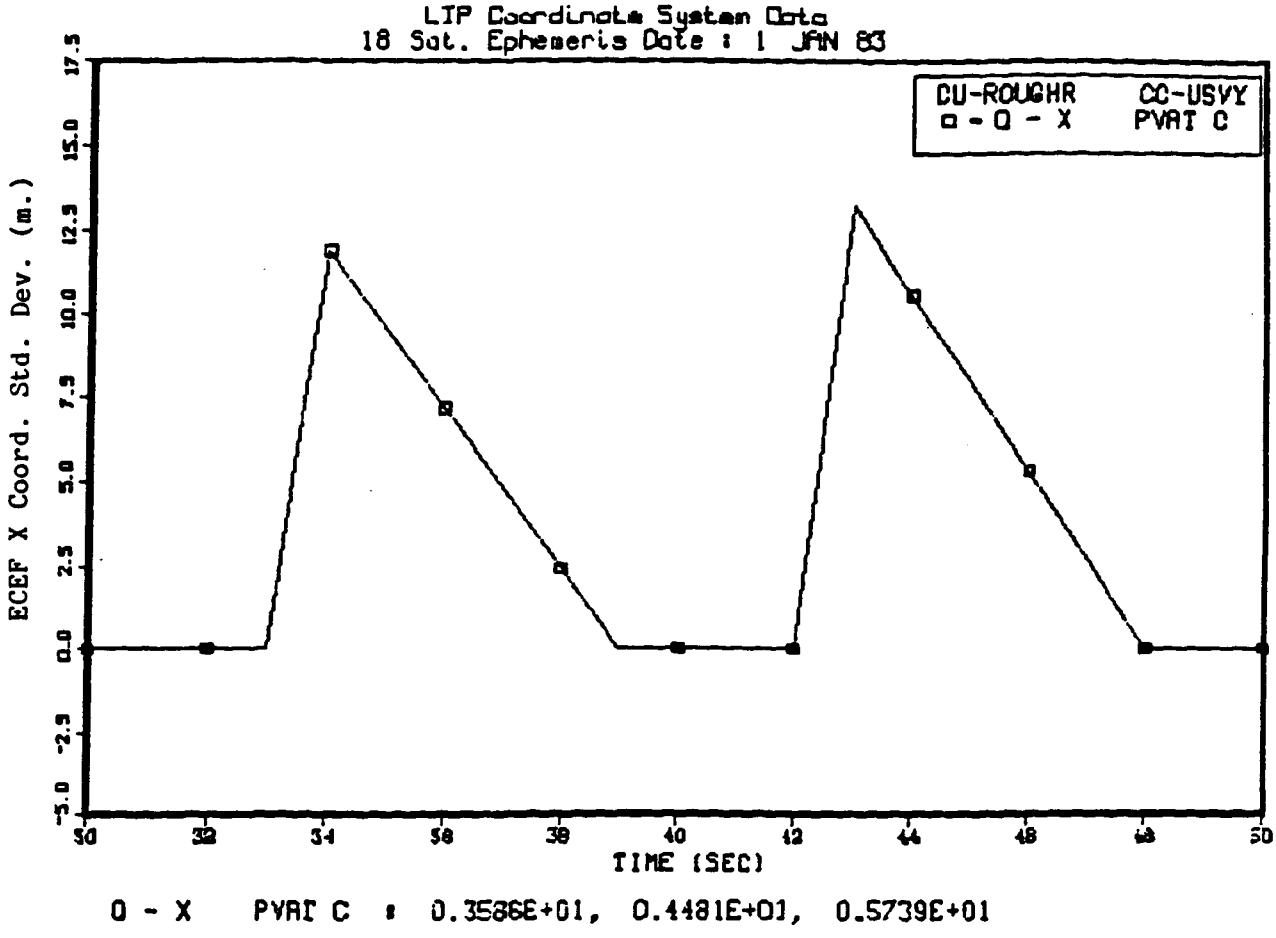

For acronym definition refer to glossary on page vi.

Figure 3-13. Process Noise History During Turn

IV. MISSION-TAILORED SATELLITE SELECTION

Much has been written on the subject of "optimal" satellite selection for GPS. Techniques generally optimize the geometry of the four satellites needed for stand-alone, continuous GPS tracking. These techniques minimize the position dilution of precision, or PDOP, which is the root sum square of the geometry-induced errors in each of three orthogonal axes. Minimum PDOP, therefore, results in the minimum sum of the squares of the errors in each axis, assuming that the satellite to user range errors are all equal and therefore can be normalized out.

Other techniques have also been proposed, some of which weigh a priori known values of each satellite's measurement error variance [5]. In addition, the satellite selection process can weigh observed errors by mathematically inferring their source. Although these more sophisticated techniques clearly make better use of all available information and will probably be significantly better if the satellites are not uniformly corrupted, they do pose computational problems. Observation of operational satellite data will decide this tradeoff. In any case, geometry-based selection algorithms can be studied independently of range variance-based methods, since geometry methods simply assume optimal performance of any range variance-based method, and thus would augment such a technique.

Of course, the subject of optimal satellite selection can be avoided altogether by employing an "all-in-view" tracking strategy. This technique observes all satellites either continuously (with a multichannel or multiplex set) or sequentially. There are tradeoffs involved in this case also, however, due to the complexity and increased uncertainty of the tracking and switching environment created.

4.1 SATELLITE SELECTION ALGORITHM CONCEPT

An immediately applicable geometry-based satellite selection concept is to consider the mission requirements in choosing satellites. This was investigated in the present study. To provide the foundation for this geometry-based analysis, however, a brief derivation of the GDOP (PDOP plus the time term) concept is first presented.

GDOP is defined for a system whose measurements, $\bar{z}$ (the pseudorange errors), are related to the error state, $\bar{x}$, by the expression:

$$\bar{z} = H\bar{x} + \bar{v}$$

where

$\bar{v}$ = unmodeled errors (white noise)

H = direction cosines to the four satellites

and

$$E[\bar{v}\,\bar{v}^T] = R$$

For a best linear unbiased estimate of $\bar{x}$ given $\bar{z}$,

$$\bar{x} = [H^T R^{-1} H]^{-1} H^T R^{-1} \bar{z}$$

The error in this estimate has the covariance:

$$\text{cov}(\bar{x}) = E[(\bar{x} - \bar{x})(\bar{x} - \bar{x})^T] = [H^T R^{-1} H]^{-1}$$

GDOP is defined by assuming that the measurement errors are uncorrelated and identically distributed so that:

$$R = \sigma^2 I$$

Thus, the error covariance is:

$$\text{cov}(\bar{x}) = \sigma^2 [H^T H]^{-1}$$

where GDOP is defined as:

$$\text{GDOP} \ (\text{tr} \ [H^T H]^{-1})^{1/2}$$

Note that the GDOP term is a "compromise" between the various components of the $[H^T H]^{-1}$ matrix, where a less than minimum DOP value in one axis of a particular constellation's GDOP may be sacrificed (accepted) to avoid selection of a very large DOP value in some other axis of another constellation.

The concept to be investigated is whether or not, for a particular mission application, one may want to weigh certain axes that are more important to mission needs. In the landing situation, the critical axes of concern are the vertical and cross-track coordinates. The vertical axis carries the most restrictive specification in the landing criteria as shown by the FAA Navigation System Accuracy Standards presented in Table 4-1 [6]. The implication from the table is that the along-track axis accuracy can be relaxed somewhat.

Table 4-1. Minimum Guidance Accuracy

	Height		Lateral		Vertical	
	(ft)	(m)	(ft)	(m)	(ft)	(m)
Category						
I	100	(30.5)	30.0	(9.1)	10.0	(3.0)
II	50	(15.3)	15.0	(4.6)	4.5	(1.4)
IIIABC	0	(0)	13.5	(4.1)	1.8	(0.5)

To pursue this possibility, the GDOP matrix was modeled in a "landing mission coordinate frame" with three orthogonal axes in the along-track, cross-track, and vertical directions as shown in Figure 4-1. GDOP, being the root sum square of all three coordinates, is the same in either coordinate frame, of course. The vertical axis is oriented normal to the local tangent

plane, although it could be tilted by the glideslope angle if desired. At a typical 3° glideslope angle, the difference would be negligible. The error covariance in the landing coordinate frame will be:

$$\text{cov}(\bar{x}) = \sigma[A^{-T}H^{T}HA^{-1}]^{-1}$$

$$= \sigma \begin{bmatrix} V_A^2 & & & \sim \\ & V_X^2 & & \\ & & V_V^2 & \\ \sim & & & V_T^2 \end{bmatrix}$$

where

V_A^2 = along-track dilution factor

V_X^2 = cross-track dilution factor

V_V^2 = vertical deviation dilution factor

V_T^2 = time dilution factor

A = Rotation matrix from normal GPS coordinate frame to A-X-V frame

A satellite selection algorithm optimized for this frame may seek to minimize V_V or some weighted combination of V_V and V_X.

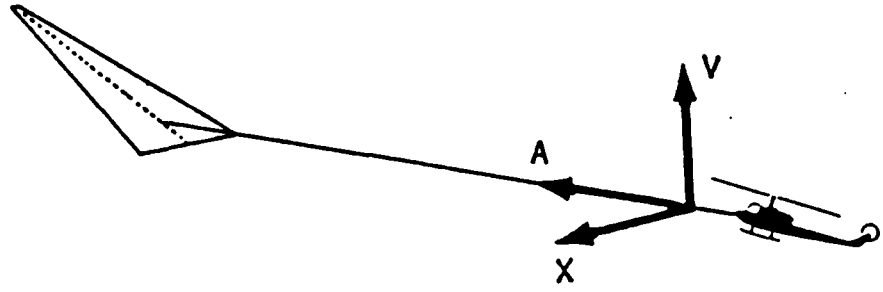

A = ALONG-TRACK
X = CROSS-TRACK
V = VERTICAL

Figure 4-1. Landing Approach Oriented Coordinate Frame

4.2 SATELLITE SELECTION ALGORITHM SIMULATION RESULTS

The above GDOP coordinate frame rotation was modeled in NASA's DIFFGPS Simulation DOPS Analysis Module. Then, representative areas of operation for the remote helicopter mission were identified, and both conventional minimum PDOP and the modified satellite selection algorithms were executed over a 12-hour period. The satellite constellation was selected as the proposed 18-satellite, 6-orbit configuration [7].

The modified satellite selection algorithm used for these runs is an even-weighted "XVDOP", where the criterion was a sum square of the cross-track and vertical error values:

$$XVDOP = \sqrt{V_X^2 + V_V^2}$$

In addition, a VDOP criterion is analyzed, which minimizes the error only in the vertical direction.

Figure 4-2 presents a typical plot of dilution of precision over a 12-hour period. The plot presents the "VDOP" (vertical dilution) component values achieved by three different satellite selection criteria. The first criterion is PDOP, position dilution of precision, which utilizes all three axes and is represented by "XYZ" in the figure. The next criterion is XVDOP as described above, represented by YZ in the figure. The last criterion is VDOP, which is the criterion of minimizing only the vertical component, regardless of the values in the other two axes (in this case, cross-track accuracy may suffer).

The XVDOP case is dependent on the azimuth orientation of the vertical plane, of course. In all cases presented here, the orientation was normal to the runway heading of the referenced city. In other analyses, not presented here, the sensitivity of satellite selection to azimuth orientation of the vertical plane was studied. Although differences did exist, they were generally not significant to the VDOP value. Therefore, the random sample presented here is considered "representative."

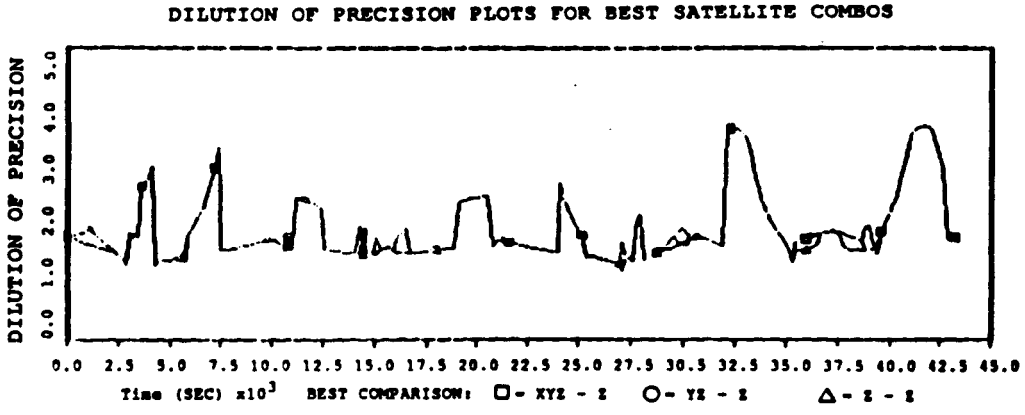

Figure 4-2. Dilution of Precision, Seattle

The statistical results are calculated as follows. First, the PDOP value is calculated. Next, the percentage of time over the 12 hours that VDOP differed from the nominal PDOP selection case is calculated. Finally, the per-

centage improvement of VDOP, during those periods when it differs from the nominal case, is calculated. The results are tabulated in Table 4-2.

Table 4-2. VDOP Statistics for Seattle, WA Case

	Selection Criterion	
	XVDOP	VDOP
Nominal PDOP	5.2	5.2
VDOP		
Percentage of Time Different from PDOP Criterion	22.8%	32.4%
Improvement Amount When Better than PDOP Criterion	.35	.35

The improvement in VDOP of .35 represents about a 10% improvement, which as indicated, occurs about 23% of the time for the XVDOP selection criterion case and 32% of the time for the VDOP selection criterion case. Table 4-3 presents results for several other representative locations, for the XVDOP criterion only. It should be noted that VDOP is not always better, when different, in the XVDOP selection criterion case. For these results, it was better on the average over 75% of the time. Better weighting of the cross-track and vertical terms would correct this.

One notable result illustrated by the plot in Figure 4-2 is that this improvement occurs primarily when overall DOPs are "good", and not during the VDOP "spikes" that occur due to changing geometry. This result is in general true for all cases tested; this is an unfortunate result since it would be beneficial to find a means to improve VDOP during these "bad" periods.

A possible complementary solution would be to add an altimeter measurement and state. The altimeter's inherent inaccuracies would probably eliminate its influence during periods where the VDOP is "good," but this is where the XVDOP selection algorithm improves performance. However, in periods where the VDOP is poor and where the XVDOP algorithm was shown to have no effect, the altimeter input is likely to be more heavily weighted thereby substituting its vertical "measurement" for the poorly resolved GPS vertical observation.

Table 4-3. VDOP Results for XVDOP

Location	Selection Criterion: Percent of Time Different	Selection Criterion: Improvement in VDOP
Fairbanks	14.9	.12
Kodiak	41.5	.24
Cold Bay	19.1	.20
Juneau	45.6	.23
Seattle	22.8	.35
Seattle W.	21.2	.26
Portland	58.1	.24
Portland W.	70.5	.17
SFO	7.9	.32
SFO W.	7.9	.26
L.A.	11.2	.23
L.A. W.	11.6	.21
Bangor	18.7	.29
Bangor E.	18.7	.25
St. John	12.0	.30
St. John E.	12.4	.27
Average	17.4	.25

W. = 100 miles west of city

E. = 100 miles east of city

V. SENSOR AIDING

5.1 BAROMETRIC ALTIMETER

The addition of baroaltimeter inputs provides improved vertical accuracy in high VDOP conditions. A PVAC filter was modified to include a baro state, and its performance was compared to that of the original PVAC filter. The selected baro state is $(h_{GPS} - h_{Baro})$.

Two modes are used; the calibrate mode when baro measurements are not used (PDOP < 5) in the position calculation and the measurement mode, when baro measurements are used (PDOP > 5). In the calibrate mode, $h_{GPS} - h_{Baro}$ is estimated by filtering the $h_{GPS} - h_{Baro}$ measurements. The baro error equation is:

$$\delta h_b(k) = \left(1 - \frac{\Delta t}{\tau_b}\right) \delta h_b(k-1) + W_b(k-1)\Delta t$$

with $W_b \simeq N(0, N_b)$

$N_b = (9.6 \text{ ft})^2/\text{sec}$

$\delta h_b(0) = 500$ ft

$\tau_b = 10{,}667$ sec

In the measurement mode, the h_{Baro} measurements are processed directly and contribute to the position solution.

$$h_{Baro} = H_{GPS} - (h_{GPS} - h_{Baro})$$

5.1.1 Truth Baro Model

The baro error model is

$$\delta h_b = e_{p_o} + e_{hsf}\, h + c_{sp}\, v^2$$

with

$$(e_{p_o})_{k+1} = (1 - \omega_{alt}\Delta t)(e_{p_o})_k + w_{p_o}\Delta t$$

with

$w_{p_o} \sim N(0, Q_{p_o})$

$e_{p_o}(0) = 20$ ft

$Q_{p_o} = 2\omega_{alt}\sigma_{alt}^2 = (6.9 \text{ ft})^2/\text{sec}$

$\omega_{alt} = v/d_{alt} \simeq 10^{-4}\ \text{sec}^{-1}$

where

e_{p_o} = error due to the variation in altitude of a constant pressure surface

e_{hsf} = scale factor error due to non-standard temperature

c_{sp} = coefficient of static pressure measurement error

d_{alt} = correlation distance of weather patterns

σ_{alt} = standard deviation of the variation in altitude of a constant pressure surface

v = speed

The baro measurement error consists of a bias with a "small amount" of noise. Let us select:

$$R = 25 \text{ ft}^2$$

The process noise is

$$Q = 2\omega_{alt}\sigma_{alt}^2 t + 2e_{hsf}^2 h|\Delta h| + 4c_{sp}^2 v^3|\Delta v|$$

with

$$\Delta h = 5 \text{ ft}$$

$$\Delta v = 1 \text{ ft/sec}$$

or

$$Q = (9.6 \text{ ft})^2$$

5.1.2 Simulations

The Constant Acceleration Turn pattern used previously was used for the baroaltimeter simulations. A forced satellite switch was implemented leading to a PDOP history as shown in Figure 5-1. The PVAC filter without baro inputs was run as a benchmark. Figure 5-2 shows its performance. The baroaltimeter filter was run in both the calibrate mode (no baro measurements are processed when PDOP is less than five) and in the measurement mode (baro measurements are processed throughout). These results are provided in Figures 5-3 and 5-4, respectively. There is little difference in performance between the calibrate mode and the measurement mode. In the calibrate mode, the baro measurements are not used to calculate the position when PDOP is less than five. The baro bias error is, however, estimated continuously. The vertical accuracy is slightly better in the non-calibrate mode (i.e., when baro measurements are always processed in the position determination), due to the additional information in the vertical direction provided by the baro measurements. If these measurements are well-modeled in the filter, they will provide increased accuracy. It is therefore advantageous to always process them in the calculation of the position.

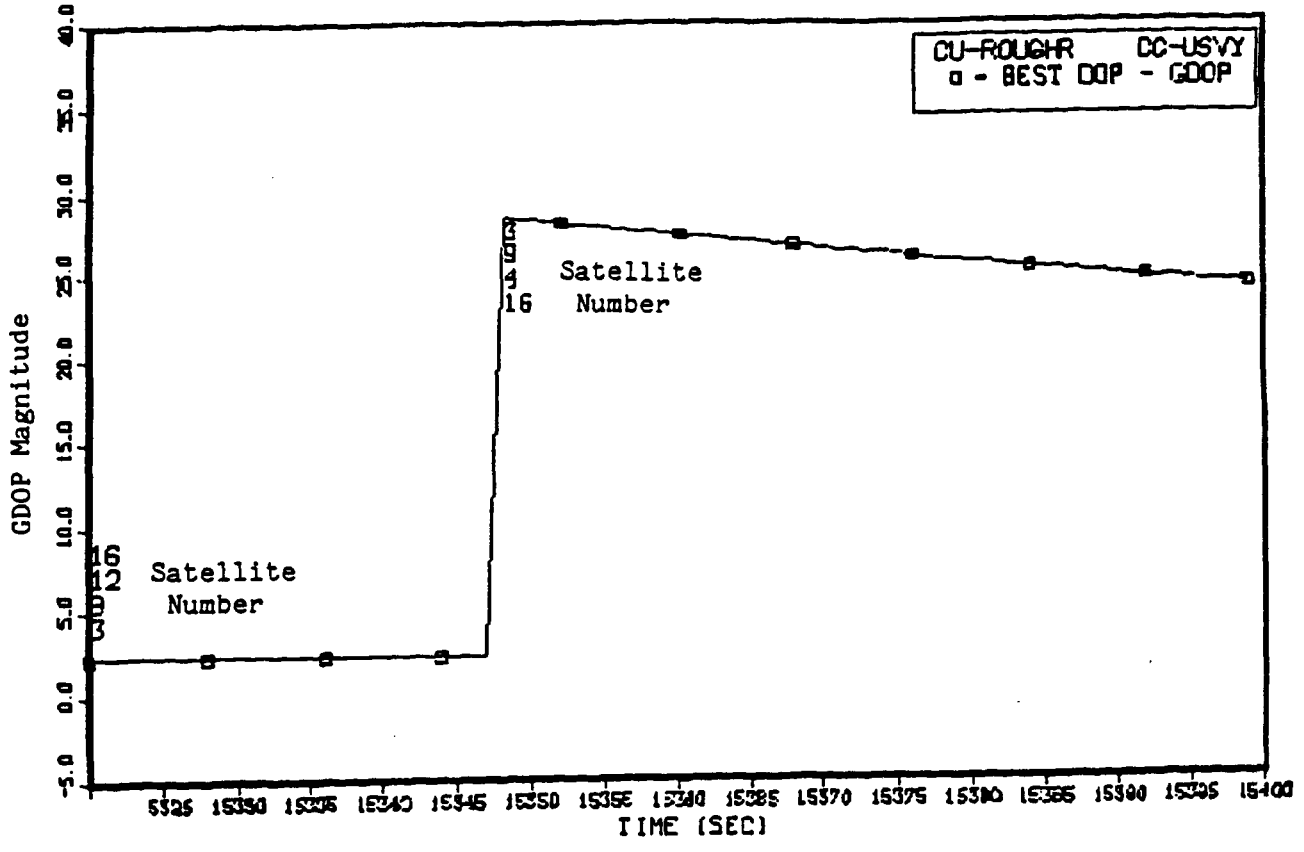

For acronym definition refer to glossary on page vi.

Figure 5-1. GDOP History

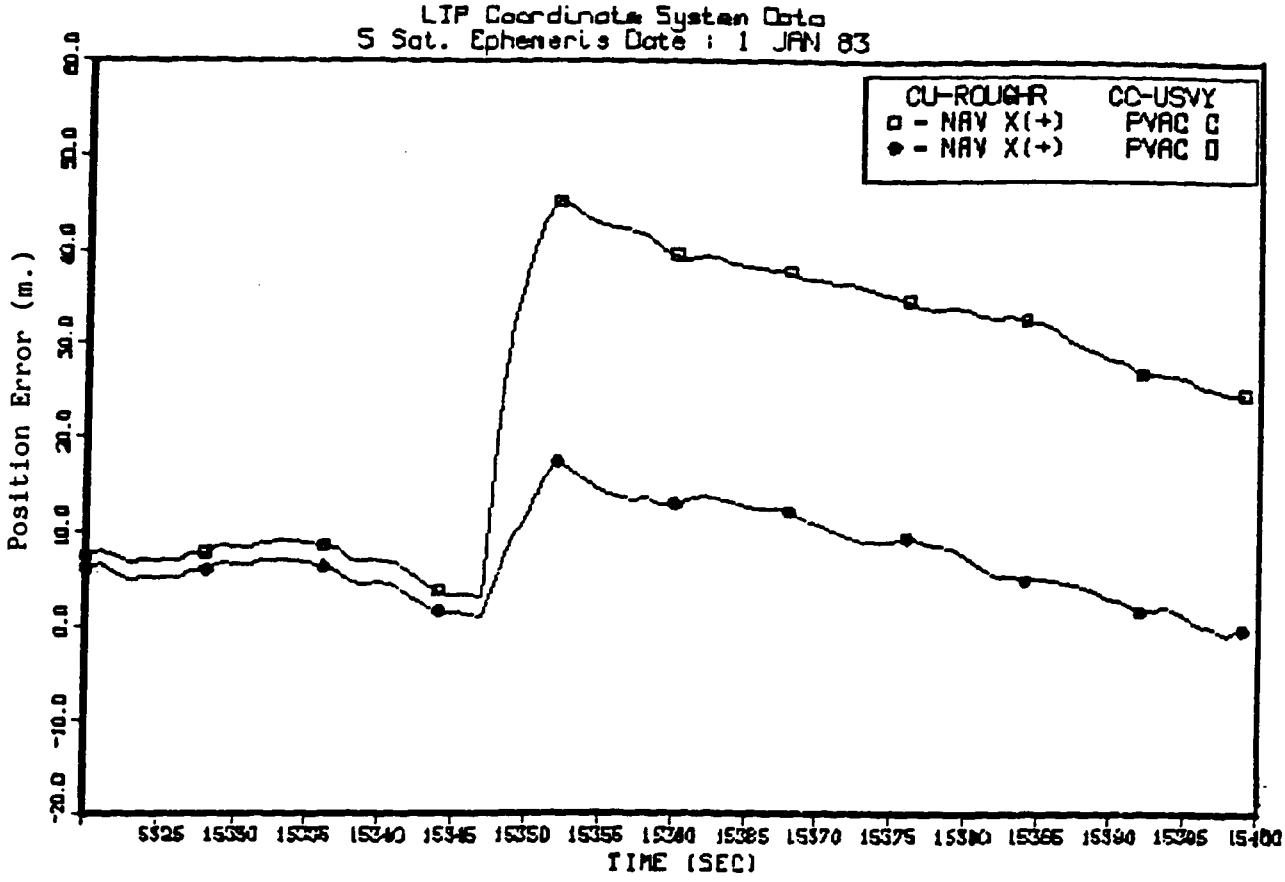

NAV X(+)	PVAC C	:	0.2495E+02,	0.1401E+02,	0.2862E+02
NAV X(+)	PVAC D	:	0.7332E+01,	0.1460E+01,	0.8582E+01

For acronym definition refer to glossary on page vi.

Figure 5-2a. PVAT Filter Performance, X-Axis Degraded PDOP

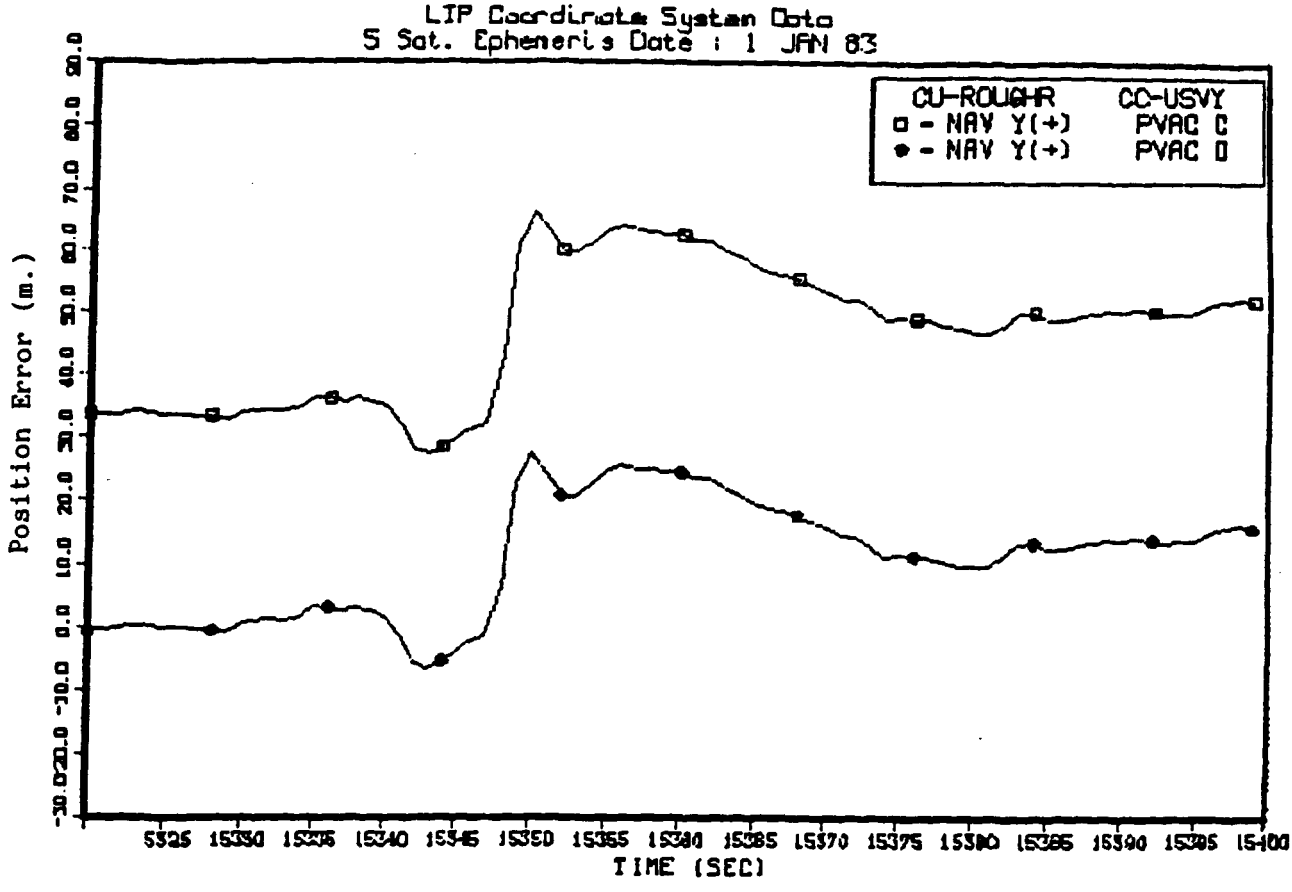

NAV Y(+) PVAC C : 0.4690E+02, 0.1122E+02, 0.4822E+02
NAV Y(+) PVAC D : 0.1077E+02, 0.9277E+01, 0.1421E+02

For acronym definition refer to glossary on page vi.

Figure 5-2b. PVAT Filter Performance, Y-Axis Degraded PDOP

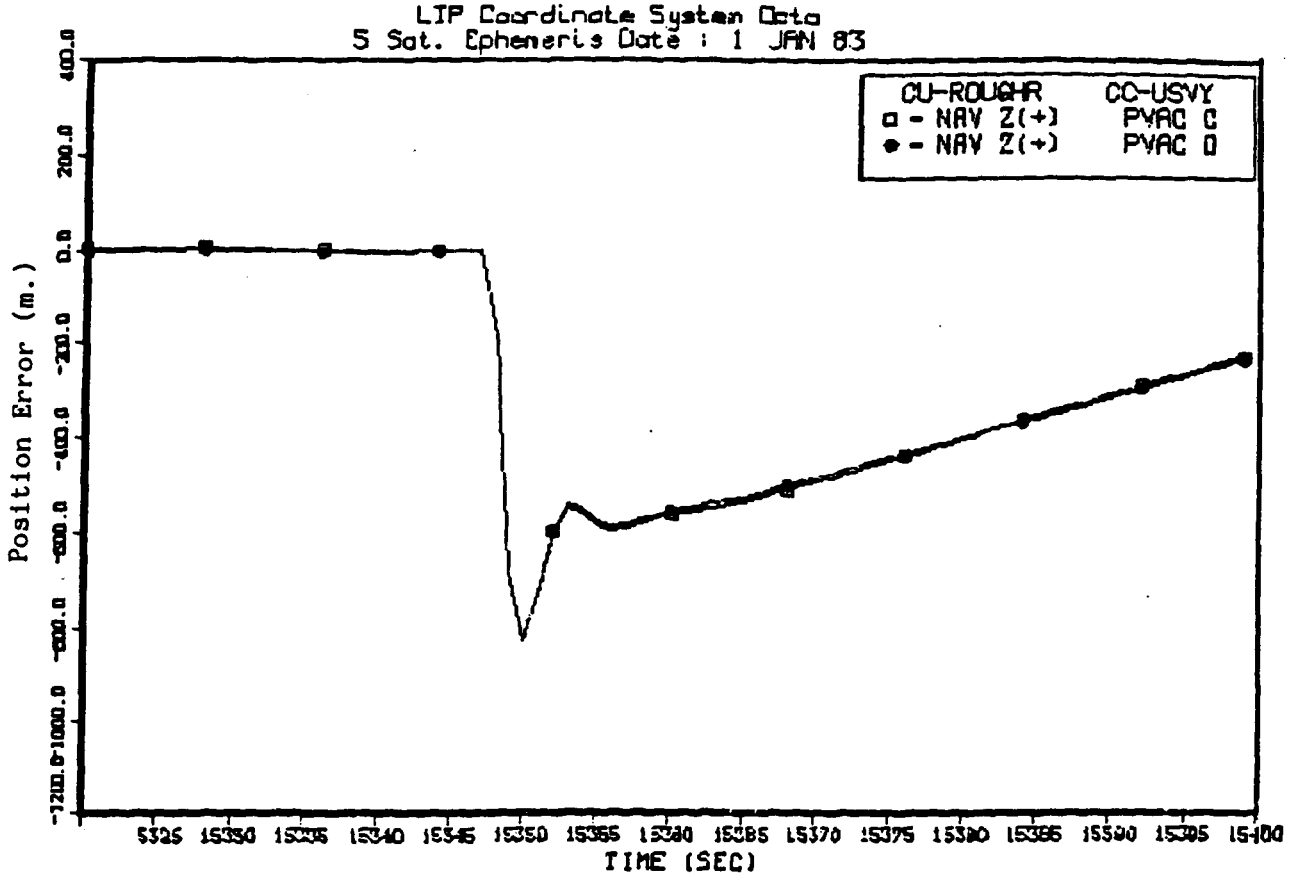

NAV Z(+) PVAC C : -0.2899E+03, 0.2410E+03, 0.3770E+03
NAV Z(+) PVAC D : -0.2896E+03, 0.2368E+03, 0.3741E+03

For acronym definition refer to glossary on page vi.

Figure 5-2c. PVAT Filter Performance, Z-Axis Degraded PDOP

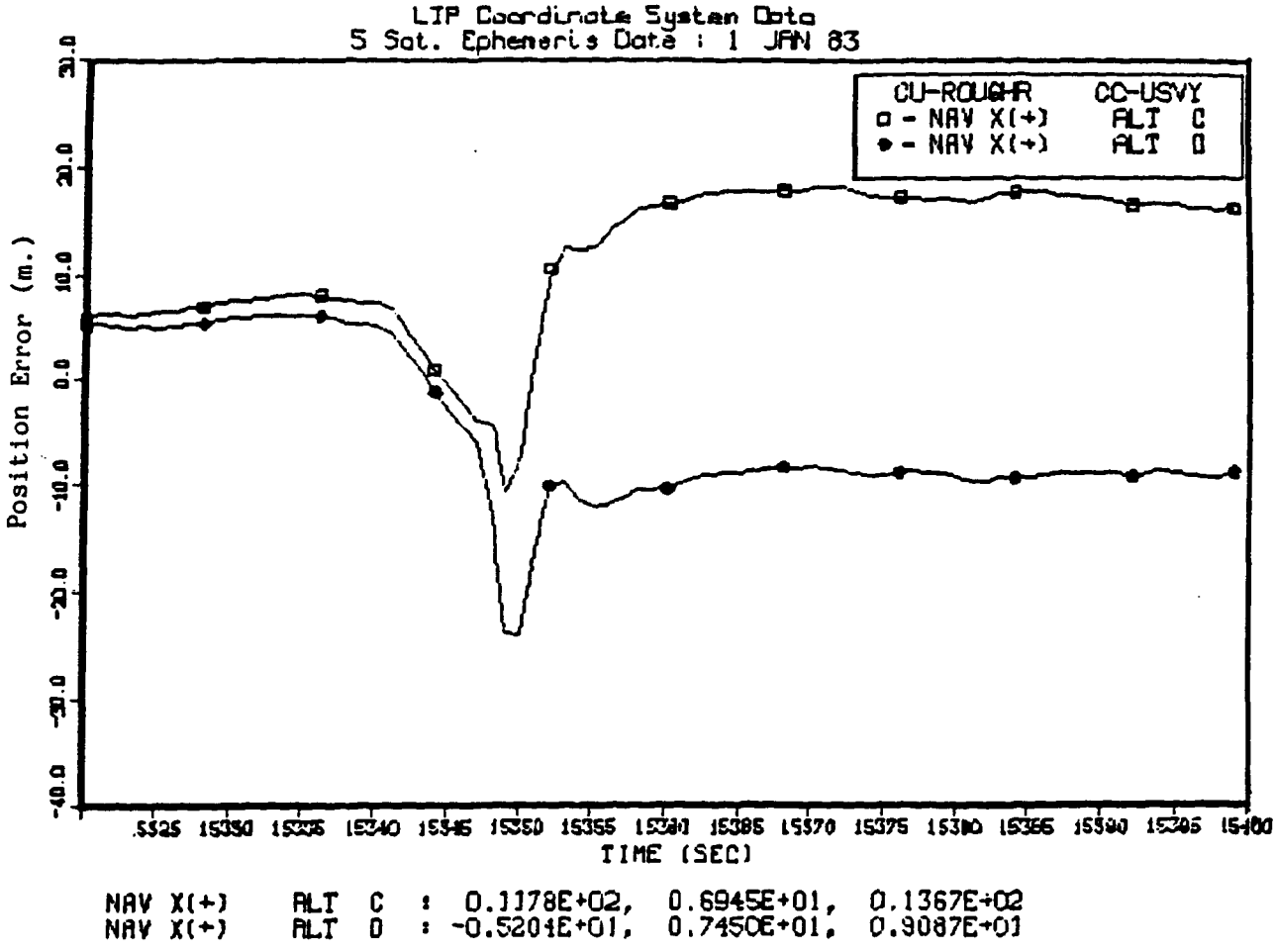

For acronym definition refer to glossary on page vi.

Figure 5-3a. ALT Filter Performance, X-Axis Calibrate Mode

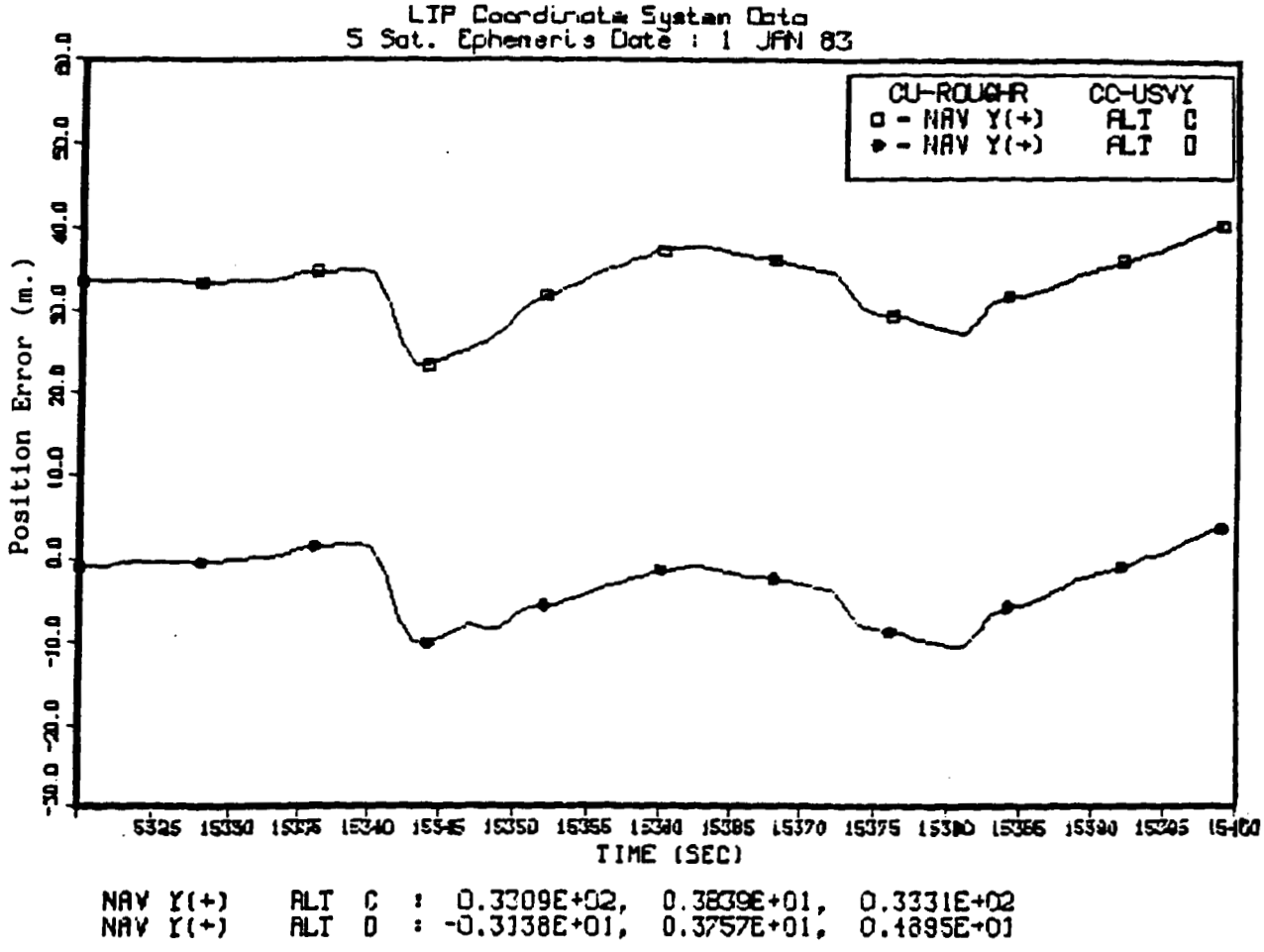

NAV Y(+) ALT C : 0.3309E+02, 0.3839E+01, 0.3331E+02
NAV Y(+) ALT D : -0.3138E+01, 0.3757E+01, 0.4895E+01

For acronym definition refer to glossary on page vi.

Figure 5-3b. ALT Filter Performance, Y-Axis Calibrate Mode

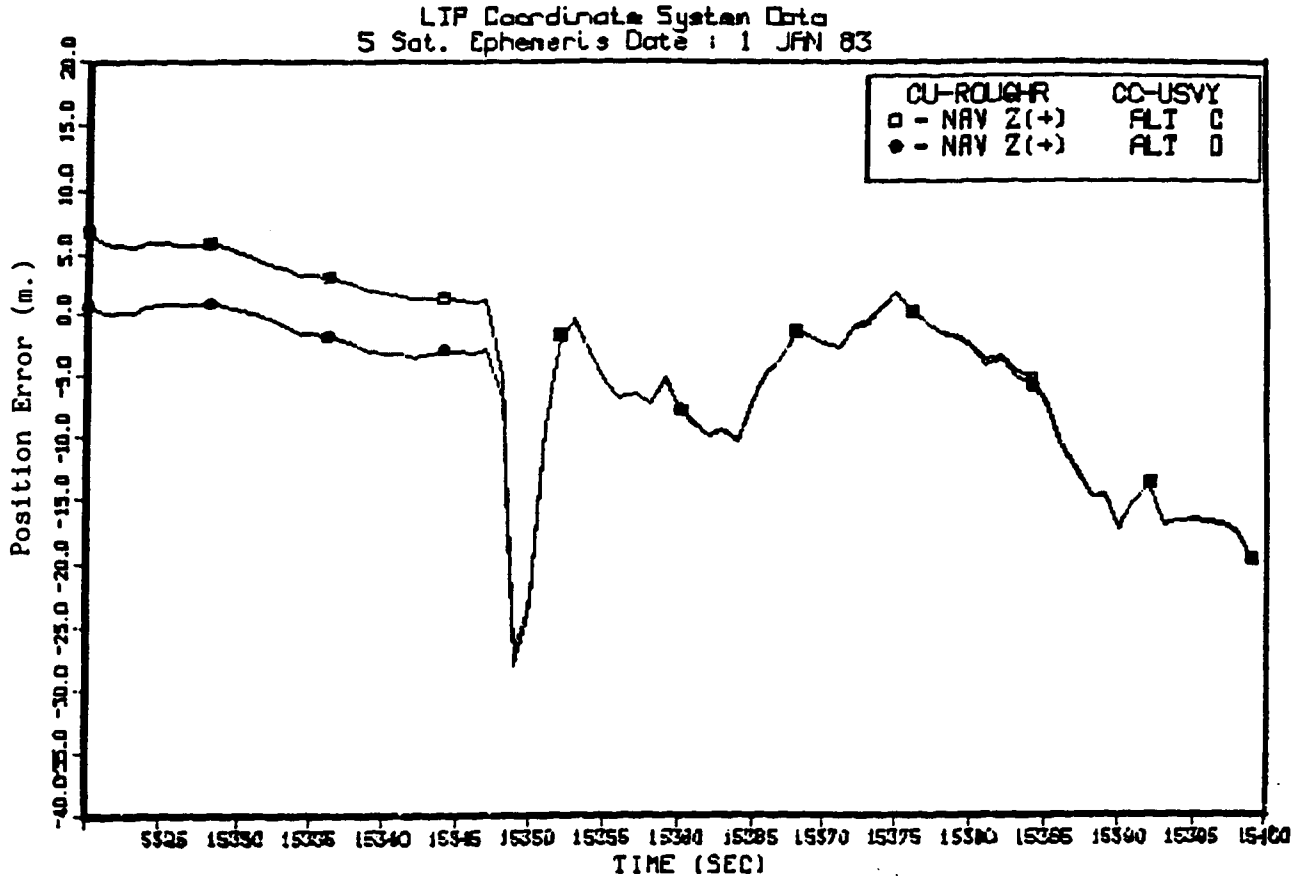

NAV Z(+) ALT C : -0.4012E+01, 0.7860E+01, 0.8824E+01
NAV Z(+) ALT D : -0.5816E+01, 0.6462E+01, 0.8694E+01

For acronym definition refer to glossary on page vi.

Figure 5-3c. ALT Filter Performance, Z-Axis Calibrate Mode

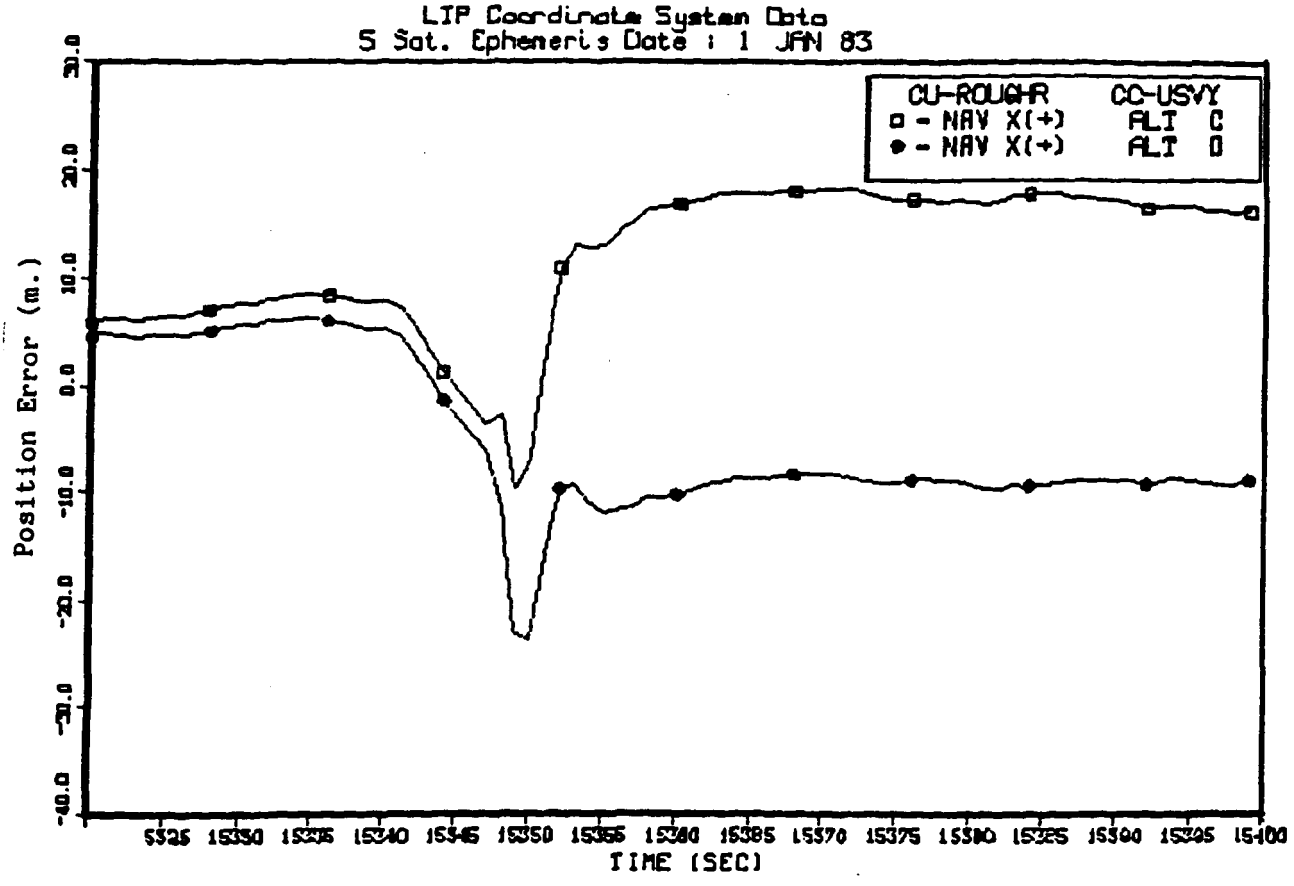

NAV X(+) ALT C : 0.1192E+02, 0.6785E+01, 0.1371E+02
NAV X(+) ALT D : -0.5232E+01, 0.7228E+01, 0.8923E+01

For acronym definition refer to glossary on page vi.

Figure 5-4a. ALT Filter Performance, X-Axis Measurement Mode

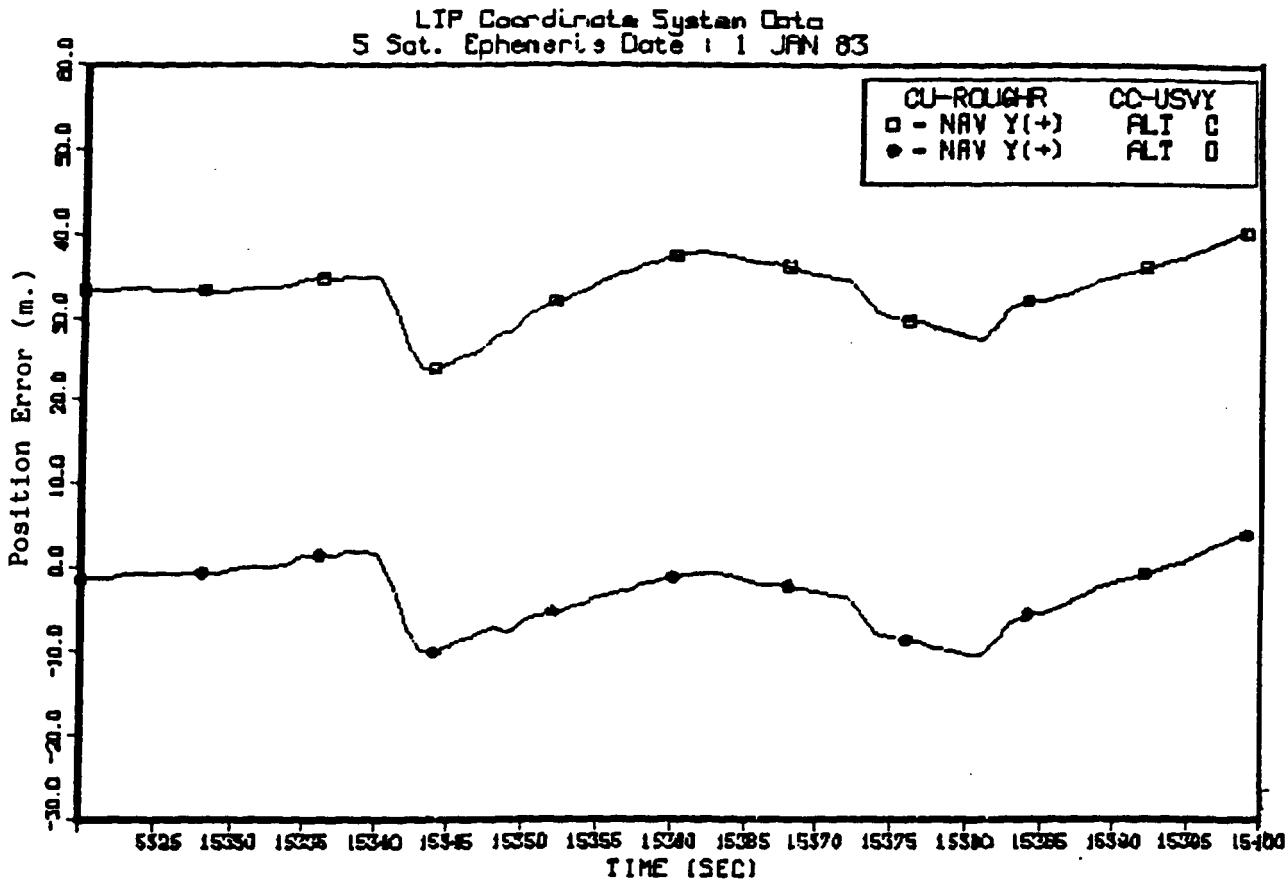

NAV Y(+) ALT C : 0.3316E+02, 0.3776E+01, 0.3337E+02
NAV Y(+) ALT D : -0.3179E+01, 0.3666E+01, 0.4853E+01

For acronym definition refer to glossary on page vi.

Figure 5-4b. ALT Filter Performance, Y-Axis Measurement Mode

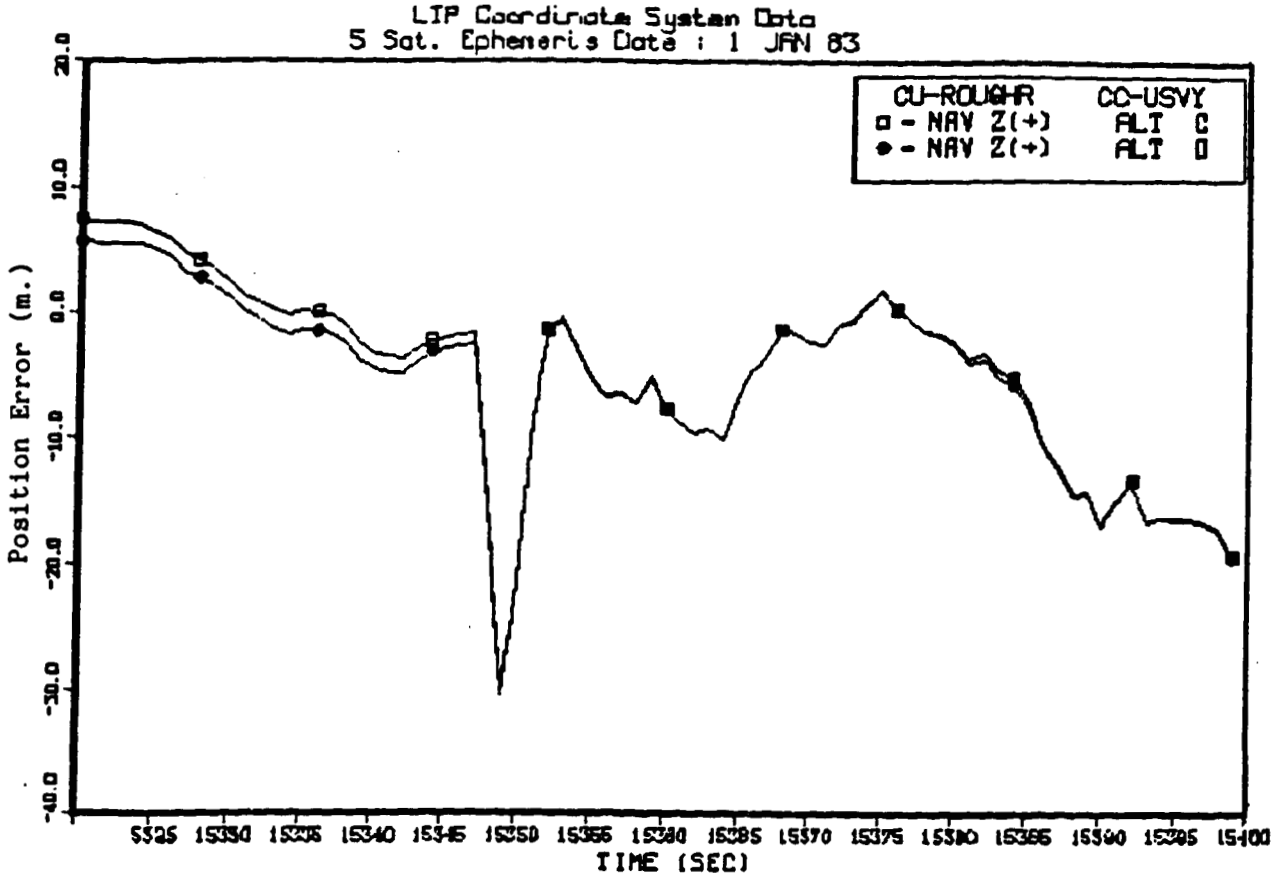

NAV Z(+) ALT C : -0.4735E+01, 0.7567E+01, 0.8927E+01
NAV Z(+) ALT D : -0.5307E+01, 0.7225E+01, 0.8965E+01

For acronym definition refer to glossary on page vi.

Figure 5-4c. ALT Filter Performance, Z-Axis Measurement Mode

RMS and standard deviations of the errors in all axes are provided in Table 5-1 for both the PVAC filter and the PVAC/baroaltimeter filter (in the calibrate mode).

Table 5-1. ALT Filter Performance (Meters), Versus PVAC Filter Performance Constant Acceleration Turn Pattern

		PVAC		ALT	
		RMS	STANDARD DEVIATION	RMS	STANDARD DEVIATION
CONVENTIONAL GPS	x	28.8	14.0	13.7	6.8
	y	48.2	11.2	33.4	3.8
	z	377.0	241.0	8.9	7.6
DIFFERENTIAL GPS	x	8.6	4.5	8.3	7.2
	y	14.2	9.3	4.5	3.7
	z	374.0	237.0	8.4	7.2

Clearly, the performance of the ALT filter is superior, especially in the vertical direction. Differential GPS helps remove the common biases in the measurements for both filters. It is not improving much vertical accuracy of the PVAC filter. This is because the common biases in this direction are small and the geometry is poor (large VDOP). Range errors will therefore translate into large altitude errors. For the ALT filter, the altitude solution will be heavily based on baromeasurements and will therefore be much more accurate. In the PVAC performance to be better, the process noise should be decreased when the DOP is increased so as to rely more heavily on a priori information and less on new GPS measurements. This would be more in line with the corrector filter tuning and should provide for better error cancellation in the differential mode. It is clear, however, that the inclusion of baroaltimeter inputs dramatically improve performance without the need for adaptive process noise features.

The ALT filter performance is studied further in the next section using a landing type profile.

5.2 INERTIAL COMPONENTS

Although inertial sensors were not modeled and simulated in this effort, because of their potentially large contribution to an integrated GPS landing guidance system, conceptual analysis was performed. Use of inertial sensors could substantially change the modeling used by the Kalman filter processing the GPS measurements, for example.

The inertial sensors considered here are of the "low cost" variety, that is, not including complete stabilized platform (inertial navigation system) configurations. Instead, the emphasis is on isolated accelerometers and gyros.

Since the major objective in a GPS-based landing guidance system is to reduce the vertical component of error, the logical choice is to incorporate a vertical accelerometer. The vertical accelerometer outputs precise changes in velocity, so it would provide an excellent source of information about motion in a "vertical" direction. Roll and pitch motions of the aircraft would distort this output as a measure of local level vertical, but since only the landing domain is of interest in this design, such effects would be minimal. For example, a 10° bank angle (reasonably severe maneuver in a typical final approach) would resolve a .2 g local level axis-vertical maneuver (again reasonably severe) into an erroneous .203 g vertical maneuver. Similarly, a flat 10° bank turn maneuver would be interpreted as a little over 1/100 of a g climb. Appropriate modeling and weighing in the Kalman filter would not respond to these small values for short durations.

To incorporate a single vertical accelerometer in an integrated GPS Kalman filter, several options are available. The accelerometer error states (e.g., bias and scale factor) could be modeled in the state vector, enhancing the accuracy of the delta velocity information while increasing the dimensionality of the processing and therefore processing load. Such modeling is frequently used in full INS/GPS integration, but the major objectives for such applications are long term stability, constant calibration for GPS outages, and stability of information under maneuvering conditions for precise carrier loop aiding (doppler prediction). For this application, most of these objectives are not relevant.

Alternatively, the small accelerometer errors which impact this application only in a short term sense can be ignored and handled by a small amount of process noise. The delta velocity output is used to propagate the vertical velocity state of the filter between measurement updates instead of the acceleration modeling studied in the earlier sections of this report. Note the significance of this concept; the acceleration measurement from the accelerometer is likely to be far superior to any <u>a priori</u> model or computation, and yet the state vector can actually be reduced in size by eliminating the vertical acceleration state (since it is known so need not be estimated). In fact, it may also be inconsequential to model lateral accelerations as well given that the vertical axis of concern is well modeled.

Extending this concept, a couple or triad of accelerometers could be used to measure the other axis or axes. Small mounting errors could be adequately handled by a small amount of process noise.

Use of other on-board instruments could be made to further resolve the accelerometer outputs, especially if performance in dynamics is important. The attitude indicator provides a fairly good steady-state bank and pitch attitude. This would be easy to integrate if digital outputs were available with sufficient resolution, latency, and time tag accuracy.

These various concepts provide several possible low cost enhancements to stand-alone GPS operation. Their relative benefits and practical significance must be determined by simulation and eventual flight test.

VI. APPROACH AND LANDING SIMULATION

To create a realistic landing scenario for the DIFFGPS Monte Carlo Simulation, a landing path was devised that emulated an actual manual helicopter landing approach. The objective was to accurately model the dynamics of a manual approach. Accuracy of the dynamics was important since the GPS filter modifications were designed to model essentially constant acceleration dynamics which may or may not be true of the actual approach path.

6.1 DEVELOPMENT OF SIMULATED LANDING PATH

An accurate simulation could be produced by explicitly modeling a helicopter, instrument landing system, and closed loop pilot, of course. However, it was felt that the complexity of such a model, along with the difficulty in tuning the aircraft and pilot models, was excessive for this effort.

Instead, an analysis was made of manual helicopter landing data and a mathematical description of the profile was devised. Figure 6-1 shows a sample of the landing data from Reference 5. These tracking data were gathered during NASA Beacon Landing System tests on an SH-3 helicopter. Other example data included helicopter MLS Approaches and curved approach tests. Analysis of the data in Figure 6-1 reveals a basic oscillatory pattern about the glidepath, particularly in the lateral axis. The vertical axis exhibits some of these oscillations although less pronounced and more heavily damped.

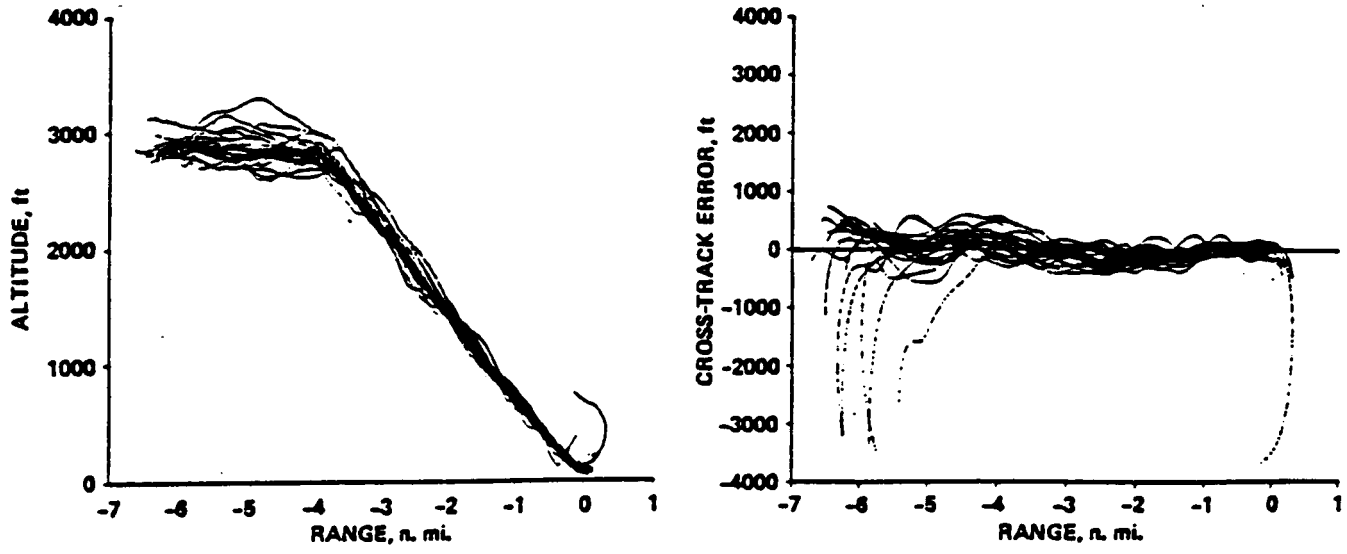

Figure 6-1. Actual Helicopter Landing Tracking Data

Based on these data, a "randomized" sinusoidal path motion was selected in the lateral and vertical axes. The form of the model (for the lateral case) was:

$$y(x) = Ae^{Bx} \sin(Cxe^{Dx} + E) + F$$

where

A, B, C, D are exponentially correlated random variables
E is a constant randomly initialized
F is a Gaussian random variable for gust term

Note that both the period and the amplitude of the sinusoid were allowed to randomly adjust, of course ensuring that the path was nevertheless continuous. The period and amplitude of the motion were also designed to generally reduce in magnitude as the approach neared touchdown, again consistent with the appearance of the data.

To calculate the parameters in the models, coarse measurements were made of the period and amplitude of the glidepath deviations at each end of the approach for both the horizontal and vertical axes. These data are shown in Table 6-1. Note that any bias in the glidepath deviation was ignored; it is not significant in determining aircraft dynamics during approach for small values. The final lateral and longitudinal path equations were:

$$f(x) = Ae^{Bx} \sin(Cxe^{Dx} + E) + F$$

For A, B, C, D, E:

$$x = xe^{-G/G_o \Delta+} + \sigma_x \sqrt{1 - e^{-26/G_o \Delta+}}\, N(0,1)$$

where the values are:

	Lateral	Vertical
σ_A	80 90	17 21.4
G_A	1	1
G_{OA}	3040	3040
$\bar{B}$	.0000153	.0000228
σ_B	.0000031	.0000047

	Lateral	Vertical
G_B	1	1
G_{OB}	50	50
$\bar{C}$	.0032	.004
σ_C	.00064	.0008
G_C	1	1
G_{OC}	1500	1500
$\bar{D}$	-.0000224	-.0000224
σ_D	.00002	.00002
G_D	1	1
G_{OD}	3040	3040
E	u(-3.14,3.14)	u(-3.14,3.14)
F	N(0,1)	N(0,2)

Velocity was also modulated along the path to approximate a pilot/aircraft response when maneuvering vertically. This was modeled as "speed along the path" for trajectory propagation purposes:

$$V(x) = \begin{cases} V(x-1)+N(0,.5) & x > .75D \\ V(x-1)+32.2\left[\frac{z(x-1)-z(x)}{(x-1)-x} - \tan 6°\right] & x \leq .75D \\ V_o = 135 \text{ ft/sec} & \end{cases}$$

where:

x is distance along path
D is total approach path distance (i.e., glideslope starts at .75D)

While it can be argued that this model is not an exact representation of the observed data, the fact that the match is approximate, the dynamics have infinite derivatives, and the randomness induced should provide more than adequate "realism" for the Kalman filter attempting to follow this motion. Figures 6-2 and 6-3 present plots of 10 approaches in each axis which can be favorably compared with the recorded actual data of Figure 6-1 (again noting the absence of glidepath bias errors in the simulated data).

Table 6-1. Path Dynamics for Landing Data

	Beginning of Approach			End of Approach		
	Peak-Peak Oscillation	Standard Deviation (2s)	Period	Peak-Peak Oscillation	Standard Deviation (2s)	Period
Vertical	102	156	3541	47	63	1672
Horizontal	313	406	4459	188	141	2108

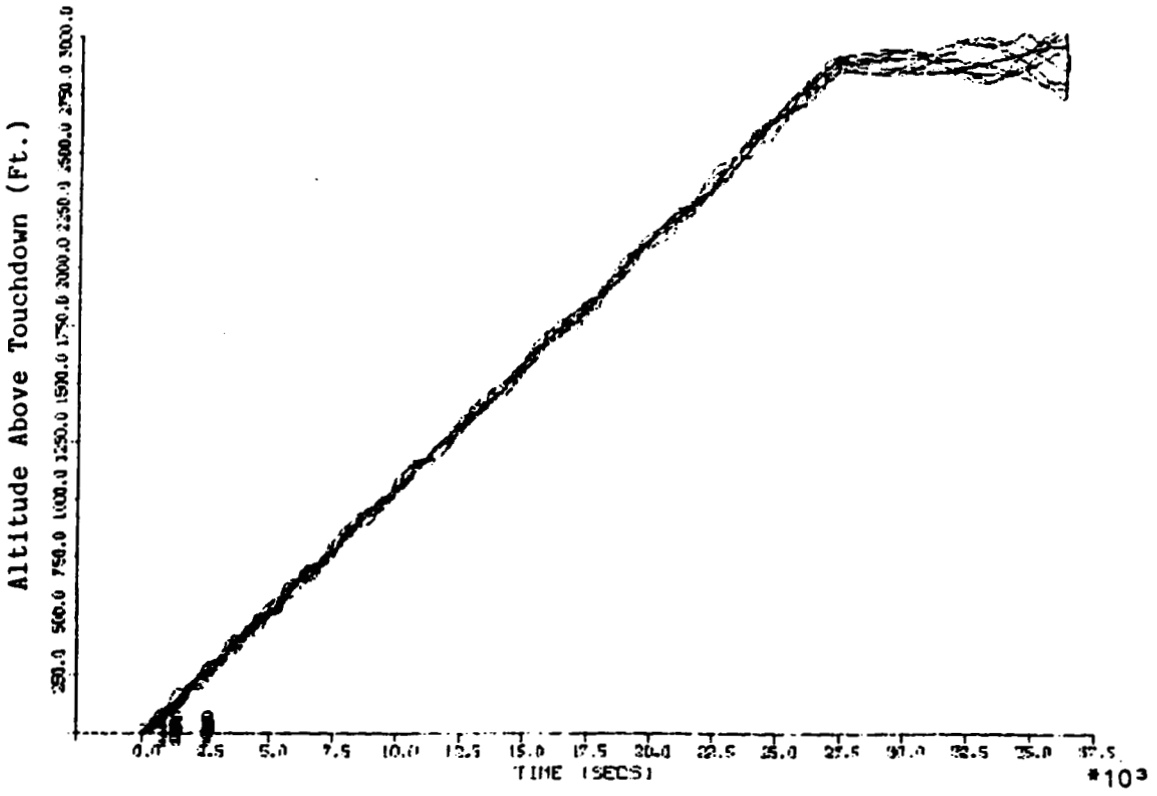

Figure 6-2. Vertical Axis Simulated Landing Approaches

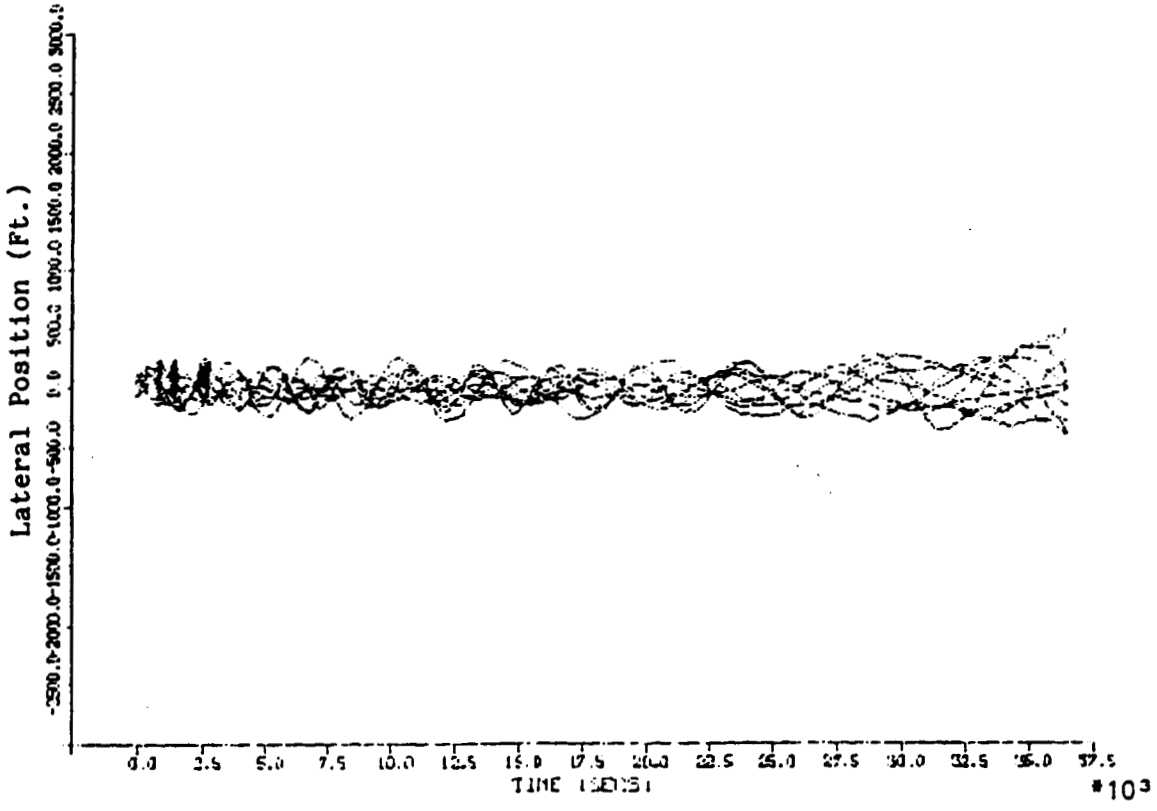

Figure 6-3. Horizontal Axis Simulated Landing Approaches

6.2 LANDING SIMULATION FILTER PERFORMANCE

The flight path described in the previous section was used to test the filters designed earlier in this study, namely, the PV, PVAC, PVAT, and ALT filters. The filters were tuned for a level Constant Acceleration Turn pattern and their performance was descussed in Sections 3 and 5. In the landing simulation, the vehicle experiences more dynamics (of a sinusoidal nature) in all axes. Although we found out that the PVAC filter was probably the best choice for the Constant Acceleration Turn pattern, it is possible that the PV filter will perform just as well for the landing path. This is because of the continuously changing acceleration (in a sinusoidal way). Modeling of the acceleration as constant or even centripetal will result in filter lagging and could degrade performance as compared to the PV filter. In the next sections, performance of the filters is compared, and the results of Monte Carlo runs are provided.

6.2.1 PV, PVAC, PVAT Filters Comparisons

The landing profile described in Section 6.1 was flown with the PV, PVAC, and PVAT filters. Three cases were tested for the PVAT filter; constant process noise matrix Q, variable matrix Q, and adaptive matrix Q. Results are provided in Tables 6-2 through 6-4 and in Figures 6-4 through 6-8.

The PVAC filter, as for the constant acceleration turn, out performs the PV filter in both the conventional and differential modes. The advantage is most pronounced in the East direction (lateral motion) with a 44% improvement in standard deviation in the conventional mode and a 35% improvement in the differential mode. At the RMS level, a 30% improvement is achieved in the East direction for the differential mode, with only a 5% improvement in the conventional mode. In the North directions, a small improvement is achieved with the PVAC while in the vertical direction the performance is even.

The various PVAT filters perform pretty much identically. Their accuracy is similar to that achieved with the PVAC filter. Although the PVAC performance is better than that achieved with the PV filter, the improvement is not as large as was obtained on the Constant Acceleration Turn pattern. This is because the acceleration vector is continuously changing (in a sinusoidal way) for the landing pattern, and the estimate of acceleration will therefore always be lagging, thereby reducing the performance improvement over the PV filter.

Table 6-2. PV Filter Performance (Meters) Landing Profile

		RMS	Standard Deviation
Conventional GPS	East	17.3	6.6
	North	17.3	6.8
	Up	7.1	4.0
Differential GPS	East	7.5	6.5
	North	9.5	7.8
	Up	4.2	4.2

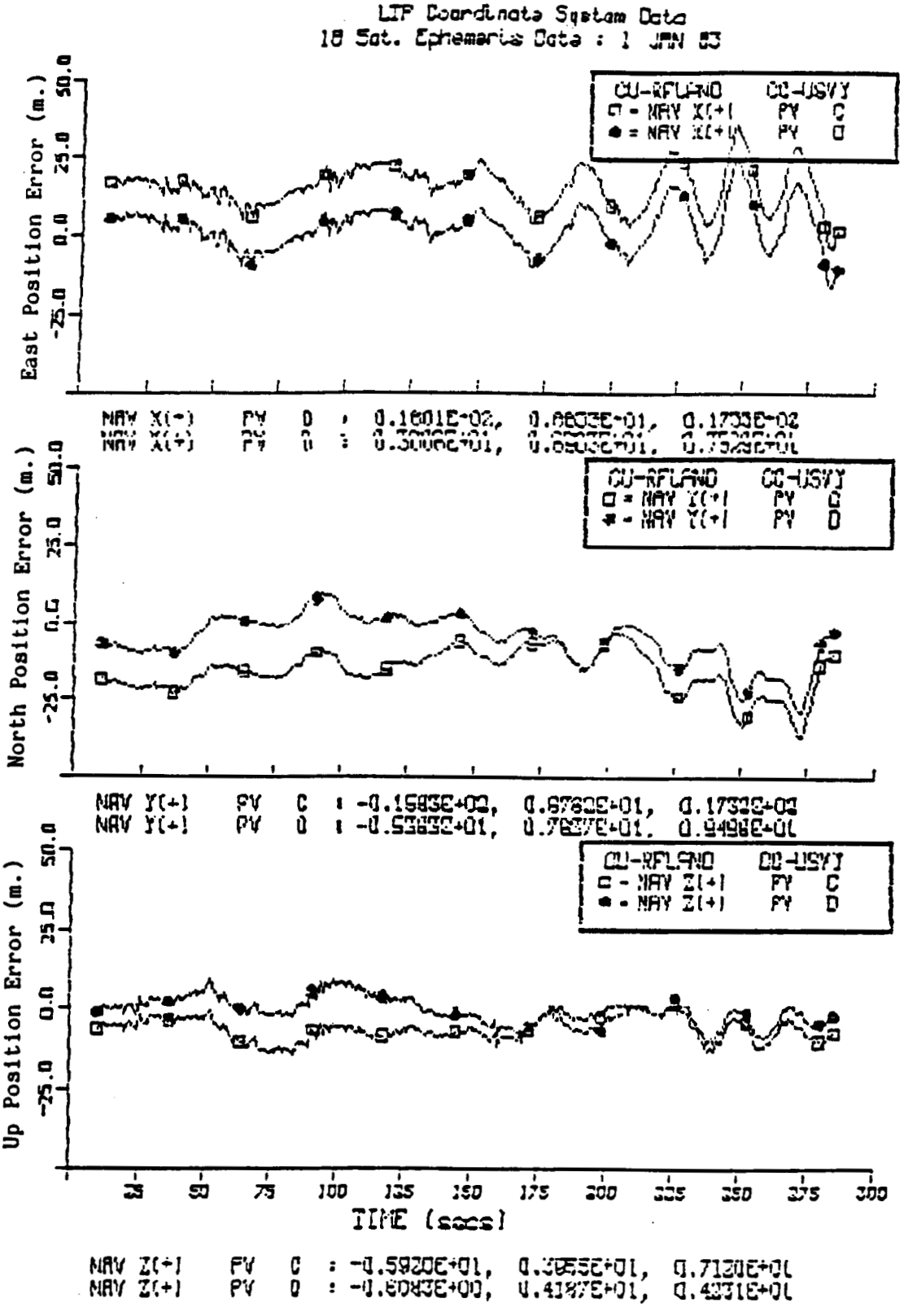

For acronym definition refer to glossary on page vi.

Figure 6-4. FV Filter Performance Landing Profile

Table 6-3. PVAC Filter Performance (Meters) Landing Profile

		RMS	Standard Deviation
Conventional GPS	East	16.5	3.7
	North	16.6	6.5
	Up	7.1	4.1
Differential GPS	East	5.2	4.2
	North	8.7	7.3
	Up	4.2	4.1

Table 6-4. PVAT Filter Performance (Meters) Landing Profile

		RMS			Standard Deviation		
		Constant Q	Variable Q	Adaptive Q	Constant Q	Variable Q	Adaptive Q
Conventional GPS	East	16.5	16.5	16.4	3.7	3.7	3.5
	North	16.8	16.9	16.7	6.7	6.5	6.5
	Up	7.1	7.1	7.7	4.1	4.1	4.6
Differential GPS	East	5.2	5.2	5.1	4.2	4.2	4.1
	North	8.8	8.8	8.5	7.4	7.2	7.0
	Up	4.2	4.2	4.5	4.1	4.1	4.4

In order to generate more meaningful statistical data on the filters performance, ten Monte Carlo runs were performed on the PV, PVAC, and PVAT (Constant Q) filters. Results are reported in Section 6.2.3.

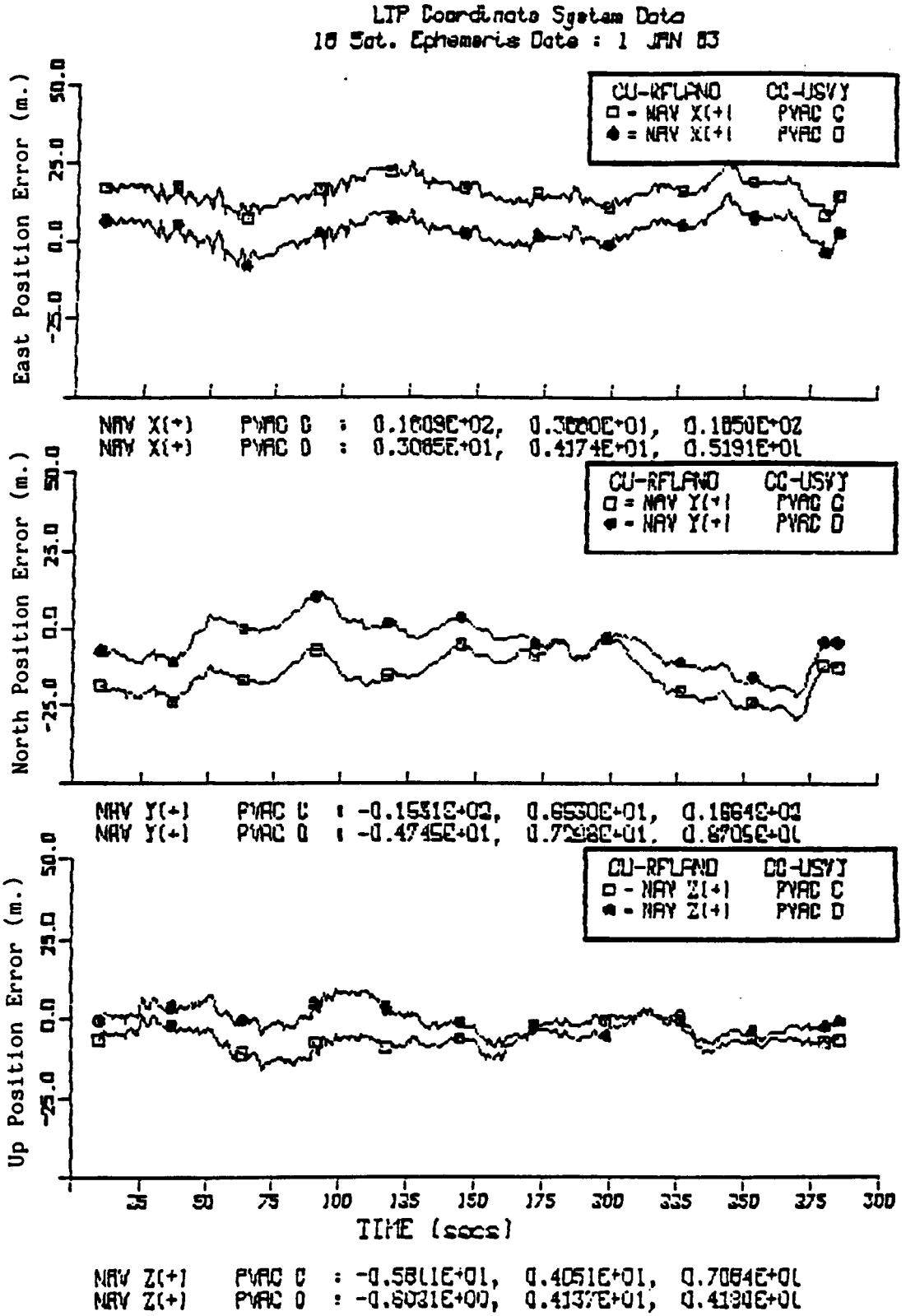

For acronym definition refer to glossary on page vi.

Figure 6-5. PVAC Filter Performance Landing Profile

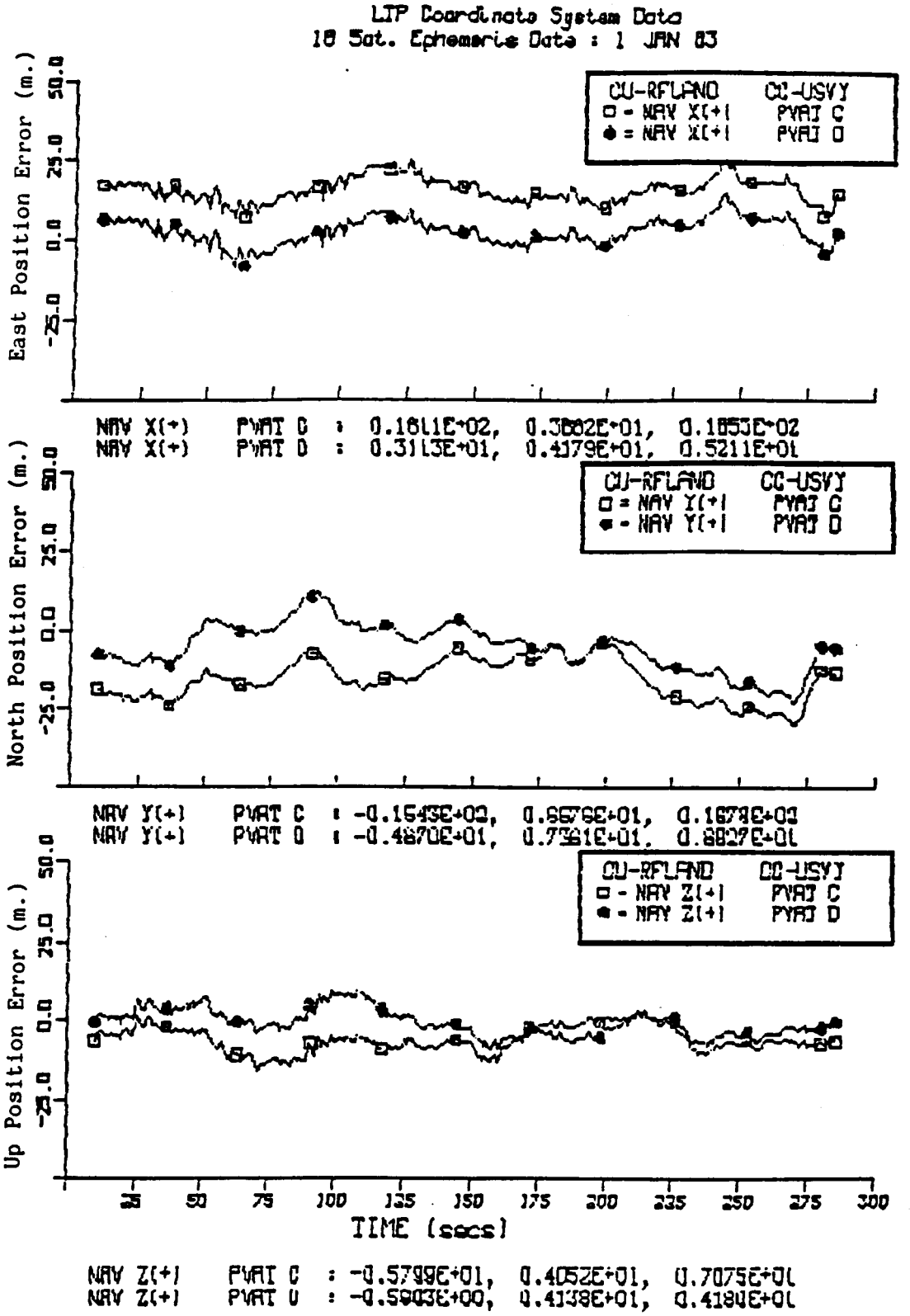

For acronym definition refer to glossary on page vi.

Figure 6-6. PVAT (Constant Q) Filter Performance Landing Profile

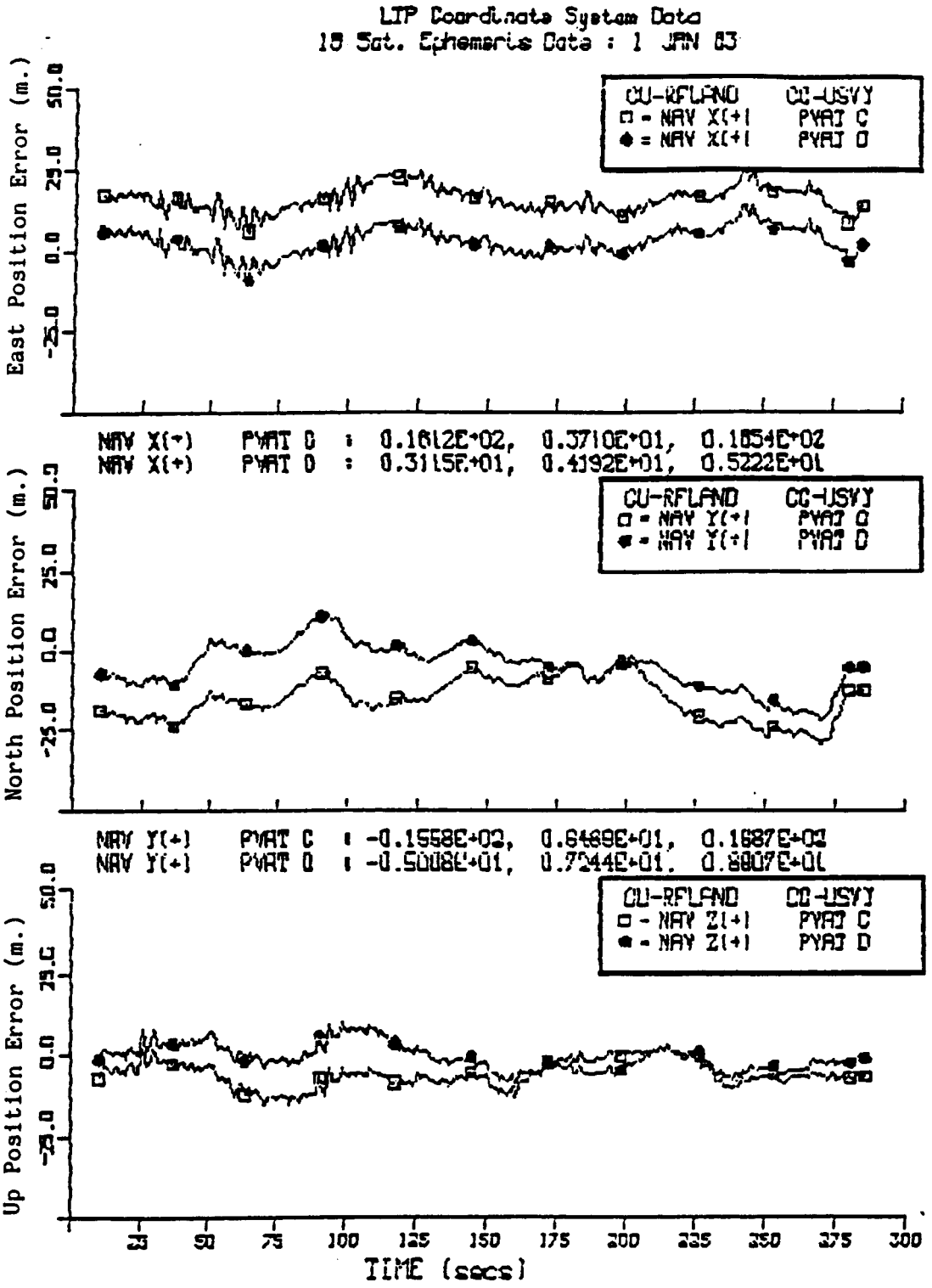

For acronym definition refer to glossary on page vi.

Figure 6-7. PVAT (Variable Q) Filter Performance Landing Profile

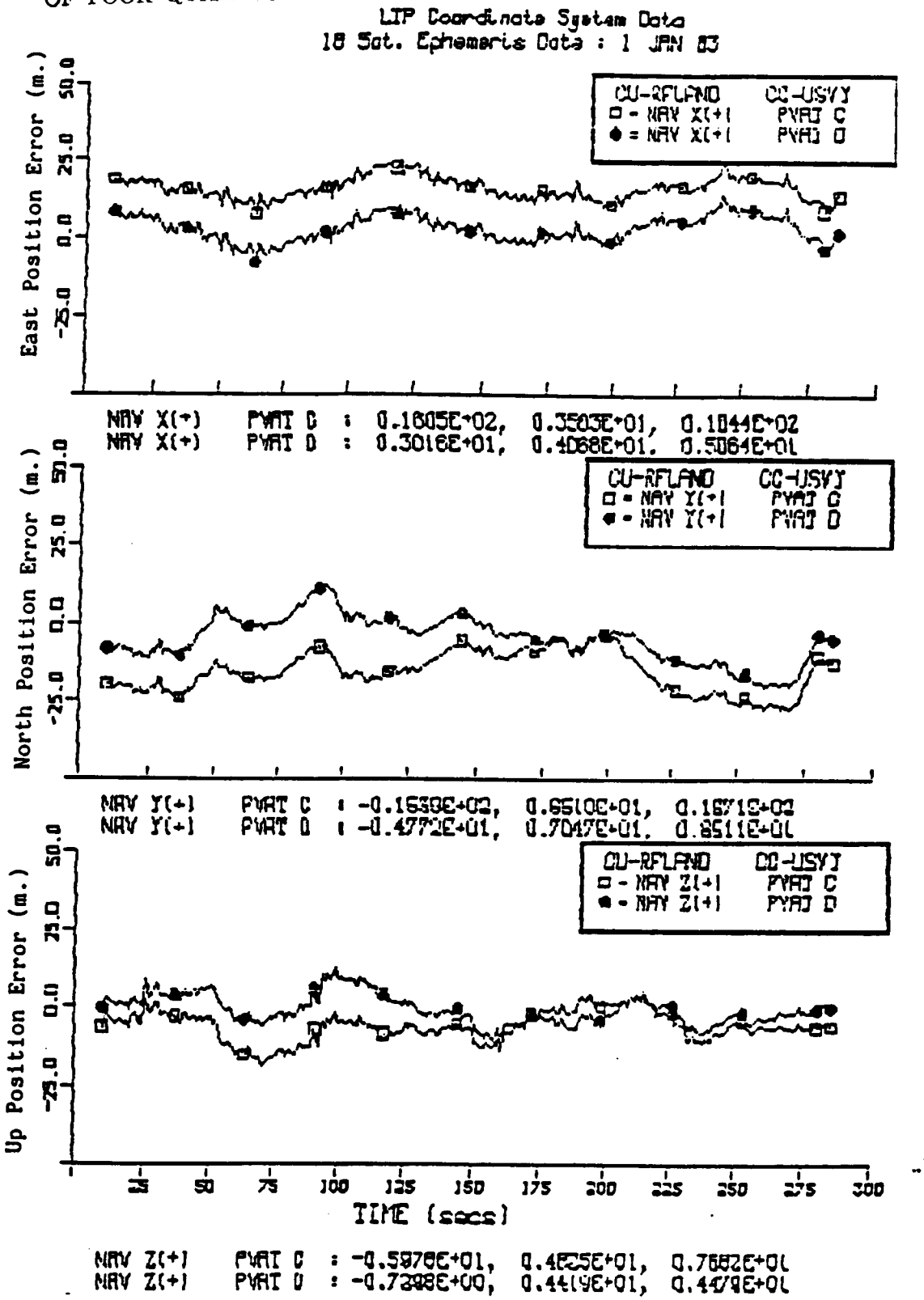

For acronym definition refer to glossary on page vi.

Figure 6-8. PVAT (Adaptive Q) Filter Performance Landing Profile

6.2.2 ALT Filter Performance

The ALT filter developed for the Constant Acceleration Turn pattern was run over the landing profile and for the same degraded DOP condition as was used for the Constant Acceleration Turn pattern. As a comparison, the PVAC filter was run under the same conditions. Position errors are shown in Figure 6-9 for the PVAC filter, Figure 6-10 for the ALT filter, and Figure 6-11 for the reference receiver filter. The GDOP history is shown in Figure 6-12. Performance comparisons are shown in Tables 6-5 and 6-6.

The performance degradation at the GDOP transition is clearly visible for the PVAC filter as the errors grow very large, especially in the vertical direction. The degradation is more subtle for the ALT filter, and although the altimeter helps substantially at the GDOP transition, the vertical accuracy degrades to 100 m error. Additional filter tuning in the vertical direction is probably required to enhance further the baro inputs over the GPS measurements and the system modeling.

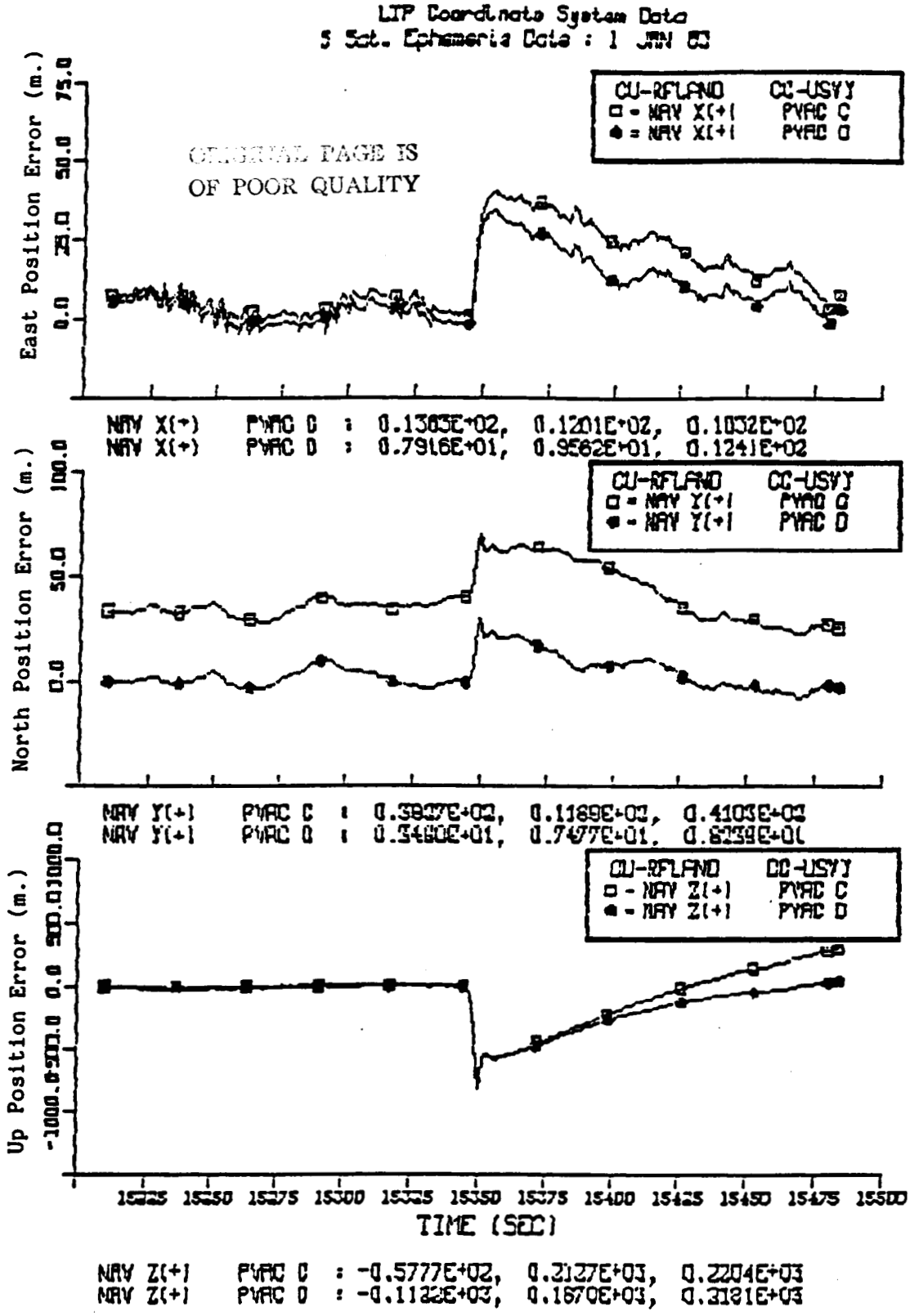

For acronym definition refer to glossary on page vi.

Figure 6-9. PVAC Filter Performance, Degraded DOP, Landing Profile

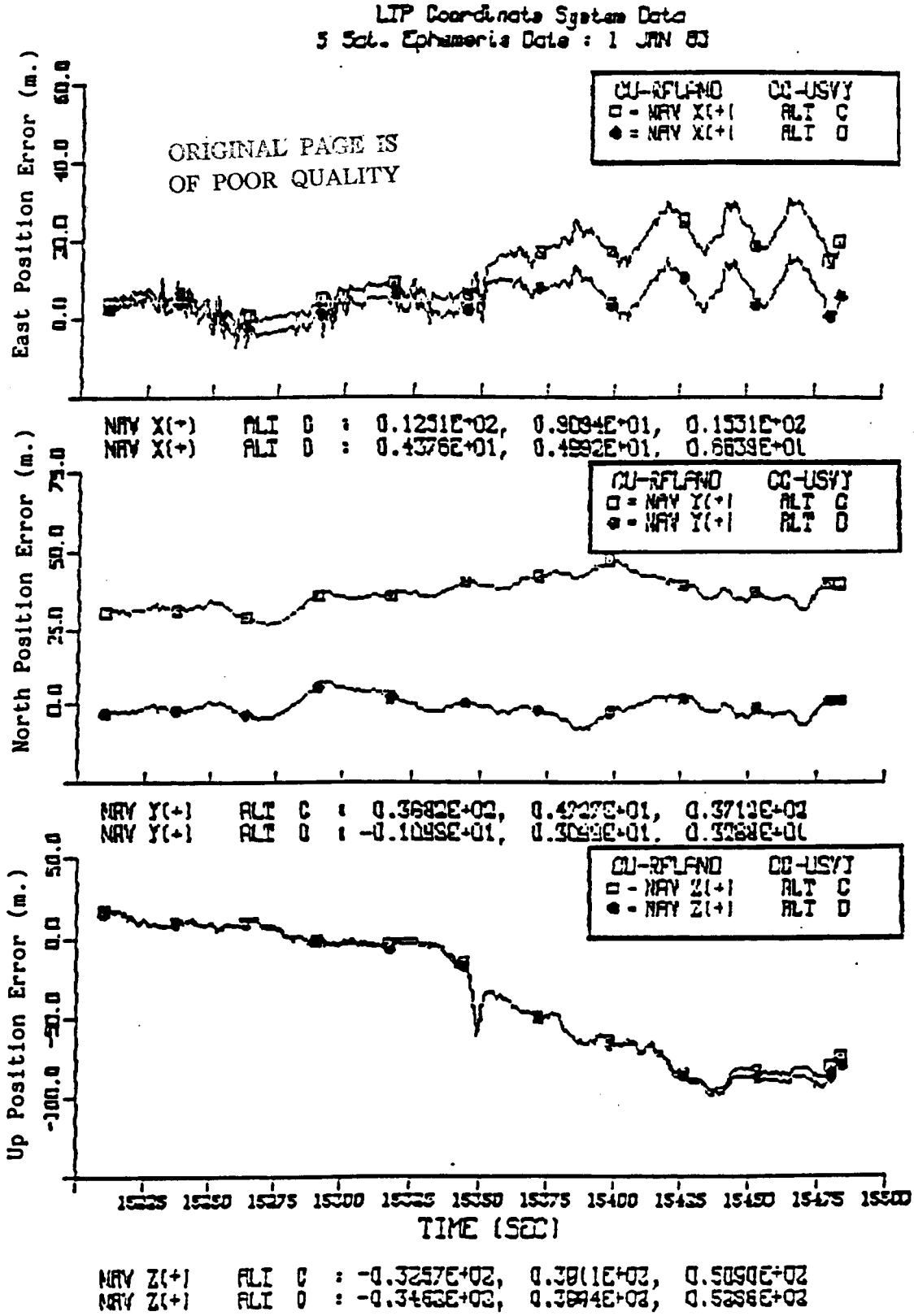

For acronym definition refer to glossary on page vi.

Figure 6-10. ALT Filter Performance, Degraded DOP, Landing Profile

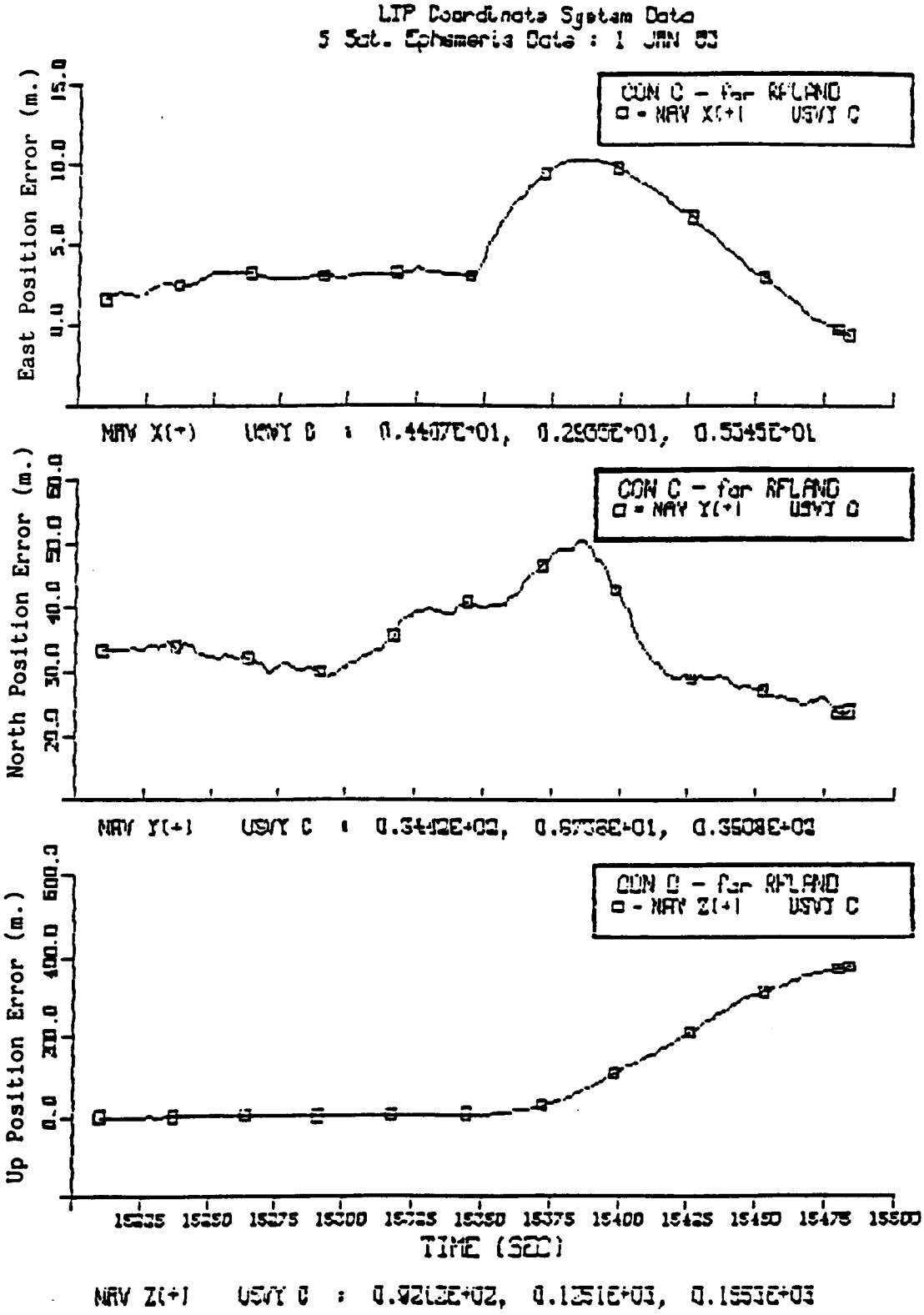

For acronym definition refer to glossary on page vi.

Figure 6-11. Reference Receiver Filter Performance, Degraded DOP

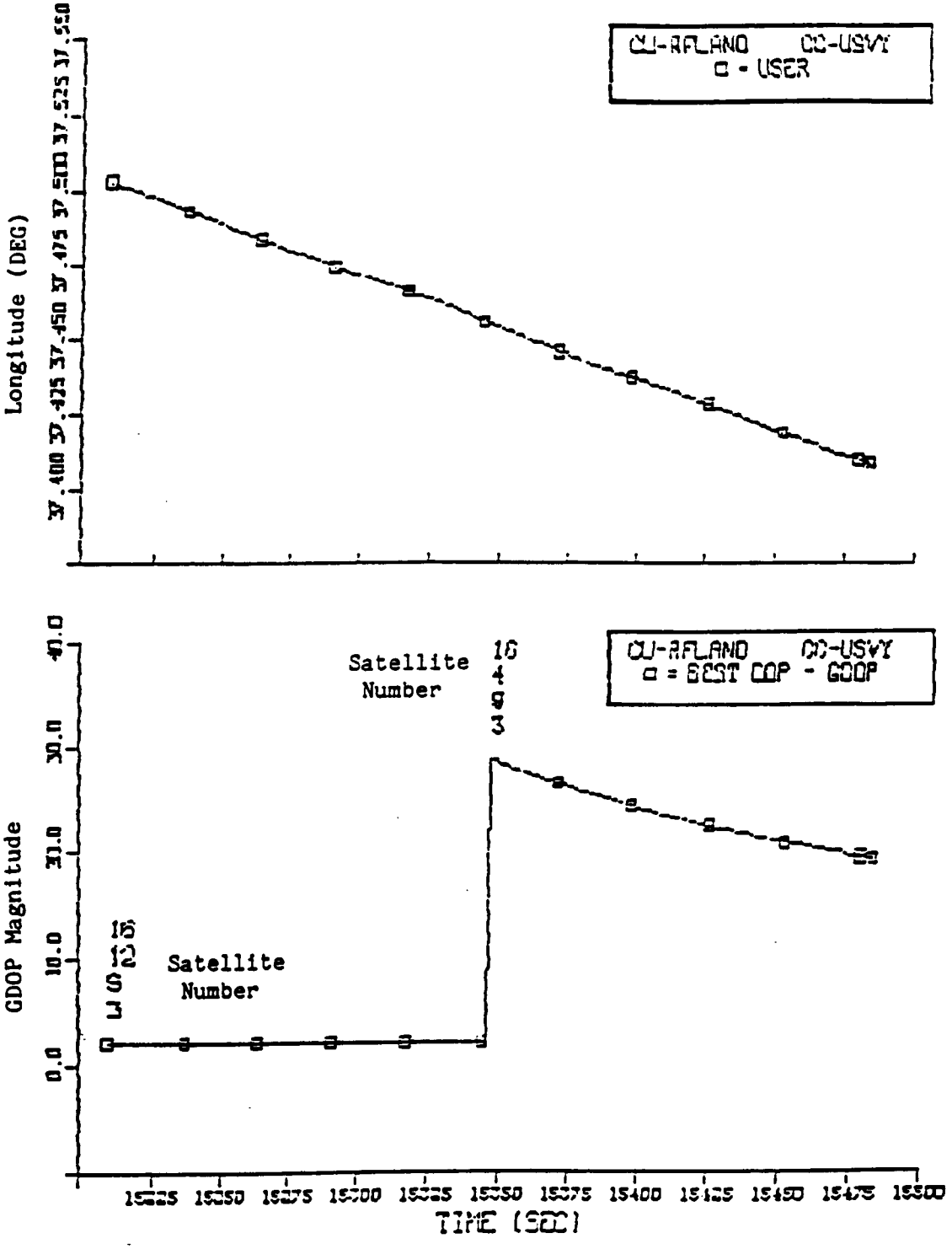

For acronym definition refer to glossary on page vi.

Figure 6-12. Landing Profile and GDOP History

Table 6-5. PVAC Filter Performance (Meters) Landing Profile Degraded DOP

		RMS	Standard Deviation
Conventional GPS	East	18.3	12.0
	North	41.3	11.9
	Up	220.4	212.7
Differential GPS	East	12.4	9.6
	North	8.2	7.5
	Up	218.1	167.0

Table 6-6. ALT Filter Performance (Meters) Landing Profile Degraded DOP

		RMS	Standard Deviation
Conventional GPS	East	15.3	9.1
	North	37.1	4.7
	Up	50.9	38.1
Differential GPS	East	6.6	5.0
	North	3.3	3.1
	Up	53.9	36.9

6.2.3 Monte Carlo Runs

Ten runs were performed for the PV, PVAC, and PVAT (Constant Q) filters using ten randomly generated seeds to drive the error models. Statistics were generated for each filter as follows. A mean and standard deviation were calculated for each run. An overall mean was then generated as the mean of the individual mean values. An overall standard deviation generated as the square root of the mean of the squares of the individual standard deviations. An overall RMS value was generated as the RSS of the overall mean and standard deviation. Results are listed in Tables 6-7 through 6-9.

In the conventional mode, the PVAC filter out performs the PV filter in both RMS and standard deviation, with a 45% improvement in East standard deviation (which pretty much corresponds to lateral motion) and a 12% improvement in North standard deviation. There is a 1% degradation in vertical standard deviation. The RMS values show smaller improvements, 22% in the East, 1% in the North, 1% in the vertical.

In the differential mode, performance comparisons are similar, with the PVAC out performing the PV filter in standard deviation by 44% in the East and 8% in the North. There is a 3% degradation in the vertical direction. For the RMS values, the PVAC has an advantage of 42% in the East and 9% in the North, but there is a 3% degradation in the vertical direction.

Performances of the PVAC and PVAT filters are virtually identical. The results above indicate that it is advantageous to estimate the acceleration in the filter. However, the model itself is of little importance, with a simple constant acceleration scheme performing just as well as more sophisticated models. In the vertical direction, however, there was actually a small degradation of accuracy when acceleration was estimated. The vastly improved lateral performance should, however, make the PVAC filter the preferred choice for the landing application.

Table 6-7. PV Filter Performance (Meters) Landing Profile
10 Runs Statistics

		RMS	Standard Deviation
Conventional GPS	x	9.0	6.8
	y	7.3	5.7
	z	31.9	6.7
Differential GPS	x	6.9	6.8
	y	6.6	6.5
	z	7.5	7.5

Table 6-8. PVAC Filter Performance (Meters) Landing Profile
10 Runs Statistics

		RMS	Standard Deviation
Conventional GPS	x	7.0	3.7
	y	7.2	5.0
	z	31.7	6.8
Differential GPS	x	4.0	3.8
	y	6.0	6.0
	z	7.7	7.7

Table 6-9. PVAT Filter Performance (Meters) Landing Profile
(Constant Q Matrix)
10 Runs Statistics

		RMS	Standard Deviation
Conventional GPS	x	7.0	3.7
	y	7.1	5.0
	z	31.7	6.8
Differential GPS	x	3.9	3.8
	y	6.0	6.0
	z	7.7	7.7

VII. LANDING GLIDEPATH STEERING GUIDANCE

This part of the effort developed navigation steering guidance for a helicopter executing a repeating touch-and-go landing pattern, including scaled lateral and vertical steering guidance during final straight-in approach.

7.1 PATTERN DESIGN

The landing pattern, shown in Figure 7-1, is designed to meet NASA flight test procedures. Settable parameters are listed in Table 7.1. Horizontal and vertical steering gains for the non-approach segments of the profile are set for nominal path guidance.

The approach gains were designed to maximize compatibility with typical pilot procedures. That is, the approach gain schedule is a function of range to glidepath intercept point (GPIP). The maximum extent of the display sensitive area converges as the aircraft approaches the GPIP in both the vertical and horizontal axes, much like the traditional glideslope and localizer signals of the Instrument Landing System (ILS). With GPS, of course, there is no reason that the "beamwidth" must converge down the glideslope; a constant gain "tube" could be implemented.

However, there are inherent advantages in a converging sensitivity boundary. In the early stages of the approach, the pilot is capturing the path in both the horizontal and vertical axes. He is establishing stable path tracking. Finally, since the aircraft is still high above the ground, the pilot is usually less precise in his tracking and unvoncerned about small path deviations. Therefore, a wide sensitivity area, or low display gain, is appropriate.

At the lower end of the approach, the situation is different, particularly in low visibility conditions. Here it is critical to maintain ground clearance and stable approach conditions, and tight path tracking is essential. Increasing the sensitivity gives more precise path deviation information to the pilot, who is now controlling the aircraft beam deviations to finer tolerances.

The other major feature of this design is separate specification of capture, mid-range, and final path sensitivity ("beamwidth") boundaries. This enables low gain on the display while capturing the horizontal and vertical paths, and higher gain once stable path tracking is established. Furthermore, the various sensitivities are selectable in flight so that successive approaches can optimize the gain selections.

Table 7-1. Settable Landing Pattern Parameters

Parameter	Description	Default
PA	Pattern Altitude	610 m. AGL
DL	Downwind Length	8 nm
BL	Base Length	2 nm
AFD	Approach Final Distance	5 nm
XCV	Max Lateral Deflection	.5 nm
YCV	Max Vertical Deflection	152.4 m
ETR	Expected Turn Radius	.5 nm
CR	Capture Range	2.5 nm
CLW	Lateral Capture Window	1219.2 m
XMLW	Middle Lateral Window	61.0 m
GPIPLW	GPIP Lateral Window	3.0 m
CVW	Vertical Capture Window	61.0 m
XMVW	Middle Vertical Window	15.2 m
GPIPVW	GPIP Vertical Window	6.1 m
GLIDE	Glideslope Angle	6 deg
APBEAR	Approach Bearing	11 deg
VF	Velocity Factor	100
SF	Scale Factor	2.5
GLAT	GPIP Location, Crows Landing	37° 24' 47.79"
GLON	GPIP Location, Crows Landing	-121° 06' 30.39'
GALT	GPIP Location, Crows Landing	5.4 m (Ellipsoid Height)

Note:

1. XMLW Location = XMVW Location

2. Middle Window Dist - GPIP = AFD-CR

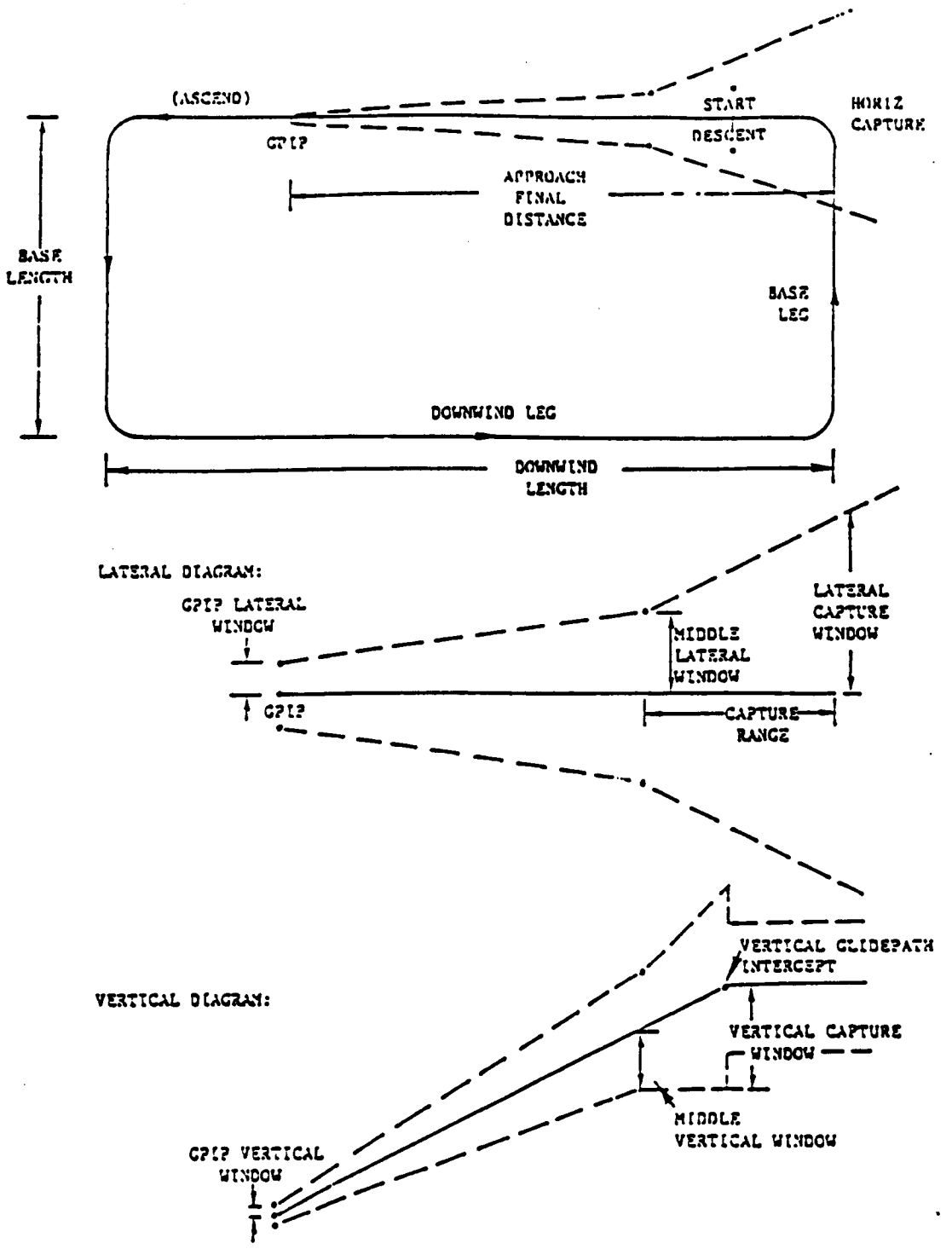

Figure 7-1. Landing Pattern

7.2 APPROACH LATERAL STEERING ALGORITHM

The lateral steering algorithm was formulated as basically a proportional plus derivative control strategy. This formulation assures that pilot steering commands are always "toward" the landing direction. Closed commands by the pilot results in "exponential" capture of the path (solution to the homogeneous first order differential equation).

A "design" approach speed of 60 knots was selected. Although this parameter could have been specified as a variable using actual total helicopter velocity, it was decided that the relationship of aircraft control and inertial path tracking was better maintained by using a design velocity. Thus instead of always commanding the same path in space regardless of velocity, the algorithm will command later and sharper turns at lower velocities.

The gain strategy was designed to handle ILS unit in use on the test aircraft. Scaling was 0 to 250, fly left, 250 to 500, fly right; 0 to 250 fly up, 250 to 500 fly down; and 0 to 200:0 to 20.0 nautical miles range to GPIP.

The derivation of the lateral steering algorithm follows:

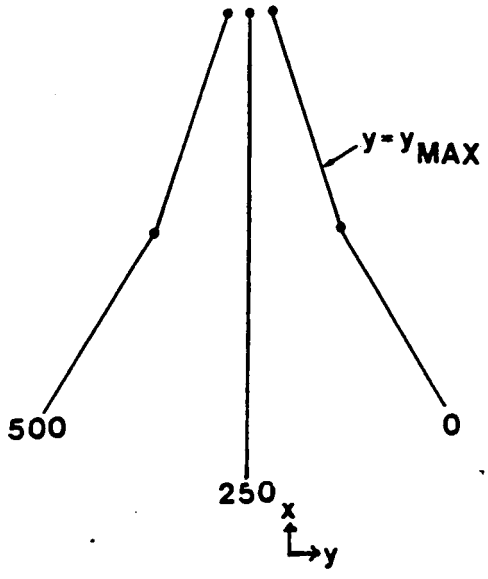

Form:

$$C = k_1(\dot{y} + \frac{1}{Y} y) + k_2$$

C = Steering command

Boundary conditions:

A. When $y = y_{max}$, $\dot{y} = 0$

Then C = 0 (Full scale left turn)

B. When $y = \dot{y} = 0$

Then C = 250 (Centered display)

C. When $y = 0$, $\dot{y} = +30.48$ m/s

Then C = 0 (Full scale left turn)

NOTE: Design approach speed 60 kts (30.89 m/s)

From (A):

$$0 = k_1(\frac{1}{\gamma} y_{max}) + k_2 \quad (1)$$

From (B):

$$250 = k_2 \quad (2)$$

From (C):

$$0 = k_1(30.48) + k_2 \quad (3)$$

Combining (2) and (3):

$$k_1 = -\frac{250}{30.48} = -8.2 \quad (4)$$

Combining (1), (2) and (4)

$$0 = -8.2\ (\frac{1}{\gamma} y_{max}) + 250$$

$$\gamma = .033\ y_{max} \quad (5)$$

Final Expression:

$$C = -8.2\ [\dot{y} + (\frac{30.48}{|y_{max}|})y] + 250 \quad (6)$$

where the absolute value sign handles the general left or right of path case.

2nd Condition:

For $\dot{x} = 0$, $\dot{y} < 0$ -> 250 <C< 500
For $\dot{x} = 0$, $\dot{y} > 0$ -> 0 <C< 250

NOTE: $y_{max} = f(x)$

The algorithm is propagated over 2.4 seconds at 0.1 second intervals. Normal updates of the 2.4 second propagation occur at the GPS measurement update rate, typically, 1.2 seconds.

7.3 APPROACH VERTICAL STEERING ALGORITHM

The approach vertical steering algorithm is identical to the approach lateral steering algorithm with three major exceptions. The gains are structured to correspond to the vertical axis parameters (YCV, CVW, XMVW, AND GPIPVW), the scaling corresponds to the instrument vertical scales, and the vertical velocity damping is adjusted for a non-zero nominal vertical velocity (due to the descent).

The derivation of the vertical steering algorithm is as follows:

From:

$$C = k_1(\dot{z}' + \frac{1}{\gamma} z') + k_2$$

C = Steering command

Boundary Conditions:

A. When $z' = -z'_{max}$, $\dot{z}' = 0$

Then C = 500 (Full scale fly down)

B. When $z' = -z' = 0$

Then C = 250 (Centered Display)

C. When $z' = 0$, $\dot{z}' = -6.4$ m/s

Then C = 500 (Full scale fly down)

NOTE: Design approach speed 60 knots (30.89 m/s)

$$z' = z - z_{GLIDE\ PATH}$$

$$z' = z - \tan(\text{Glideslope})\ x^2 + z^2$$

From (A):

$$500 = -k_1(\frac{1}{\gamma} z'_{max}) + k_2 \quad (1)$$

From (B):

$$250 = k_2 \quad (2)$$

From (C):

$$500 = -k_1(6.4) + k_2 \quad (3)$$

Combining (2) and (3):

$$k_1 = -\frac{250}{6.4} = -39.1 \quad (4)$$

Combining (1), (2), and (4)

$$500 = 39.1\ (\frac{1}{\gamma} z'_{max}) + 250 \quad (5)$$

$$\gamma = .156\ z'_{max}$$

Final Expression:

$$C = 39.1\ [z' + (\frac{6.4}{|z'_{max}|})\ z'] + 250 \qquad (6)$$

where the absolute value sign handles the general up or down of path case.

2nd Condition:

For $\dot{x} = 0$, $\dot{z}' < 0$ -> $0 < C < 250$

For $\dot{x} = 0$, $\dot{z}' > 0$ -> $250 < C < 500$

NOTE: $z'_{max} = f(x)$

The algorithm is propagated over 2.4 seconds at 0.1 second intervals. Normal updates of the 2.4 second propagation occur at the GPS measurement update rate, typically, 1.2 seconds.

7.4 PATTERN STEERING ALGORITHMS

The steering algorithm for the "non-approach" segments of the pattern, namely the ascent, downwind, and base legs, are constant gain horizontal and vertical steering rules.

The nominal horizontal steering algorithm is based on a maximum instrument deflection at ±0.5 nm (Max Lateral Deflection). The steering algorithm is of the same form as the approach lateral steering algorithm:

$$C = -8.2\ [\dot{y} + (\frac{30.48}{y_{max}})\ y] + 250$$

C = Lateral steering command

$y_{max} = 926.0$ m.

In the pattern algorithm case, of course, y_{max} is constant.

For turn to the next leg, the lateral algorithm switches to steering for the next segment at a distance of 0.5 nm (Expected Turn Radius) from the "to" waypoint. Distance is calculated from only the x (along track) component of the total distance.

For turn to localizer, the same event occurs except at the intersection of the max lateral distance and the aircraft's x distance from the corner waypoint within the lateral capture area. This turn distance will typically be greater than the nominal pattern value of 0.5 nm.

In the vertical axis, the pattern steering algorithm is also of the same form as the vertical landing algorithm, except that vertical pattern maneuvering is symmetric about $\dot{z}=0$ instead of $\dot{z}'=0$. Specifically, the pattern steering algorithm is:

$$C = 39.1 \left[\dot{z} + \left(\frac{6.4}{z_{max}}\right) z\right] + 250$$

C = Vertical steering command

z_{max} = 152.4 m.

7.5 SIMULATION EVALUATION

Figure 7-2 shows a sample landing approach path in the runway coordinate frame. Figures 7-3 and 7-4 show the steering command computation. Figure 7-5 is an enlargement of the turn portion of the command.

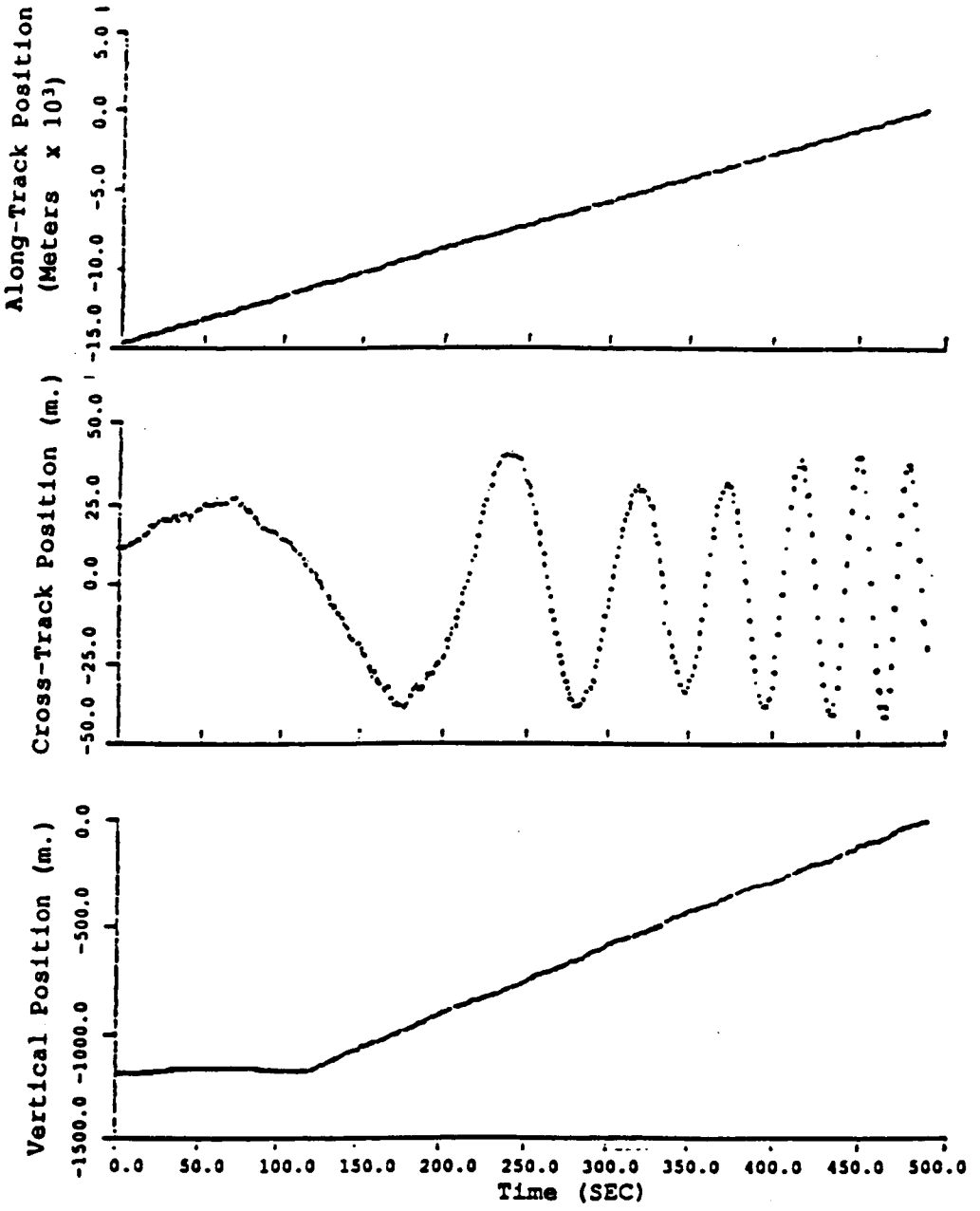

Figure 7-2. Path of Simulated Landing Approach

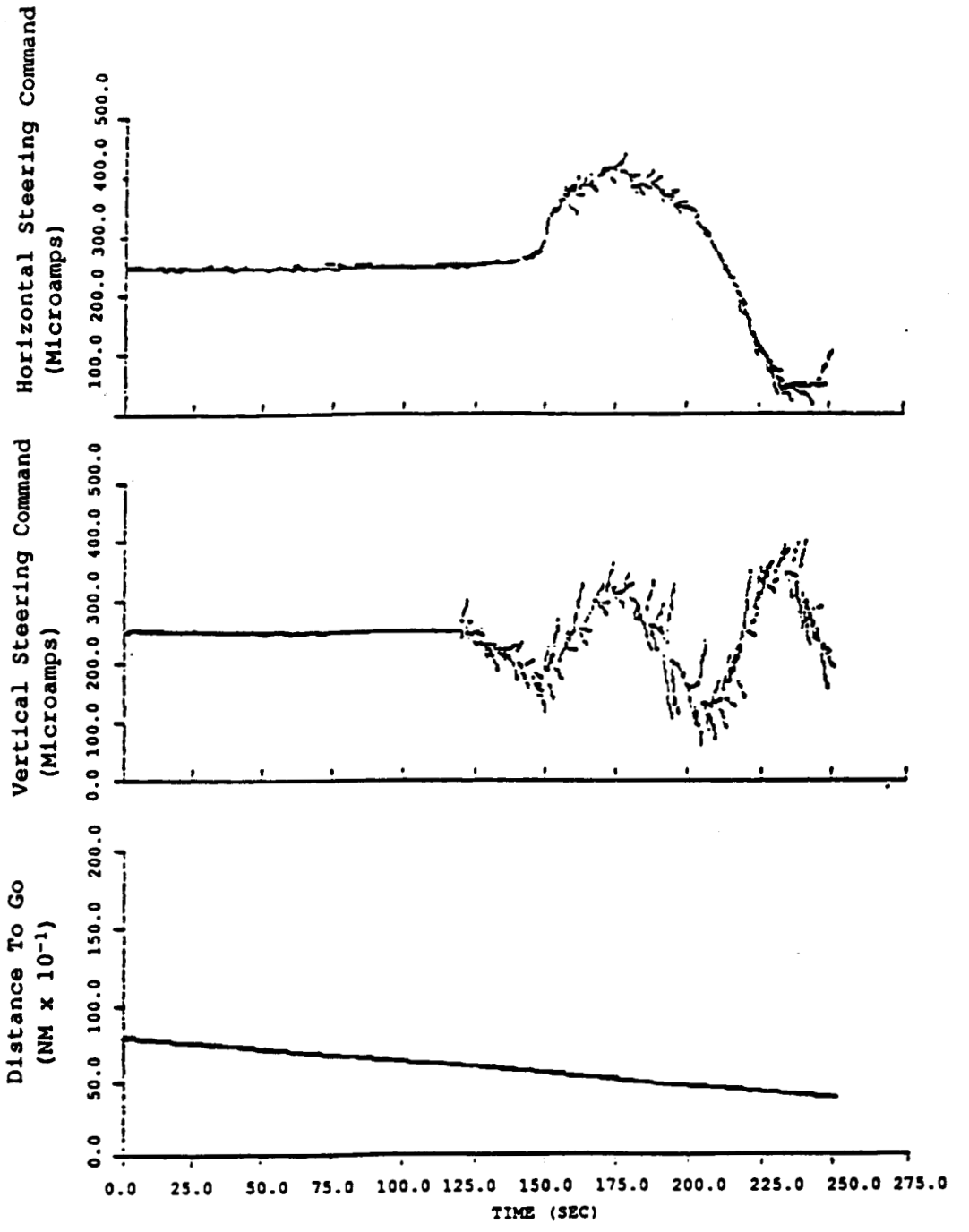

Figure 7-3. Calculated Steering Commands
(Runway Coordinate Frame, Scaled to ILS μ Amps Inputs)
First 275 Seconds

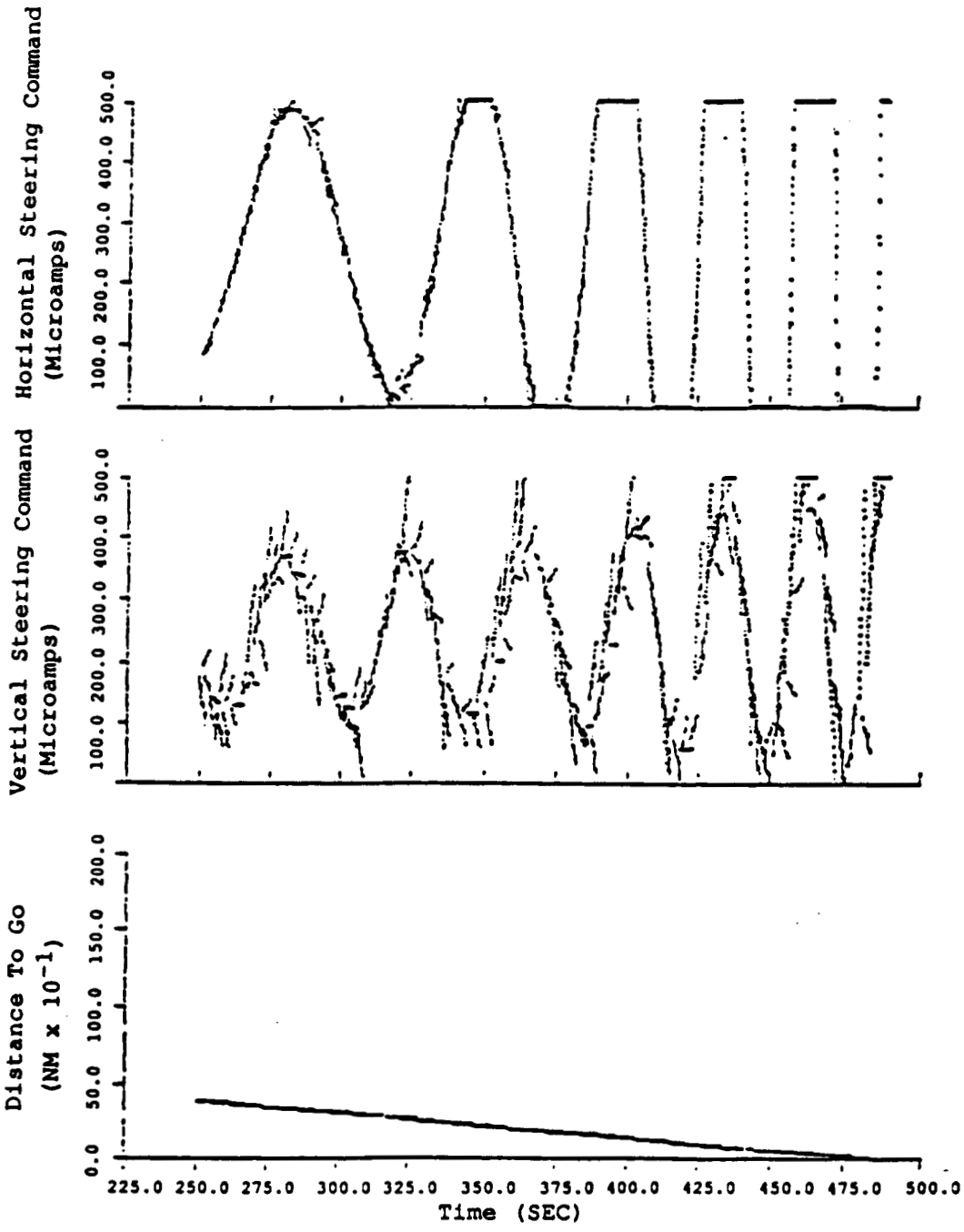

Figure 7-4. Calculated Steering Commands - 225 Seconds to Touchdown

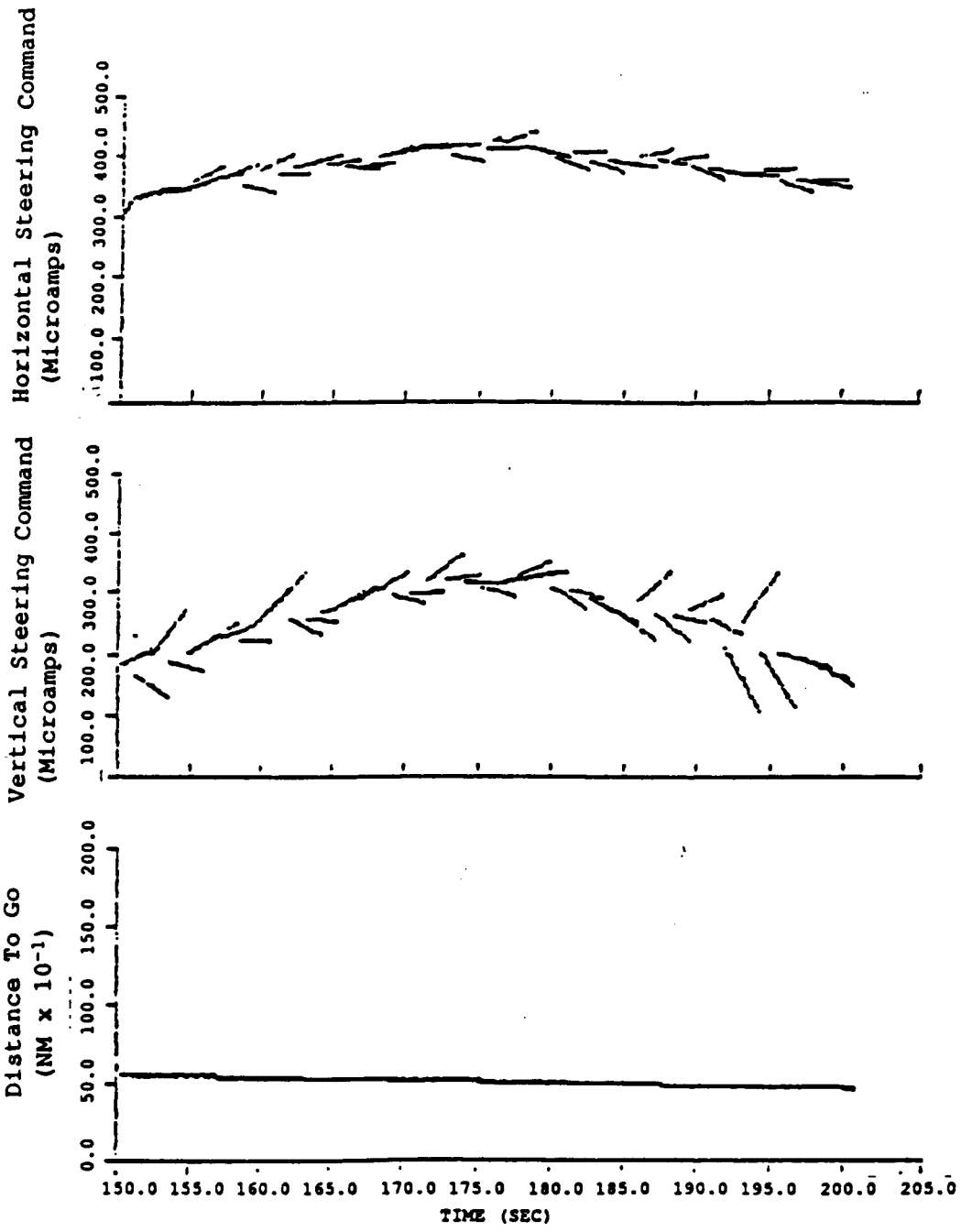

Figure 7-5. Expanded View of Calculated Steering Commands

VIII. CONCLUSIONS

Several areas were investigated for their potential contribution to improving vertical accuracy for a rotorcraft using differential GPS during a landing approach. Continuous deltaranging was studied and the potential improvement achieved by estimating acceleration was studied by comparing the performance of several filters: a position-velocity (PV) filter, a position-velocity-constant acceleration (PVAC) filter, and a position-velocity-turning acceleration (PVAT) filter. The filters were tuned for a Constant Acceleration Turn, horizontal profile, then tested on a "rough" landing profile.

The performance on the Constant Acceleration Turn pattern was best for the PVAT filter, but the improvement over the PVAC filter was negligible. The PV filter performance was inferior (factor 2 or 3 in standard deviation). The same conclusions, although to a lower extent, were also reached for the landing profile. Several different implementations of the PVAT filter were studied. They consisted of a constant turn rate (and process noise matrix), a variable turn rate (and process noise matrix) and an adaptive process noise scheme. Very minor improvements, not justifying the added processing burden, were achieved with the more complex implementations.

Overall statistics were generated for ten Monte-Carlo runs of the PV, PVAC, and PVAT (constant) filters. Results showed the PVAC filter to be the most efficient with the PVAT filter performing equally well, but being more complex. Vertical performance, however, was not significantly different (1 to 3% differences) among the various filters. The largest improvement was along the cross-track direction. Satellite selection algorithms based on vertical errors only (VDOP) and even-weighted cross-track and vertical errors (XVDOP) were tested. The resulting VDOP, when using the above criteria instead of the more common PDOP criterion, were different 32.4% of the time (VDOP) criterion) and 22.8% (XVDOP criterion). Improvement was achieved with the XVDOP criterion 75% of the time. One problem with the XVDOP criterion is that improvement was generally achieved during good DOP conditions, but not during degraded DOP conditions. By adding an altimeter, vertical accuracy should be improved during poor DOP conditions, and the XVDOP selection criterion would provide good accuracy during "good" DOP conditions.

The inclusion of an altimeter was studied by modifying the PVAC filter to include a baro bias estimate. Tests were run both on the Constant Acceleration Turn pattern and the landing approach and clearly showed the improved vertical accuracy during degraded DOP conditions, although additional tuning in the vertical direction will be necessary to acquire the required level of accuracy during landing.

Flight Test results for raw differential results, not including the effects of filter improvements studied in this simulation effort, indicated that the differential performance significantly improved overall navigation accuracy. Interestingly, the residual errors were non-dominated by geometry-independent errors such that GDOP effects were no longer obvious in the remaining error plots.

A landing glidepath steering algorithm was devised which exploits the flexibility of GPS in determining precise relative position. A method for propagating the steering command over the GPS update interval was successfully implemented.

REFERENCES

1. Edwards, F. G. and Hamlin, J. R., "Operation of a Single-Channel Sequential Navstar GPS Receiver in a Helicopter Mission Environment." The 39th Annual National Forum of the American Helicopter Society, May 1983.

2. Kalafus, R. M., "Differential Operation of Navstar GPS.: Navigation, Vol. 30, No. 3, Fall 1983.

3. Denaro, R. P. and Cabak, A. R., "Simulation and Analysis of Differential Global Positioning System for Civil Helicopter Operations." NASA CR-166534, 1983

4. Eller, D., "Transparent Covariance Matrix Formulation," IEEE, 1979.

5. Clary, George R., and John P. Chisholm, "Development and Flight Test of an X-Band Precision Approach Concept for Remote-Area Rotorcraft Operations," NASA Technical Memorandum 84398, August 1983.

6. MacMillian, A. J., "Navstar/Global Positioning System Flight Test Program Overview." AIAA/SETP et al., First Flight Testing Conference, Las Vegas, NV, November 1981.

7. Kruczynski, L. R., et al., "Global Positioning System Differential Navigation Tests at the Yuma Proving Ground." Proceedings of the National Technical Meeting of the Institute of Navigation, January 1981.

8. Connor, J. T., Sawtelle, E. M., and Till, R. D., "Fixed-Wing and Rotary-Wing Flight Testing of Navstar GPS as a Civilian Navigation System." IEEE National Telecommunication Conference, New Orleans, LA, November 1981.

9. Cardall, J. D. and Cnossen, R. S., "Civil Application of Differential GPS Using a Single-Channel Sequential Receiver." NASA CR-166168, 1981.

10. Beser, J. and Parkinson, B. W., "The Application of Navstar Differential GPS to Civil Helicopter Operations." Navigation, Vol. 29, No. 2, Summer 1982.

11. Denaro, R. P., "Application of Differential GPS to Civil Helicopter Terminal Guidance." Sixth Digital Avionics Conference, Baltimore, MD, December 1984.

12. Brogan, W. L., "Improvements and Extensions of the Geometrical Dilution of Precision (GDOP) Concept for Selecting Navigation Measurement," AFWAL-TR-81-1142, September 1981.

13. "Federal Radionavigation Plan," DOT-TSC-RSPA-81-12-1, March 1982.

14. Brady, W. and Jorgensen, P., "Worldwide Coverage of the Phase I Navstar Satellite Constellation," ION Proceedings, April 1981.

15. Kalafus, R. et al., "Navstar GPS Simulation and Analysis Program," DOT-TSC-RSPA-83-2, May 1983.

16. Denaro, R. P, and Beser, J., "Helicopter Flight Test Demonstration of Differential GPS." Proceedings of the National Technical Meeting of the Institute of Navigation, January 1985.

17. Milliken, R. J. and Zoller, C. J., "Principle of Operation of Navstar and System Characteristics." Navigation, Vol. 25, No. 2, Summer 1978.

18. Jorgensen, P. S., "Ionospheric Measurements from Navstar Satellites." SAMSO-TR-79-29, 1979.

APPENDIX A

ϕ and Q Matrix Derivations

Below are derivations for the ϕ and Q matrices for the various filters used in DIFFGPS.

Q_v, Q_a, Q_b, Q_f represent the power spectral density matrices (or scalars) for the noise in the 3 velocity equations, 3 acceleration equations, clock phase equations, and clock frequency equations, respectively.

The implementation consists of having the program user select thepower spectral densities (or their square roots) for all equations, and letting subroutines calculate the process noise matrices for the discrete implementation.

Note that these matrices are constant, except for the turn dynamics filter, where it is a function of ω.

1.0 ϕ MATRIX DERIVATIONS

1.1 NO ACCELERATION STATES

$$\dot{x} = v + \text{noise}$$
$$\dot{b} = f + \text{noise}$$
$$\dot{v} = \text{noise}$$
$$\dot{f} = -1/\tau\, f + \text{noise}$$

F matrix is

$$\begin{array}{c|c|c} x & v & b,f \\ \hline 0 & I & 0 \\ \hline 0 & 0 & 0 \\ \hline 0 & 0 & \begin{matrix} 0 & 1 \\ 0 & -1/\tau \end{matrix} \end{array}$$

ϕ matrix is: $L^{-1}\,(sI - F)^{-1}$

$(sI - F) =$

$$\left[\begin{array}{c|c|c} sI & -I & 0 \\ \hline 0 & sI & 0 \\ \hline 0 & 0 & \left\{\begin{array}{cc} s & -1 \\ 0 & s+1/\tau \end{array}\right\} B(s) \end{array}\right]$$

$(sI - F)^{-1} =$

$$\left[\begin{array}{c|c|c} sBI & B & 0 \\ \hline 0 & sBI & 0 \\ \hline 0 & 0 & s^2 I \\ & s^2 B(s) I & \end{array}\right]$$

$(sI - F)^{-1} =$

$$\left[\begin{array}{c|c|c} I/s & I/s^2 & 0 \\ \hline 0 & I/s & 0 \\ \hline 0 & 0 & \begin{array}{l} 1/s \;\; \dfrac{1}{s(s + 1/\tau)} \\ 0 \;\; \dfrac{1}{s + 1/\tau} \end{array} \end{array}\right]$$

$0 =$

$$\left[\begin{array}{c|c|c} I & \Delta t I & 0 \\ \hline 0 & I & 0 \\ \hline 0 & 0 & \begin{array}{cc} 1 & \Delta t \\ 0 & e^{-\Delta t/\tau} \end{array} \end{array}\right]$$

1.2 CONSTANT ACCELERATION

The clock equations are the same as for Section 1.1 and are left out here. The equations are:

$$\dot{x} = v$$

$$\dot{v} = a$$

$$\dot{a} = o + \text{noise}$$

F matrix is

$$\begin{bmatrix} o & I & o \\ o & o & I \\ o & o & o \end{bmatrix}$$

ϕ is $L^{-1}(sI-F)^{-1}$

$(sI - F) =$

$$\begin{bmatrix} sI & -I & o \\ o & sI & -I \\ o & o & sI \end{bmatrix}$$

$(sI - F)^{-1} =$

$$\begin{bmatrix} s^2I & sI & I \\ o & s^2I & sI \\ o & o & s^2I \end{bmatrix} \quad \frac{I}{s^3}$$

$(sI - F)^{-1} =$

$$\begin{bmatrix} I/s & I/s^2 & I/s^3 \\ o & I/s & I/s^2 \\ o & o & I/s \end{bmatrix}$$

$$0 = \left[\begin{array}{c|c|c} I & \Delta t I & \frac{\Delta t^2}{2} I \\ \hline 0 & I & \Delta t I \\ \hline 0 & 0 & I \end{array}\right]$$

1.3 TURNING SEGMENT

The clock equations are the same as for Section 1.1 and are left our here. The equations are:

$$\dot{x} = v$$

$$\dot{v} = a$$

$$\dot{a} = -\omega^2 v + \text{noise}$$

or F matrix is

$$\begin{bmatrix} 0 & I & 0 \\ 0 & 0 & I \\ 0 & -\omega^2 I & 0 \end{bmatrix}$$

ϕ matrix $= -L^{-1}(sI - F)^{-1}$

$(sI - F) =$

$$\begin{bmatrix} sI & -I & 0 \\ 0 & sI & -I \\ 0 & \omega^2 I & sI \end{bmatrix}$$

$(sI - F)^{-1} =$

$$\begin{bmatrix} s^2 I + \omega^2 I & sI & I \\ 0 & s^2 I & sI \\ 0 & -\omega^2 sI & s^2 I \end{bmatrix}$$

$$sI(s^2 I + \omega^2 I)$$

$$(sI - F)^{-1} = \begin{bmatrix} \frac{I}{s} & \frac{I}{(s^2+\omega^2)} & \frac{I}{(s^2+\omega^2)s} \\ 0 & \frac{sI}{(s^2+\omega^2)} & \frac{I}{(s^2+\omega^2)} \\ 0 & \frac{-\omega^2 I}{s^2+\omega^2} & \frac{sI}{s^2+\omega^2} \end{bmatrix}$$

$$\Phi(\Delta t) = \begin{bmatrix} I & \frac{\sin\omega\Delta t}{\omega} I & \int_0^{\Delta t} \frac{\sin\omega\Delta t}{\omega} I \, dt \\ 0 & \cos\omega\Delta t I & \frac{\sin\omega\Delta t}{\omega} I \\ 0 & -\omega\sin\omega\Delta t I & \cos\omega\Delta t I \end{bmatrix}$$

$$\int_0^{\Delta t} I \frac{\sin\omega\Delta t}{\omega} d(\Delta t) = \frac{-I}{\omega^2} \cos\omega\Delta t \Big|_0^{\Delta t}$$

$$= -\frac{I}{\omega^2}(\cos\omega\Delta t - 1) = \frac{1-\cos\omega\Delta t}{\omega^2} I$$

For ω very small, Φ becomes:

$$\begin{bmatrix} I & \Delta t I & \frac{\Delta t^2}{2} I \\ 0 & I & \Delta t I \\ 0 & 0 & I \end{bmatrix}$$

which, as expected, is the constant acceleration ϕ matrix.

0 matrix is

$$\begin{bmatrix} I & \frac{\sin\omega\Delta t}{\omega} I & \frac{1-\cos\omega\Delta t}{\omega^2} I \\ 0 & \cos\omega\Delta t\, I & \frac{\sin\omega\Delta t}{\omega} I \\ 0 & -\omega\sin\omega\Delta t\, I & \cos\omega\Delta t\, I \end{bmatrix}$$

$$\vec{\omega} = \frac{\vec{v} \times \vec{a}}{|\vec{v}|^2}$$

Derivation of ω

Assume central acceleration only. Coordinated turn,

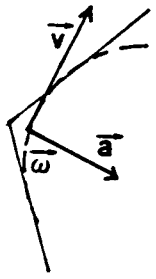

$$\vec{v} \times \vec{a} = \alpha|\vec{\omega}$$

$$\vec{\omega} = \omega|\vec{\omega}$$

$$\vec{\omega} = \alpha|\vec{\omega}\ (\tfrac{\omega}{\alpha}) = \vec{v} \times \vec{a}\ (\omega/\alpha)$$

$$\omega/\alpha = \frac{\omega}{va}$$

and,

$$a = \omega v$$

$$\rightarrow \frac{\omega}{\alpha} = \frac{\omega}{\omega v^2} = \frac{1}{v^2}$$

$$\rightarrow \vec{\omega} = \frac{\vec{v} \times \vec{a}}{v^2}$$

2.0 Q MATRIX DERIVATIONS

2.1 NO ACCELERATION STATES

The ϕ matrix was calculated as

$$\phi = \begin{bmatrix} I & \Delta t I & 0 \\ 0 & I & 0 \\ 0 & 0 & \begin{matrix} 1 & \Delta t \\ 0 & e^{\frac{-\Delta t}{\tau}} \end{matrix} \end{bmatrix}$$

Q matrix is

$$\begin{bmatrix} 0 & 0 & 0 \\ 0 & Q_v I & 0 \\ 0 & 0 & \begin{matrix} Q_b & 0 \\ 0 & Q_f \end{matrix} \end{bmatrix}$$

$$Q_k = \int_0^{\Delta t} \phi Q \phi^T dt$$

$$= \int_0^{\Delta t} \begin{bmatrix} 0 & Q_v \Delta t & 0 \\ 0 & Q_v I & 0 \\ 0 & 0 & \begin{matrix} Q_b & Q_f \Delta t \\ 0 & e^{-\Delta t/\tau} Q_f \end{matrix} \end{bmatrix} \phi^T dt$$

$$= \int_0^{\Delta t} \begin{bmatrix} Q_v \Delta t^2 & Q_v \Delta t & 0 \\ Q_v \Delta t & Q_v & 0 \\ 0 & 0 & \begin{matrix} Q_f \Delta t^2 + Q_b Q_f \Delta t e^{-\Delta t/\tau} & \\ Q_f \Delta t e^{-\Delta t/\tau} & Q_f e^{-2\Delta t/\tau} \end{matrix} \end{bmatrix} dt$$

$$Q_k = \begin{bmatrix} \frac{Q_v \Delta t^3}{3} & \frac{Q_v \Delta t^2}{2} & 0 \\ \frac{Q_v \Delta t^2}{2} & Q_v \Delta t & 0 \\ 0 & 0 & \frac{Q_f \Delta t^3}{3} + Q_b \Delta t \quad Q_f \frac{(\Delta t^2)}{2} \\ & & Q_f \frac{(\Delta t^2)}{2} \quad Q_f \Delta t \end{bmatrix}$$

The σ's below are the square roots of the noise P.S.D. for the applicable equations (i.e., σ_{vx} for the x velocity equation).

$Q(1) = \sigma_{v_x}^2 \frac{\Delta t^3}{3}$ $\quad Q(2) = Q(4) = Q(5) = 0$

$Q(3) = \sigma_{v_y}^2 \Delta t^3/3$ $\quad Q(7) = Q(8) = Q(9) = 0$

$Q(6) = \sigma_{v_z}^2 \Delta t^3/3$ $\quad Q(11) = \sigma_{v_x}^2 \Delta t^2/2$

$Q(10) = \sigma_b^2 \Delta t + \sigma_f^2 \frac{\Delta t^3}{3}$ $\quad Q(12) = Q(13) = Q(14) = 0$

$Q(15) = \sigma_{v_x}^2 \Delta t$ $\quad 0 = Q(16) = Q(18) = Q(19) = Q(20)$

$Q(21) = \sigma_{v_y}^2 \Delta t$ $\quad Q(17) = \sigma_{v_y}^2 \Delta t^2/2$

$Q(28) = \sigma_{v_z}^2 \Delta t$ $\quad Q(22) = Q(23) = Q(25) = Q(26) = 0 = Q(27)$

$Q(36) = \sigma_f^2 \Delta t$ $\quad Q(24) = \sigma_{v_z}^2 \Delta t^2/2$

$Q(29) = Q(30) = Q(31) = 0$

$0 = Q(33) = Q(34) = Q(35)$

$Q(32) = \sigma_f^2 \frac{(\Delta t^2)}{2}$

2.2 CONSTANT ACCELERATION

The clock equations are the same as for 2.1 and are not repeated here.

$\phi =$

$$\begin{bmatrix} I & \Delta t I & \Delta t^2/2\ I \\ 0 & I & \Delta t I \\ 0 & 0 & I \end{bmatrix}$$

$Q_k = \int_0^{\Delta t} \phi\ Q\ \phi^T\ dt$

$Q =$

$$\begin{bmatrix} 0 & 0 & 0 \\ 0 & 0 & 0 \\ 0 & 0 & Q_a \end{bmatrix}$$

$$Q_k = \int_0^{\Delta t} \left[\begin{array}{c|c|c} 0 & 0 & \frac{Q_a \Delta t^2}{2} \\ 0 & 0 & Q_a \Delta t \\ 0 & 0 & Q_a \end{array}\right] \left[\begin{array}{c|c|c} I & 0 & 0 \\ \Delta t I & I & 0 \\ \frac{\Delta t^2}{2} I & \Delta t I & I \end{array}\right]$$

$$Q_k = \int_0^{\Delta t} \left[\begin{array}{c|c|c} Q_a \frac{\Delta t^4}{4} & Q_a \frac{\Delta t^3}{2} & Q_a \frac{\Delta t^2}{2} \\ Q_a \frac{\Delta t^3}{2} & Q_a \Delta t^2 & Q_a \Delta t \\ Q_a \frac{\Delta t 2}{2} & Q_a \Delta t & Q_a \end{array}\right] dt$$

$$Q_k = \left[\begin{array}{c|c|c} Q_a \frac{\Delta t^5}{20} & Q_a \frac{\Delta t^4}{8} & Q_a \Delta t^3/6 \\ Q_a \frac{\Delta t^4}{8} & Q_a \frac{\Delta t^3}{3} & Q_a \Delta t^2/2 \\ Q_a \frac{\Delta t^3}{6} & Q_a \frac{\Delta t^2}{2} & Q_a \Delta t \end{array}\right]$$

2.3 TURNING DYNAMICS

The clock equations are the same as for 2.1 and are not repeated here.

$$\phi = \left[\begin{array}{c|c|c} I & \frac{\sin \omega\Delta t}{\omega} I & \frac{1-\cos \omega\Delta t}{\omega^2} I \\ 0 & \cos \omega\Delta t I & \frac{\sin \omega\Delta t}{\omega^2} I \\ 0 & -\omega \sin \omega\Delta t I & \cos \omega\Delta t I \end{array}\right]$$

$$Q_k = \int_0^{\Delta t} \phi Q \phi^T dt$$

$$Q = \left[\begin{array}{c|c|c} 0 & 0 & 0 \\ 0 & 0 & 0 \\ 0 & 0 & Q_a \end{array}\right]$$

$$Q_k = \int_0^{\Delta t} \left[\begin{array}{c|c|c} 0 & 0 & \frac{1-\cos\omega\Delta t}{\omega^2} Q_a \\ 0 & 0 & \frac{\sin\omega\Delta t}{\omega} Q_a \\ 0 & 0 & \cos\omega\Delta t\, Q_a \end{array}\right] \left[\begin{array}{c|c|c} I & 0 & 0 \\ \frac{s}{\omega} & c & -\omega s \\ \frac{1-c}{\omega^2} & \frac{s}{\omega} & c \end{array}\right] dt$$

$$= \int_0^{\Delta t} \left[\begin{array}{c|c|c} \frac{(1-c)^2}{\omega^4} Q_a & \frac{(1-c)}{\omega^3} s Q_a & \frac{(1-c)}{\omega^2} c Q_a \\ \frac{s}{\omega^3}(1-c)\, Q_a & \frac{s^2}{\omega^2} Q_a & \frac{cs}{\omega} Q_a \\ \frac{c(1-c)}{\omega^2} Q_a & \frac{cs}{\omega} Q_a & c^2 Q_a \end{array}\right]$$

$$Q_k(1,1) = \frac{Q_a}{\omega^5}\left\{\frac{3\omega\Delta t}{2} - 1\sin\omega\Delta t + \frac{\sin 2\omega\Delta t}{4}\right\}$$

$$Q_k(1,2) = \frac{Q_a}{\omega^3}\left\{\frac{1}{\omega}(1-\cos\omega\Delta t) - \frac{1}{4\omega}(1-\cos 2\omega\Delta t)\right\}$$

$$= \frac{Q_a}{\omega^4}\left\{3\frac{3}{4} - \cos\omega\Delta t + \frac{1}{4}\cos 2\omega\Delta t\right\}$$

$$Q_k(1,3) = \frac{Q_a}{\omega^3}\left\{\sin\omega\Delta t - \frac{\omega\Delta t}{2} - \frac{1}{4}\sin 2\omega\Delta t\right\}$$

$$Q_k(2,2) = \frac{Q_a}{\omega^3}\left\{\frac{\omega\Delta t}{2} - \frac{1}{4}\sin 2\omega\Delta t\right\}$$

$$Q_k(2,3) = \frac{Q_a}{4\omega^2}(1-\cos 2\omega\Delta t)$$

$$= \frac{Q_a}{4\omega^2}(1-\cos 2\omega\Delta t)$$

$$Q_k(3,3) = \frac{Q_a}{\omega}\left\{\frac{\omega\Delta t}{2} + \frac{1}{4}\sin 2\omega\Delta t\right\}$$

If $\omega \ll \xi$, then Q_k is same as for constant acceleration case.

$$\int_0^{\Delta t}\sin^2(\omega\Delta t)\, d(\Delta t) = \frac{1}{\omega}\int_0^{\omega\Delta t}\sin^2(\omega\Delta t)\, d(\omega\Delta t)$$

$$= \frac{1}{\omega}\left[\frac{\omega\Delta t}{2} - \frac{1}{4}\sin 2\omega\Delta t\right]^{\omega\Delta t}$$

$$= \frac{1}{\omega}\left[\frac{\omega\Delta t}{2} - \frac{1}{4}\sin 2\omega\Delta t\right]^{0}$$

$$\int_0^{\Delta t}\cos^2(\omega\Delta t)\, d(\Delta t) = \frac{1}{\omega}\int_0^{\omega\Delta t}\cos^2(\omega\Delta t)\, d(\omega\Delta t) = \frac{1}{\omega}\left[\frac{\omega\Delta t}{2} + \frac{1}{4}\sin 2\omega\Delta t\right]$$

$$\int_0^{\Delta t}(1-\cos\omega\Delta t)^2\,d\Delta t = \frac{8}{\omega}\int\frac{\omega\Delta t}{2}\sin^4\frac{\omega\Delta t}{2}\frac{d(\omega\Delta t)}{2} = \frac{8}{\omega}\left[\frac{3}{8}\left(\frac{\omega\Delta t}{2}\right) - \frac{\sin\omega\Delta t}{4} + \frac{\sin 2\omega\Delta t}{32}\right]$$
$$= \frac{1}{\omega}\left[\frac{3}{2}\,\omega\Delta t - 2\sin\omega\Delta t + \frac{\sin 2\omega\Delta t}{4}\right]$$

$$\int_0^{\Delta t}\sin\omega\Delta t\,\cos\omega\Delta t\,d(\Delta t) = \frac{1}{4\omega}\int_0^{2\omega\Delta t}\sin(2\omega\Delta t)\,d(2\omega\Delta t) = -\frac{1}{4\omega}\left[\cos(2\omega\Delta t)\right]_0^{\omega\Delta t}$$
$$= \frac{1}{4\omega}(1-\cos 2\omega\Delta t)$$

$$\int_0^{\Delta t}\sin\omega\Delta t\,d(\Delta t) = \frac{1}{\omega}\int_0^{\omega\Delta t}\sin\omega\Delta t\,d(\omega\Delta t) = -\frac{1}{\omega}\left[\cos\phi\Delta t\right]_0^{\omega\Delta t} = \frac{1}{\omega}(1-\cos\omega\Delta t)$$

$$\int_0^{\Delta t}\cos\omega\Delta t\,d(\Delta t) = \frac{1}{\omega}\int_0^{\omega\Delta t}\cos\omega\Delta t\,d(\omega\Delta t) = \frac{1}{\omega}(\sin\omega\Delta t)_0^{\omega\Delta t} = \frac{1}{\omega}\sin\omega\Delta t$$

---

1. Report No.	2. Government Accession No.	3. Recipient's Catalog No.
CR 177443		

4. Title and Subtitle	5. Report Date
GPS Vertical Axis Performance Enhancement for Helicopter Precision Landing Approach	September 1986
	6. Performing Organization Code

7. Author(s)	8. Performing Organization Report No.
Robert Denaro and Jacques Beser	

9. Performing Organization Name and Address	10. Work Unit No.
Theory and Applications Unlimited 485 Alberto Way; Bldg D Los Gatos, CA 95030	505-66-11
	11. Contract or Grant No.
	NAS2-11791

12. Sponsoring Agency Name and Address	13. Type of Report and Period Covered
Ames Research Center Moffett Field, CA 94035	NASA Contractor Report
	14. Sponsoring Agency Code

15. Supplementary Notes

Point of Contact: Fred Edwards, Ames Research Center, MS 210-9
Moffett Field, CA 94035 - (415) 694-5437 or FTS 464-5437

16. Abstract

The Navstar Global Positioning System (GPS) is a highly accurate radio-navigation system being developed for military and civil use by the Department of Defense (DoD). Due to the proposed global availability of this extremely accurate positioning system, GPS promises to be a major national resource for civil aviation and other navigation users. Of particular interest to NASA is a derivative of GPS, called differential GPS, which has direct applicability to many high-priority rotorcraft operations. Differential GPS affords increased levels of precision which will be essential for such rotorcraft applications as non-precision approach, offshore oil operations, search and rescue, and oil pipeline servicing. Preliminary studies conducted by NASA show that GPS performance, even in the differential mode, may be inadequate to support precision approach. This is particularly true of the vertical axis accuracy of differential GPS, which must meet the most demanding specifications. However, several attractive alternatives exist for improving GPS vertical axis performance, such as receiver "tuning" and aiding. The objective of this report was to investigate such techniques through simulation, and recommend a composite system which meets approach and landing navigation accuracy requirements. In addition, flight tests were conducted with post-test differential GPS processing to establish a performance baseline for future flight tests of these advanced concepts. Results of this preliminary flight test are presented.

17. Key Words (Suggested by Author(s))	18. Distribution Statement
NAVSTAR GPS NAVIGATION HELICOPTER APPROACH	Unlimited Subject Category: 04

19. Security Classif. (of this report)	20. Security Classif. (of this page)	21. No. of Pages	22. Price*
UNCLASSIFIED	U	125	

*For sale by the National Technical Information Service, Springfield, Virginia 22161